



FIU UNIVERSITYCITY PROSPERITY PEDESTRIAN BRIDGE PROJECT

Research and Analysis Related to Collapse during Construction

Miami and Sweetwater, Florida



Final Report

September 18, 2019

WJE No. 2018.1774

Prepared for:

FIGG Bridge Engineers, Inc.

Prepared by:

Wiss, Janney, Elstner Associates, Inc.



FIU UNIVERSITY CITY PROSPERITY PEDESTRIAN BRIDGE PROJECT

Research and Analysis Related to Collapse during Construction

Miami and Sweetwater, Florida

A blue ink signature of Gary J. Klein is shown, with the name obscured by a black rectangular redaction box.

Gary J. Klein
Licensed Professional Engineer
Florida 86154



Final Report

September 18, 2019

WJE No. 2018.1774

Prepared for:

FIGG Bridge Engineers, Inc.

Prepared by:

Wiss, Janney, Elstner Associates, Inc.

TABLE OF CONTENTS

1	Introduction and Background	1
1.1	Introduction	1
1.2	Project Background	1
1.3	Structure Description.....	2
1.4	Collapse Background	3
2	Evaluation of Failure Pattern	5
2.1	Document Review	5
2.1.1	Photographs	5
2.1.2	Video	5
2.1.3	OSHA Report	6
2.2	Analysis of Photos and Videos.....	6
2.2.1	Pre-Move (Before March 9, 2018): Exhibits 2.1.1 to 2.1.3.....	6
2.2.2	Post-Move and before De-tensioning (March 10, 2018): Exhibits 2.2.1 to 2.2.3	7
2.2.3	Two Days after Move (March 12, 2018): Exhibits 2.3.1 to 2.3.3	7
2.2.4	One Day before Collapse (March 14, 2018): Exhibits 2.4.1 to 2.4.3	7
2.2.5	Post Collapse: Exhibits 2.5.1 to 2.5.4.....	7
2.3	Findings	8
3	Evaluation of Construction Joint Conditions.....	25
3.1	Document Review	25
3.1.1	Construction Documents	25
3.1.2	Pre-Construction Email Correspondence	26
3.1.3	Concrete Placement Video	26
3.1.4	OSHA Report	27
3.1.5	WJE Interface Shear Transfer Specimens	28
3.2	Discussion	29
3.2.1	Project Records	29
3.2.2	Photographs and Laser Scans	30
3.3	Findings	30
4	Interface Shear Transfer Testing	31
4.1	Experimental Program.....	31
4.1.1	Introduction and Specimen Description	31
4.1.2	Specimen Reinforcement	31
4.1.3	Concrete Mixture Proportions	33
4.1.4	Concrete Placement	35
4.1.5	Construction Joint Interface	37
4.1.6	Test Set-up and Instrumentation.....	41
4.1.7	Loading Protocol	43
4.1.8	Interface Shear Transfer Results	44
4.1.9	Slant Shear Tests	48
4.2	Discussion	50
4.2.1	Results Relative to AASHTO Code	50
4.2.2	Florida Krome vs Chicago Limestone.....	51
4.2.3	Roughened vs As-Placed (Non-Roughened) Interface.....	52
4.3	Findings	52
5	Structural Analyses	62
5.1	Finite Element Analysis	62

5.1.1	Model Description and Assumptions	62
5.1.2	Loading	63
5.1.3	Post-Tensioning Force in Member 11	63
5.1.4	Results	64
5.2	Code Evaluation of Member 11/12 Deck Connection (As-built Condition)	64
5.2.1	Limit State	64
5.2.2	Demand	65
5.2.3	Capacity	66
5.2.4	Findings: Design Conditions	68
5.2.5	Findings: Design Conditions (Non-Roughened Surface)	69
5.3	Test-based Evaluation of Member 11/12 Deck Connection for As-built conditions	69
5.3.1	Failure Sequence and Pattern	69
5.3.2	Calculated Forces at Time of Collapse	69
5.3.3	Connection Strength (As-Built)	70
5.3.4	Discussion	72
5.3.5	Findings	73
6	Evaluation of Peer Review	74
6.1	Document Review	74
6.1.1	Request for Proposals (RFP)	74
6.1.2	Berger Agreement with FIGG	74
6.1.3	FDOT Plans Preparation Manual: Chapter 26	75
6.1.4	Released for Construction (RFC) Plans	76
6.1.5	Berger Peer Review Comments	76
6.1.6	Email Correspondence	77
6.1.7	Berger Analytical Model	77
6.1.8	Berger Web Member Checks	79
6.1.9	Certification Letters	79
6.2	Expected and Provided Peer Review Documents	79
6.3	Discussion	79
6.3.1	Quality and Completeness of Berger Peer Review.	79
6.4	Findings	80
7	Evaluation of Tilt Exceedances During Main Span Transport	87
7.1	Background on Transport of Main Span	87
7.2	Document Review	87
7.2.1	Photos of North-End Distress before and After Move	87
7.2.2	SPMT Bridge Movement Monitoring Plan	87
7.2.3	BDI Monitoring Report	88
7.3	Structural Analyses	89
7.4	Discussion	90
7.5	Findings	91
8	Re-Stressing of Member 11	102
8.1	Timeline and History of Cracking near the North End	102
8.2	Re-Stressing of Member 11	103
8.3	Actual Crack Monitoring	103
8.4	Possible Crack Monitoring	105
8.5	Discussion and Findings	107
9	Summary of Findings and Conclusion	127

1 INTRODUCTION AND BACKGROUND

1.1 Introduction

Wiss, Janney, Elstner Associates, Inc. (WJE) has carried out research and analysis related to collapse of main span of the FIU UniversityCity Prosperity Pedestrian Bridge during construction. Studies were carried out in the areas listed in the table shown below. The corresponding sections of the report are indicated.

Area of Research and Analysis	Report Section
Evaluation of failure pattern	2
Evaluation of construction joint conditions	3
Interface shear transfer testing	4
Structural analyses: <ul style="list-style-type: none"> Finite element analysis Code evaluation of Member 11/12 deck connection (construction condition) Test-based Evaluation of Member 11/12 Deck Connection (construction condition) 	5
Evaluation of peer review	6
Evaluation of tilt exceedances during main span transport	7
Re-stressing of Member 11	8

WJE's studies were led by Gary J. Klein (Florida PE 85164), Senior Principal and Executive Vice President of WJE. Mr. Klein's resume is provided in Exhibit 1.1.

1.2 Project Background

The UniversityCity Prosperity Project was created by Florida International University (FIU) to connect the university campus in Miami with the City of Sweetwater. The centerpiece of the project was a pedestrian bridge over SW Eighth Street west of SW 109th Avenue. FIU awarded the design-build contract to Munilla Construction Management, Inc. (MCM). The designer, who was a consultant to MCM, was Figg Bridge Engineers, Inc. (FIGG).

Funding sources included federal, state, local and University contributions. The project was administered by FIU with support from the Florida Department of Transportation (FDOT). The primary parties involved in design and construction of the bridge are listed in Table 1.1.

Table 1.1. Involved Parties

Organization	Role
Florida International University (FIU)	Owner
Florida Department of Transportation (FDOT)	Project oversight and administration
Bolton Perez and Associates, Inc. (BPA)	Certified Engineering Inspector (CEI) for FIU
The Corradino Group (Corradino)	CEI Post-tensioning inspector for BPA
Munilla Construction Management, Inc. (MCM)	General contractor (design-build team leader)
The Structural Group of South Florida (Structural)	Concrete subcontractor to MCM
Structural Technologies /VSL, LLC (Structural/VSL)	Post-tensioning subcontractor to MCM
RC Group, LLC (RC Group)	Formwork and scaffold subcontractor to MCM
Barnhart Crane & Rigging Company (Barnhart)	Precast bridge transporter to MCM
Georges Crane Service, Inc. (Georges)	Crane supplier to MCM
Cemex (Cemex)	Concrete supplier to MCM
FIGG Bridge Engineers, Inc. (FIGG)	Lead structural designer to MCM
The Louis Berger Group, Inc. (Berger)	Independent peer review to FIGG

1.3 Structure Description

The pedestrian bridge design employed a post-tensioned concrete deck and canopy connected by structural concrete columns and diagonals along the centerline to form a two-span continuous truss. The design also featured a tapered pylon extending from the center support with stay pipes connected to the canopy that were intended to increase bridge stiffness and mitigate vibration from pedestrian loading. See cover photo for a rendering of the completed bridge.

Figure 1.1 is a photo of the main (south) span being moved to its final position on the south pier and central pier.

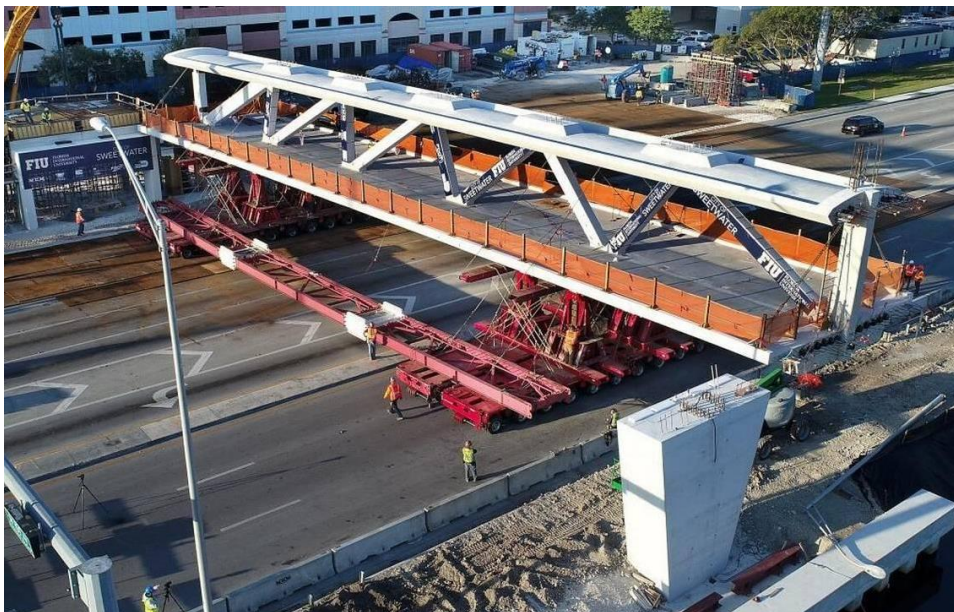


Figure 1.1. Main span being moved into its final position (Barnhart photo, March 10, 2018)

Figure 1.2 shows the key members at the north end of the main span. Member 11 is the northernmost diagonal framing between the canopy and deck. Member 12 supports the north end of the canopy in the main span. A 2-foot-wide diaphragm extends about 4 feet below the deck at the north end.

In the casting yard, the main span was oriented such that Members 11 and 12 were at the west end; however, cardinal directions referred to in this report are relative to the final position of the main span (Members 11 and 12 at the north end).

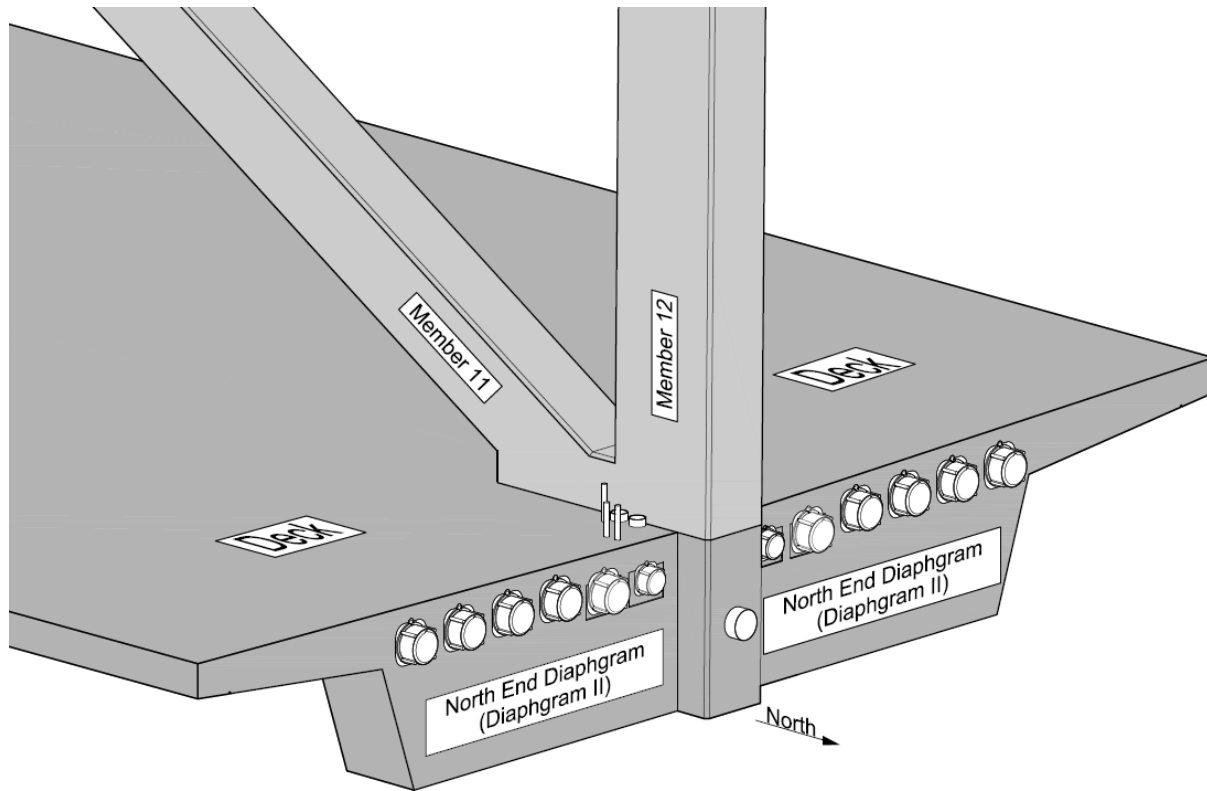


Figure 1.2. Key members at north end

1.4 Collapse Background

On March 15, 2018, at approximately 1:45 p.m., the main span collapsed as post-tensioning bars in the northernmost diagonal (Member 11) were being re-stressed. The collapse was triggered by failure of the connection between the Members 11 and 12 and the deck.

Exhibit 1.1



PERSONNEL QUALIFICATIONS

Gary J. Klein, P.E., S.E. | Executive Vice President and Senior Principal



EXPERIENCE

Gary Klein joined WJE in 1979 and has since investigated hundreds of concrete, steel, and wood structures. Most assignments have involved deterioration, distress, or failure of buildings and bridges. Mr. Klein's experience also includes the investigation of parking structures, tunnels, transit structures, stadiums, piers, environmental facilities, and wind turbines. Many of these studies have included repair design and construction observation services. He also has experience in vibration studies, nondestructive testing, load testing of structures and components, computer modeling of structures, and underwater inspection.

From 1973 to 1979, Mr. Klein worked at the Chicago firms of McDonough Engineering, Inc. (formerly Murphy Engineering, Inc.) and Howard Needles Tammen and Bergendoff (HNTB). While with these firms, he was responsible for structural design and plan preparation for new construction as well as investigation and rehabilitation of existing structures.

REPRESENTATIVE PROJECTS

Bridge Engineering

- Loop Road Bridge - VA: Structural investigation, repair design, and expert testimony
- Wacker Drive Viaduct - Chicago, IL: Durability research, prototype testing, and health monitoring
- Ford Parkway Bridge - Minneapolis, MN: Structural investigation and preservation recommendations
- Venetian Causeway - Miami, FL: Historic preservation study
- Hamakua Coast Steel Trestle Bridges - Hilo, HI: Structural investigation and load testing
- Illinois River Bridge - IL: Design of a twin segmental box-girder bridge (with HNTB)

Collapse Investigation

- I-35W Mississippi River Bridge - Minneapolis, MN: Participated in collapse investigation for MnDOT in cooperation with NTSB
- Kansas City Hyatt Regency Hotel - Kansas City, MO: Suspended walkway collapse
- I-80/94/294 Interchange at IL 394 - Lansing, IL: Collapse of Ramp J framing during erection
- Koror-Babeldaob Bridge - Republic of Palau: 790-foot concrete box-girder span over the Toegel Channel
- Los Angeles Metro Red Line - Los Angeles, CA: Subway tunnel collapse during re-mining
- Central Artery /Tunnel Project (The Big Dig) - Boston MA: Safety audit of tunnel and bridge structures following ceiling collapse

Repair and Rehabilitation Design

- Chicago and Northwestern Trainshed - Chicago, IL: Structural rehabilitation
- Grant Park North Garage - Chicago, IL: Structural rehabilitation
- Soldier Field - Chicago, IL: Structural rehabilitation

Research and Testing

- Dapped Ends Prestressed Concrete Thin-Stemmed Members , PCI 2016
- Development of a Rational Design Methodology for Precast Concrete Slender Spandrel Beams, PCI 2011
- Predicting Volume Change Movements and Forces in Buildings, PCI 2002

TECHNICAL COMMITTEES

- ACI 318 - Standard Building Code
- ACI 318J - Joints and Connections
- ACI 318E - Section and Member Strength
- ACI 378 - Wind Turbines
- ACI 445 - Shear and Torsion
- ACI 445A - Strut-and-Tie Method
- National Construction Safety Team Advisory Committee

EDUCATION

- University of Illinois at Urbana-Champaign
- Bachelor of Science, Civil Engineering, 1973
- Master of Science, Civil Engineering, 1975

PRACTICE AREAS

- Bridge Engineering
- Collapse Investigation
- Historic Preservation
- Repair and Rehabilitation Design
- Structural Research and Testing
- Structural Analysis/Computer Modeling
- Structural Investigation
- Underwater Inspection

REGISTRATIONS

- Professional Engineer in AZ, FL, IL, KY, and MI
- Structural Engineer in IL and MA

PROFESSIONAL AFFILIATIONS

- National Academy of Engineering
- American Concrete Institute
- American Society of Civil Engineers
- Precast/Prestressed Concrete Institute
- Structural Engineers Association of Illinois

2 EVALUATION OF FAILURE PATTERN

The objective of this evaluation is to assess the sequence of distress and failure in vicinity of the Member 11/12 deck connection that led to the collapse of the bridge. Evaluation of the failure sequence is based on photographs taken before and after the collapse.

2.1 Document Review

Assessment of the progression of the cracking at the Member 11/12 region was mainly based on available photographs. Explanation of the sources and observation of key documents pertaining to the cracking are provided in the following sections.

2.1.1 Photographs

Assessment of the failure sequence was dependent on photographs from various sources. A list of sources of photographs used in this report are included in Table 2.1.

Table 2.1. Source of Figures

Source	Dates	Notes
OSHA Report: <i>"Investigation of March 15, 2018 Pedestrian Bridge Collapse at Florida International University, Miami, FL"</i>	Photos: Feb 24, 2018-Apr 2019 Report: June 2019	Pre-collapse and post-collapse photos credited to BPA
Corradino	Mar 10, 2018	
MCM	Mar 12, 2018	Email from MCM to FIGG
WJE	Mar 19, 2018	

2.1.2 Video

Several videos of the collapse were reviewed by WJE. The only non-time-lapse video available to WJE was taken from a vehicle's dashboard camera as the vehicle headed east on SW Eighth Street. Frames extracted from the video at the time of the collapse are shown in Figure 2.1 to Figure 2.4. Note the frames have been cropped from the original video.



Figure 2.1. Video frame at start of collapse



Figure 2.2. Video frame during collapse

Note: Redaction in "Figures 2.1 and 2.2" as per NTSB Operations Bulletin CIO-GEN-016.



Figure 2.3. Video frame during collapse



Figure 2.4 Video frame during collapse

2.1.3 OSHA Report

OSHA produced a report summarizing its investigation into the cause of the collapse. OSHA collected photographs of the cracking in Member 11/12 region. The majority of photos in the report were taken by BPA. WJE utilized the photos taken by BPA to develop a crack sequence. WJE also used the post-collapse photographs from the OSHA report for evaluation of post-collapse conditions and the construction joint below Member 11. The OSHA report was used as a source of photographs only; WJE did not rely on or necessarily agree with findings in the OSHA report.

2.2 Analysis of Photos and Videos

WJE produced a series of images showing the sequence of cracking and the condition of the bridge after the collapse. WJE created both 2D and 3D images to assist in locating reinforcing steel, post-tensioning, deck penetrations, and crack locations.

2.2.1 Pre-Move (Before March 9, 2018): Exhibits 2.1.1 to 2.1.3

The span was precast on falsework and shoring in a staging area on the south side of SW Eighth St. Falsework and shoring removal started on February 23, 2018. Shoring at the midspan was removed first and continued outwards towards the deck-end diaphragms. All shoring was removed by February 25, 2018. The bracing for the deck-end diaphragms remained in place until the bridge was ready to be lifted by Barnhart.

The Construction Engineering Inspector for the project, BPA, completed a truss crack inspection on February 6, 2018. Minor cracks in several truss members were noted, but no cracking or distress was reported at or near the connection of Members 11 and 12 to the deck. It should be noted that debonding of the construction joint below Members 11 and 12 may have occurred before February 6 due to post-tensioning and thermal stresses, but it is highly unlikely that the crack inspection would have detected it.

The first known indication of distress in the Member 11/12 region was documented in a crack report prepared by BPA on February 28, 2018. The observed crack occurred between Member 11 and the deck chamfer or "wedge." Although difficult to see, debonding and northward sliding of Member 11 is also evident in the photograph. BPA did not measure the crack; however, a vertical marking, consistent with techniques used to visually track crack growth, is drawn across the crack.

Note: Redaction in "Figures 2.3 and 2.4" as per NTSB Operations Bulletin CIO-GEN-016.

On March 8, a Barnhart photo documented a crack on the topside of the deck, west of Member 12. Crack width was not measured. No photograph was taken on the east side of Member 12; however, WJE assumes that a matching crack likely occurred on the east side, based upon the symmetry shown by future cracking.

2.2.2 Post-Move and before De-tensioning (March 10, 2018): Exhibits 2.2.1 to 2.2.3

The bridge was placed on its final supports at approximately 12:30 p.m. on March 10, 2018. The bridge remained in this state until approximately 4:30 p.m. when VSL de-tensioned Member 11. During this time frame, at approximately 3:07 p.m., the on-site post-tensioning inspector, Corradino, took photos of the deck near Members 11 and 12. These photos show widening of the cracks documented in Exhibits 2.2.1 to 2.2.3.

These photos show widening of the “wedge” crack. Analysis of this crack profile suggests that Member 11 slid northwards while the “wedge” stayed attached to the deck. This is evident from post-collapse photographs to be discussed later. Some of the cracking on the topside of the deck, adjacent to Member 12, developed into spalls and detached from the deck. Member 11 also developed longitudinal cracks generally in line with the longitudinal PT bars.

2.2.3 Two Days after Move (March 12, 2018): Exhibits 2.3.1 to 2.3.3

Two days after the move, MCM documented the cracks and sent an email to FIGG asking for a review. Conditions generally appear similar to those shown in Exhibits 2.2.1 to 2.2.3 but with several of the cracks appearing to have slightly widened.

Several new crack patterns developed as well. It is not known if these existed on March 10 and were not documented, or if they initiated after March 10. Notably, a photograph east of Member 12, looking down on the deck, shows northward faulting of the deck-end diaphragm closest to Member 12. As the deck-end diaphragm displaces north, the base of Member 12 goes into curvature inducing flexural cracks on the north face (the tension face).

An additional longitudinal crack developed near the base of Member 11. WJE believes the development and widening of this crack is a result of additional sliding.

2.2.4 One Day before Collapse (March 14, 2018): Exhibits 2.4.1 to 2.4.3

One day before the collapse, conditions appear generally similar to those shown in Exhibits 2.3.1 to 2.3.3 with several of the cracks appearing to have widened further. Longitudinal cracking and spalling along the east and west faces at the base of Member 11 appears to have progressed. These longitudinal cracks divide Member 11 into individual laminar sections or “teeth.” As the cracks widen, Member 11 no longer acts as a fully composite member. Instead, the laminar planes begin to behave independently and each tooth is subject to flexural stress.

2.2.5 Post Collapse: Exhibits 2.5.1 to 2.5.4

In the following ways, the video and photographic evidence indicates the collapse was triggered by sudden columnar crushing of the teeth at the base of Member 11:

- Post-collapse photos show the laminar fragments or “teeth” at the base of Member 11 have completely failed and separated from Member 11 indicating a sudden failure. Photographs taken before the collapse shows progressive growth of these cracks.
- Video of the collapse shows hinging of the truss at the top of Member 11, which is consistent with shortening of Member 11 due to sudden failure near the deck. Furthermore, the video evidence does

not indicate northward movement at the base of Member 12, which would be expected if the collapse was triggered by sudden and extreme northward sliding and breakout.

- Member 12 was relatively undamaged compared to Member 11. Small portions of the deck stayed intact with Member 12. The observed damage to the lower end of Member 12 is consistent with secondary damage due to the collapse and does not coincide with the cracking observed before the collapse.
- The breakout of the deck-end diaphragm is consistent with the cracking seen in previous days. Concrete damage on areas adjacent to the breakout are shallow and consist mostly of spalling of the concrete cover.
- The construction joint between Member 11 and the deck is relatively unscathed, indicating extreme sliding of Member 11 was not part of the ultimate collapse sequence. Further assessment of the construction joint and sliding resistance is evaluated in Sections 3 and 4.
- Although the collapse was triggered by sudden failure at the base of Member 11, the underlying cause was northward movement of Members 11 and 12 relative to the deck. As described above, the northward movement started with a shear-friction failure below Member 11 that, in turn, led to breakout failure of the north-end diaphragm below Member 12.

2.3 Findings

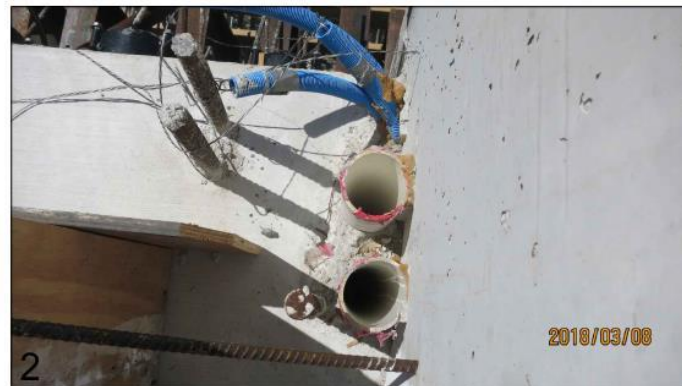
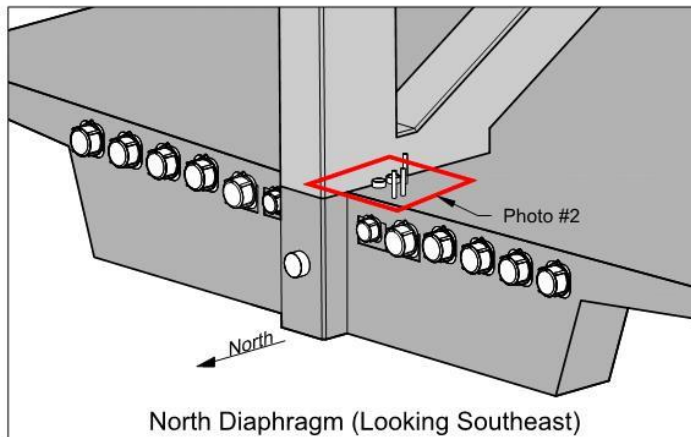
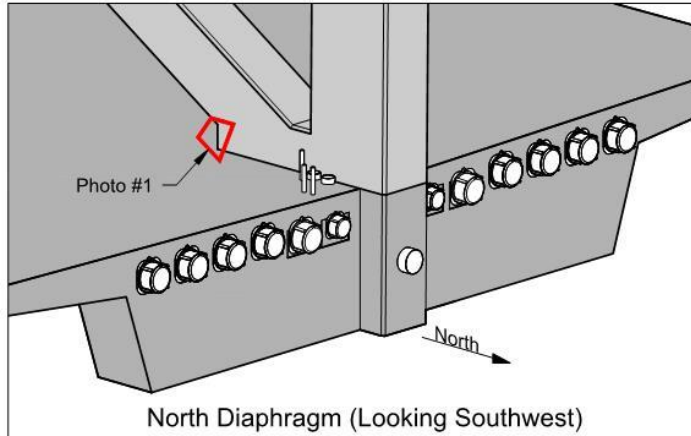
The following findings are based on the review and analysis described above:

- Cracking initiated in the Member 11/12 region after shoring was removed due to loss of bond and sliding at the construction joint below Member 11. This type of interface shear transfer failure is also referred to as a shear-friction failure.
- Cracking substantially worsened *after* the bridge was placed in its final location on south pier (End Bent 1) and central pier, *before* Member 11 was de-tensioned. Northward sliding of Member 11 led to breakout failure of the north-end diaphragm below Member 12, while existing cracks continued to widen. New cracks developed as the base of Member 11 as it separated into laminar sections or “teeth.”
- Cracking continued to worsen until the bridge collapsed. The collapse was triggered by sudden crushing of Member 11 near its base. After the base of Member 11 was lost, a hinge in the truss developed near the top of Member 11. Additional damage developed in the connection region as the collapse progressed, including severe damage to the base of Member 12 and the north-end diaphragm.

In summary, a debonding and sliding failure at the construction joint below Member 11 led to breakout failure of the north-end diaphragm and ultimately collapse, triggered by sudden crushing of Member 11 near its base. The reasons for the connection failure are addressed in subsequent sections of this report.

Exhibit 2.1.1

**OBSERVED AND ESTIMATED CRACKS AT MEMBER 11/12 DECK CONNECTION
Shoring Removal to Pre-Move (Before March 9, 2018)**



Photos

1. East side of Member 11. Included in crack report email on February 28, 2018 from Jose Morales (BPA) to Rodrigo Isaza (MCM).
2. Topside of deck end diaphragm II, west of Member 11. Produced by Barnhart. Photo dated March 8, 2018.

Exhibit 2.1.2
OBSERVED AND ESTIMATED CRACKS AT MEMBER 11/12 DECK CONNECTION
Shoring Removal to Pre-Move (Before March 9, 2018)

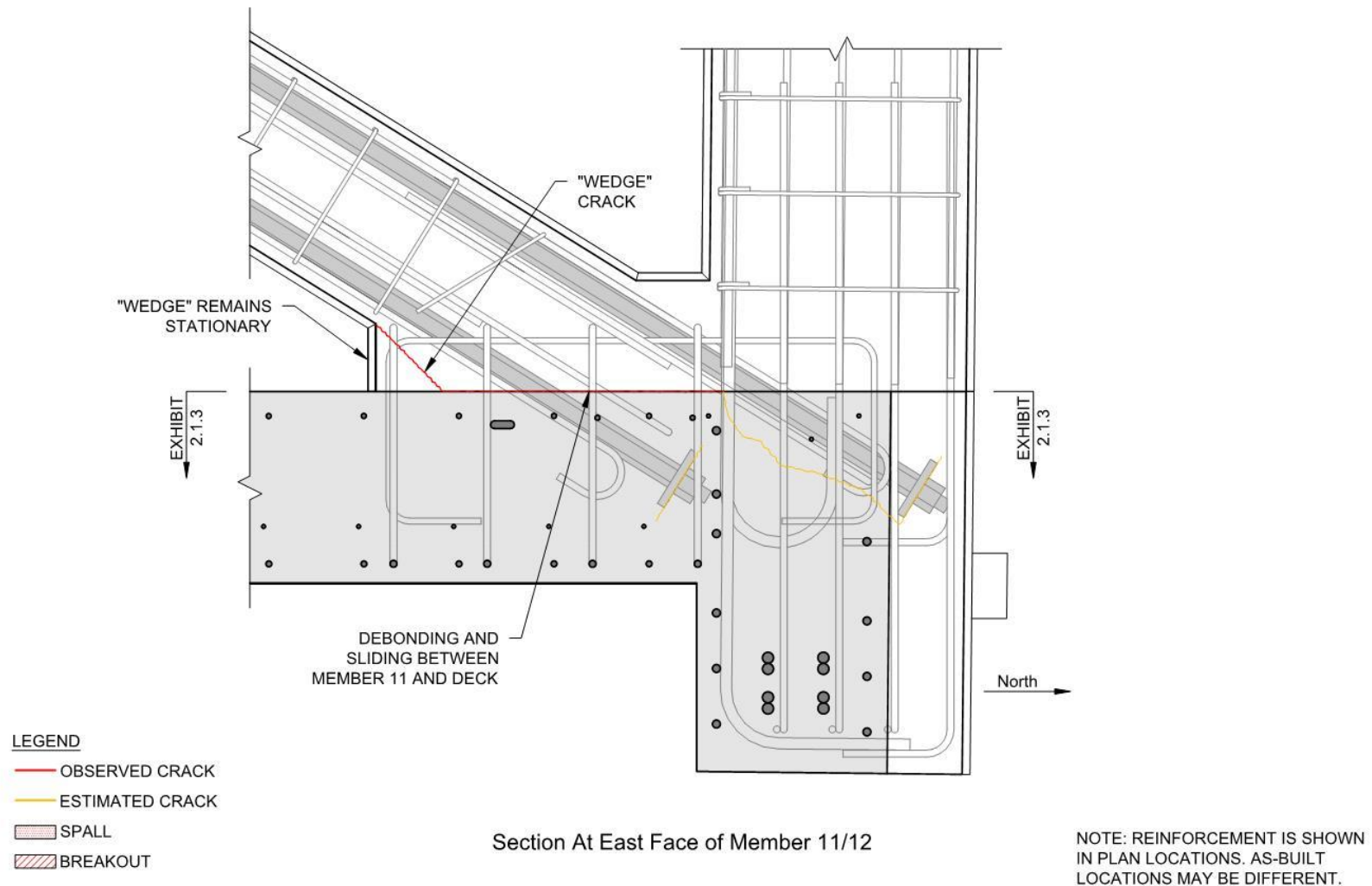


Exhibit 2.1.3
OBSERVED AND ESTIMATED CRACKS AT MEMBER 11/12 DECK CONNECTION
Shoring Removal to Pre-Move (Before March 9, 2临时)

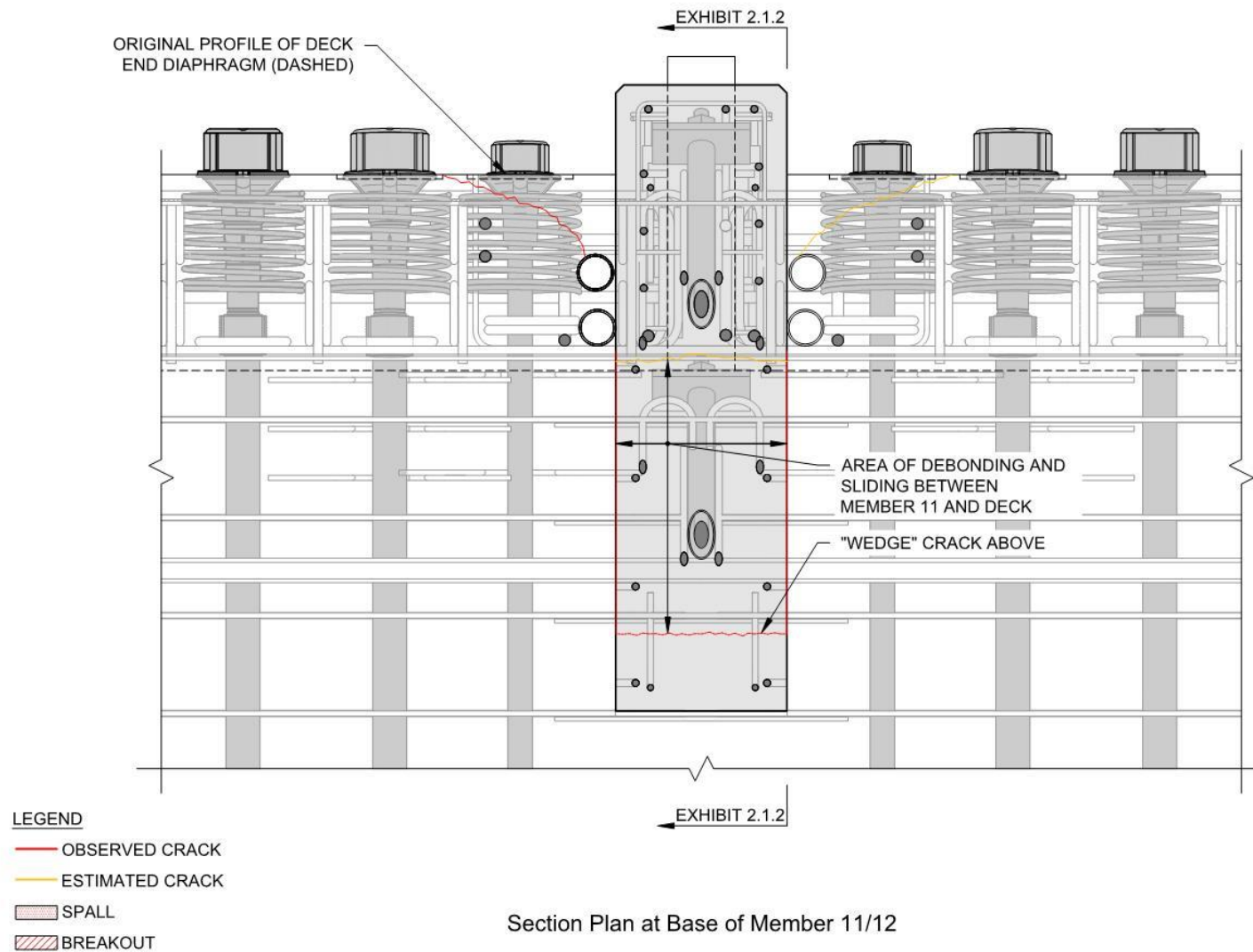
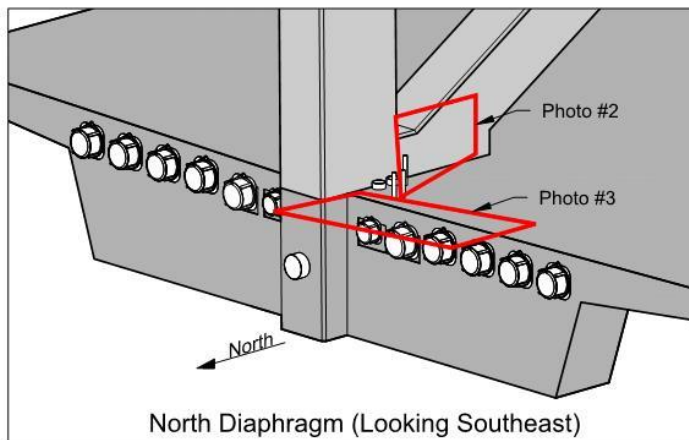
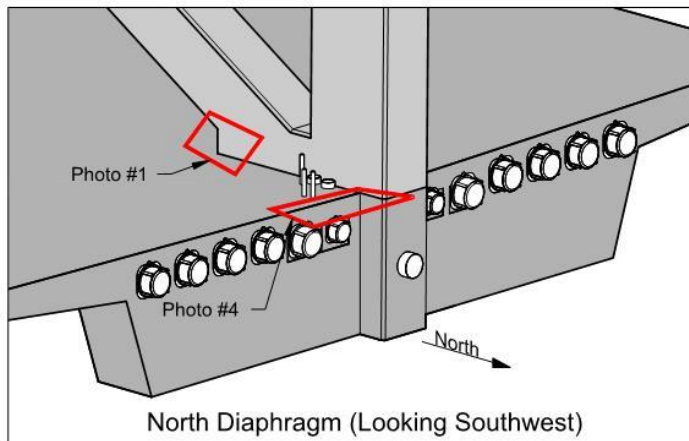


Exhibit 2.2.1
OBSERVED AND ESTIMATED CRACKS AT MEMBER 11/12 DECK CONNECTION
Post-Move (March 10, 2018)



Photos

1. East side of Member 11. Photo taken by Coradino. Photo metadata is time stamped 3:07 PM on March 10, 2018.
2. West side of Member 11. Photo taken by Coradino. Photo metadata is time stamped 3:07 PM on March 10, 2018.
3. Topside of deck end diaphragm II, west of Member 12. Photo taken by Coradino. Photo metadata is time stamped 3:14 PM on March 10, 2018.
4. Topside of deck end diaphragm II, west of Member 12. Photo taken by Coradino. Photo metadata is time stamped 3:14 PM on March 10, 2018.

Exhibit 2.2.2
OBSERVED AND ESTIMATED CRACKS AT MEMBER 11/12 DECK CONNECTION
Post-Move (March 10, 2018)

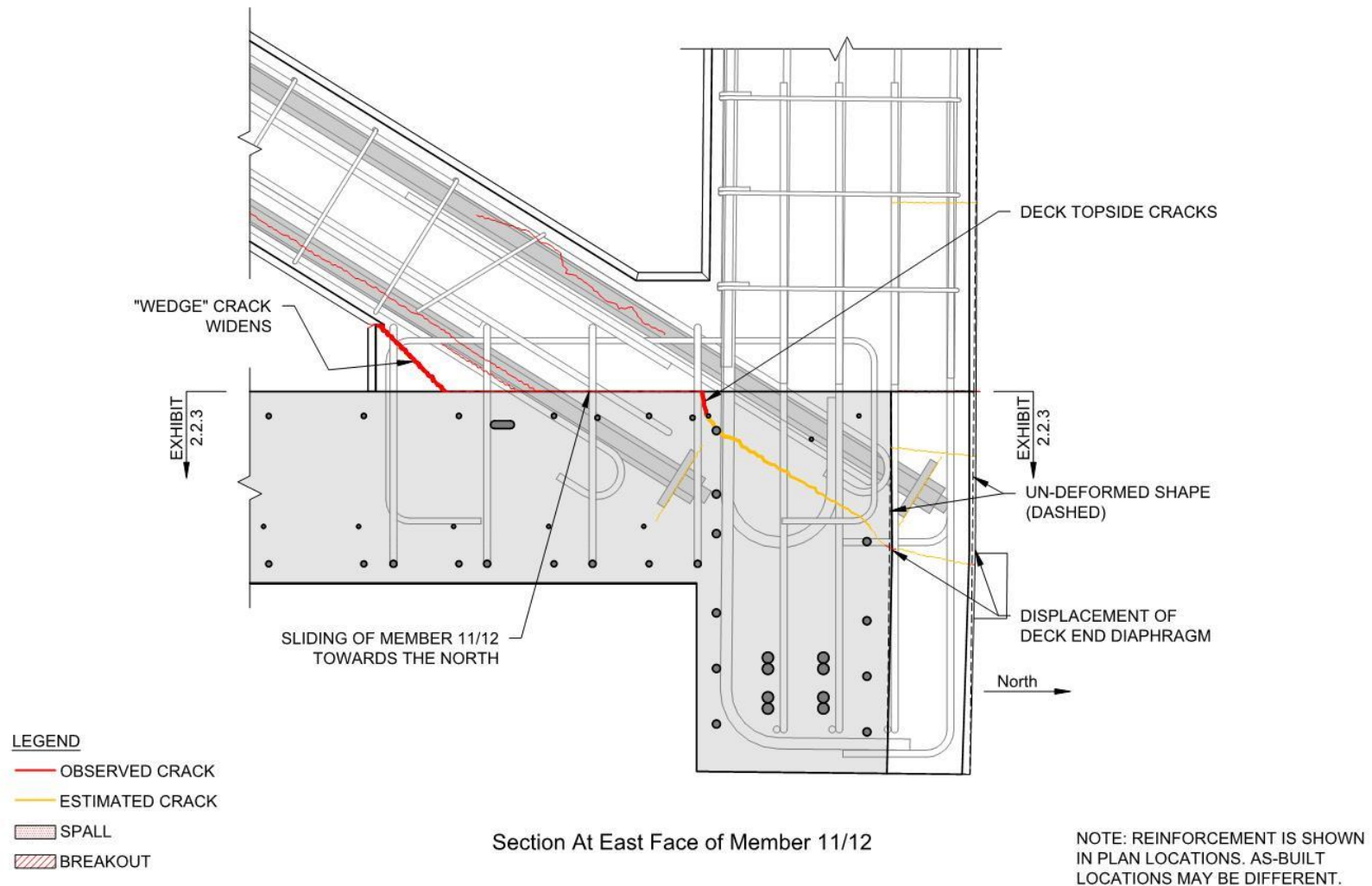


Exhibit 2.2.3
OBSERVED AND ESTIMATED CRACKS AT MEMBER 11/12 DECK CONNECTION
Post-Move (March 10, 2018)

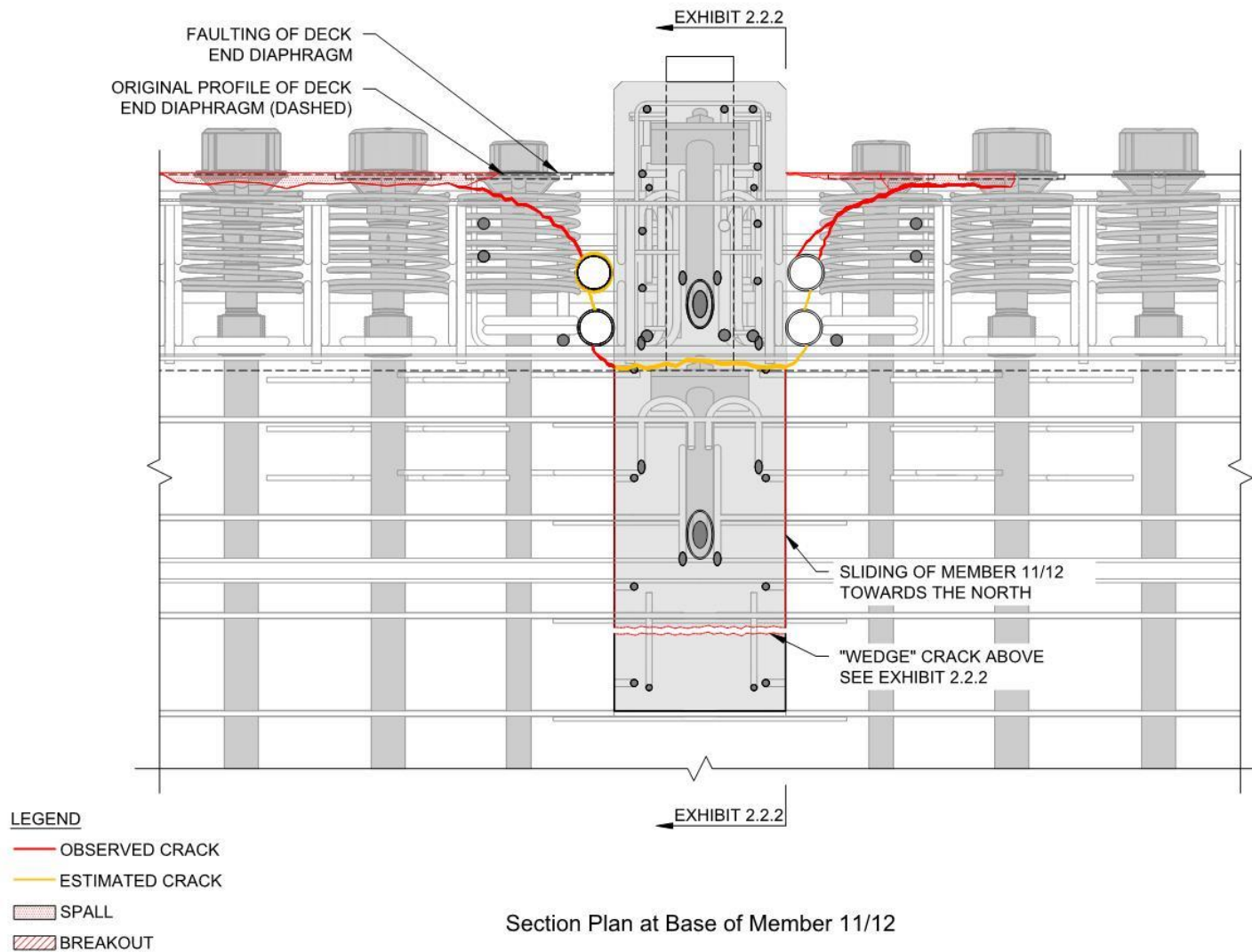
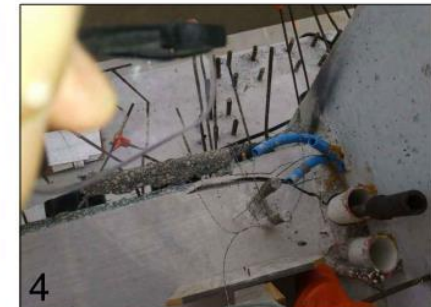
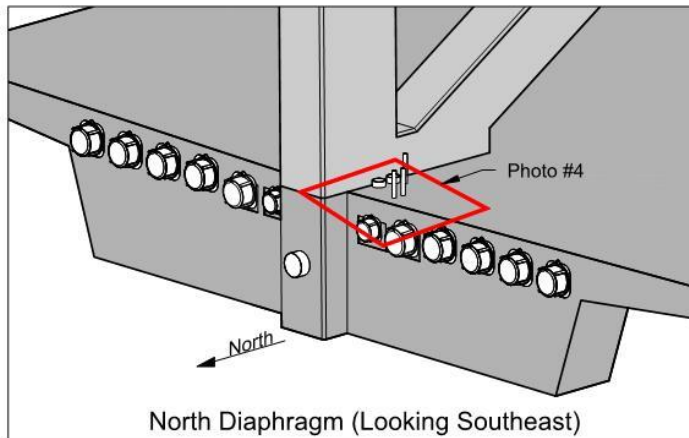
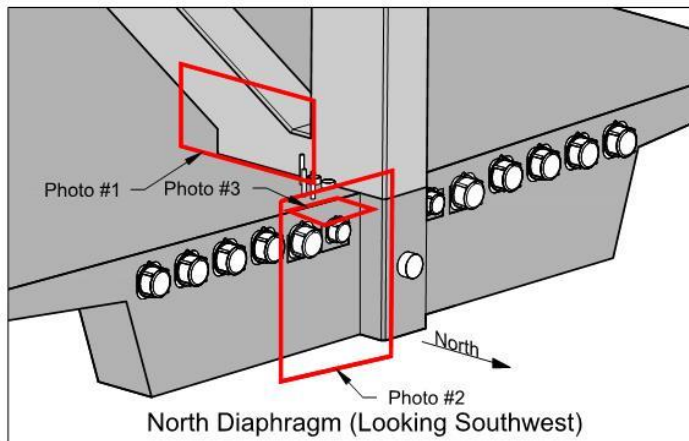


Exhibit 2.3.1

OBSERVED AND ESTIMATED CRACKS AT MEMBER 11/12 DECK CONNECTION Two Days After Move (March 12, 2018)



Photos

1. East of member 11, looking west. Photo included in email from MCM to FIGG on March 12, 2018.
2. North end of deck end diaphragm II, east of Member 12, looking south west. Photo included in email from MCM to FIGG on March 12, 2018.
3. North end of deck end diaphragm, east of Member 12, looking down. Photo included in email from MCM to FIGG on March 12, 2018.
4. Topside of deck end diaphragm II, west of Member 12. Photo included in email from MCM to FIGG on March 12, 2018.

Exhibit 2.3.2
OBSERVED AND ESTIMATED CRACKS AT MEMBER 11/12 DECK CONNECTION
Two Days After Move (March 12, 2018)

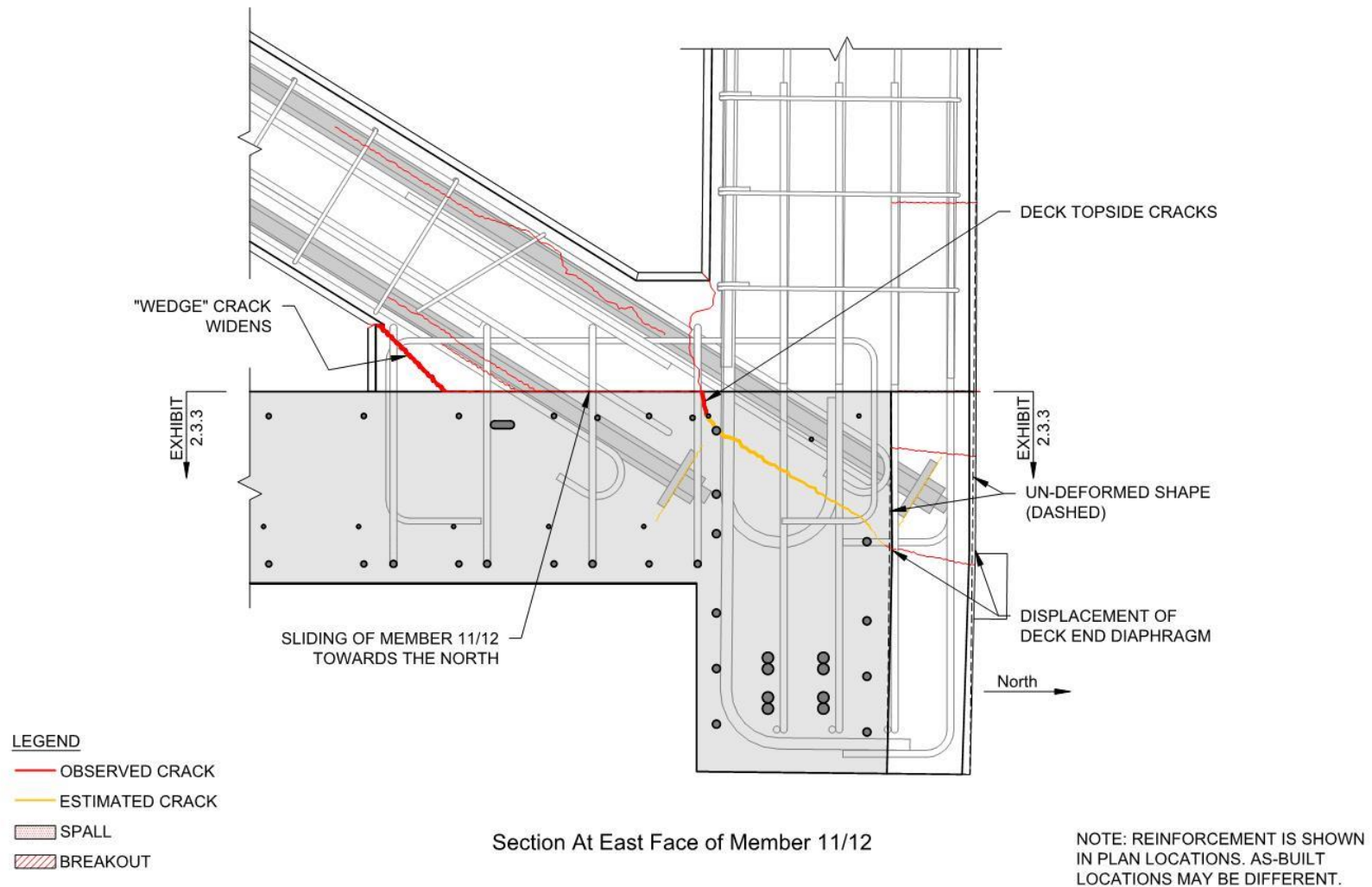


Exhibit 2.3.3
OBSERVED AND ESTIMATED CRACKS AT MEMBER 11/12 DECK CONNECTION
Two Days After Move (March 12, 2018)

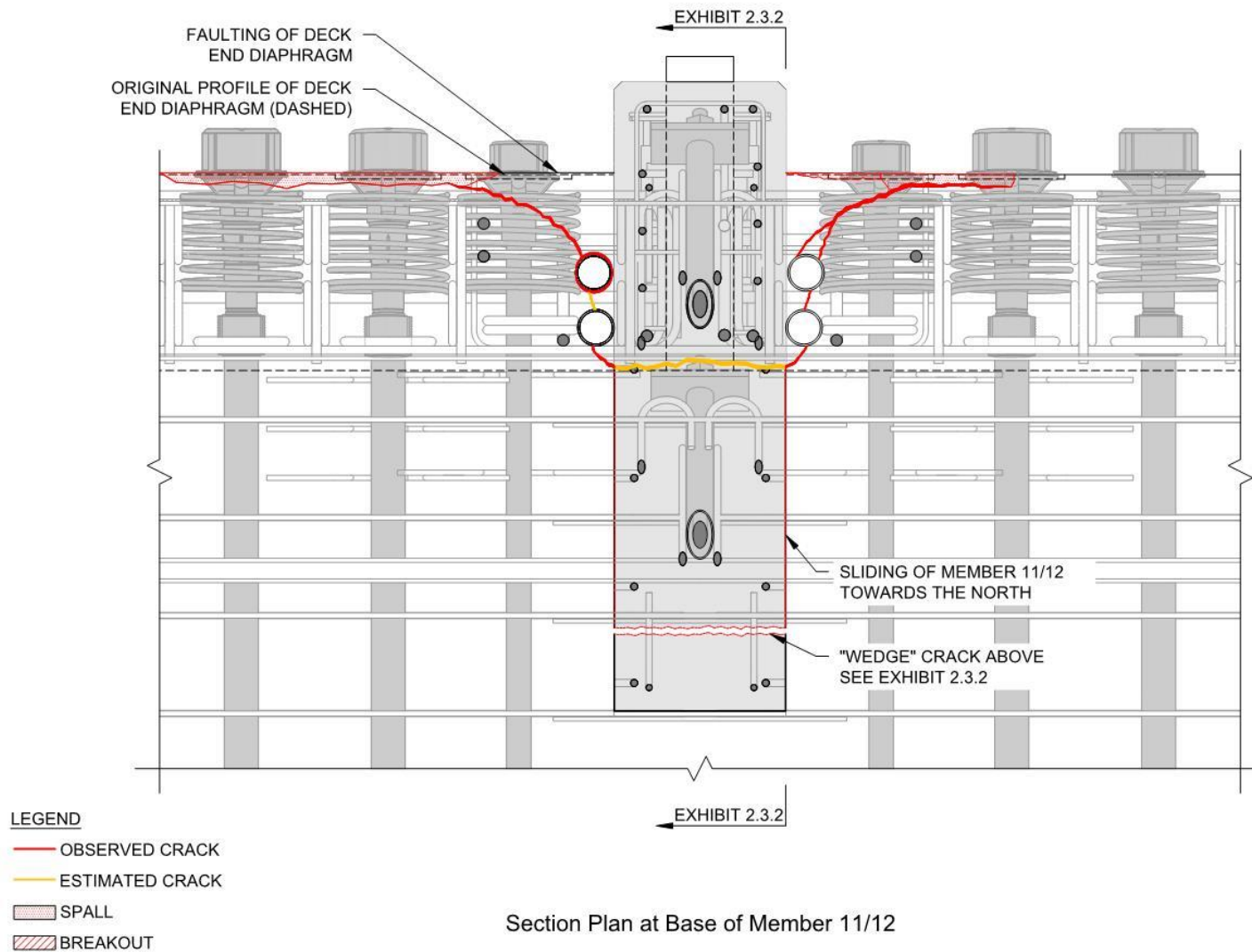
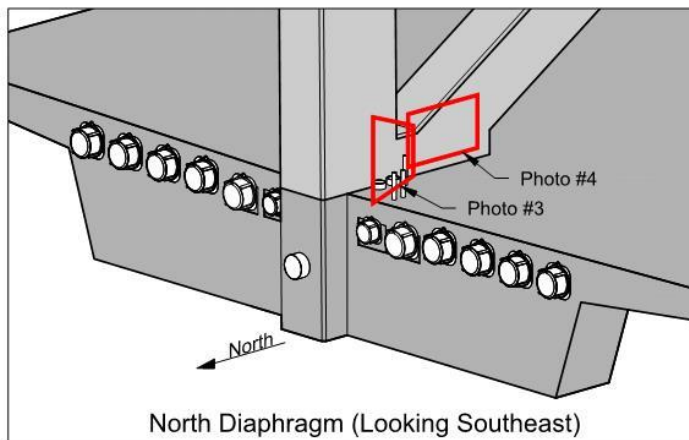
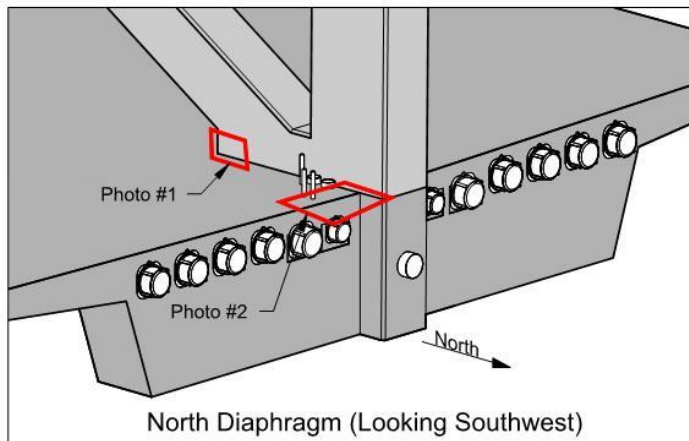


Exhibit 2.4.1

OBSERVED AND ESTIMATED CRACKS AT MEMBER 11/12 DECK CONNECTION

One Day Before Collapse (March 14, 2018)



Photos

1. East side of Member 11. Photo taken on March 14, 2018 by BPA.
2. Topside of deck end diaphragm II and east side of Member 11/12, looking northeast. Photo taken on March 14, 2018 by BPA.
3. Topside of deck end diaphragm II, east of Member 12, looking down. Photo taken on March 14, 2018 by BPA.
4. West side of Member 11. Photo taken on March 14, 2018 by BPA.

Exhibit 2.4.2
OBSERVED AND ESTIMATED CRACKS AT MEMBER 11/12 DECK CONNECTION
One Day Before Collapse (March 14, 2018)

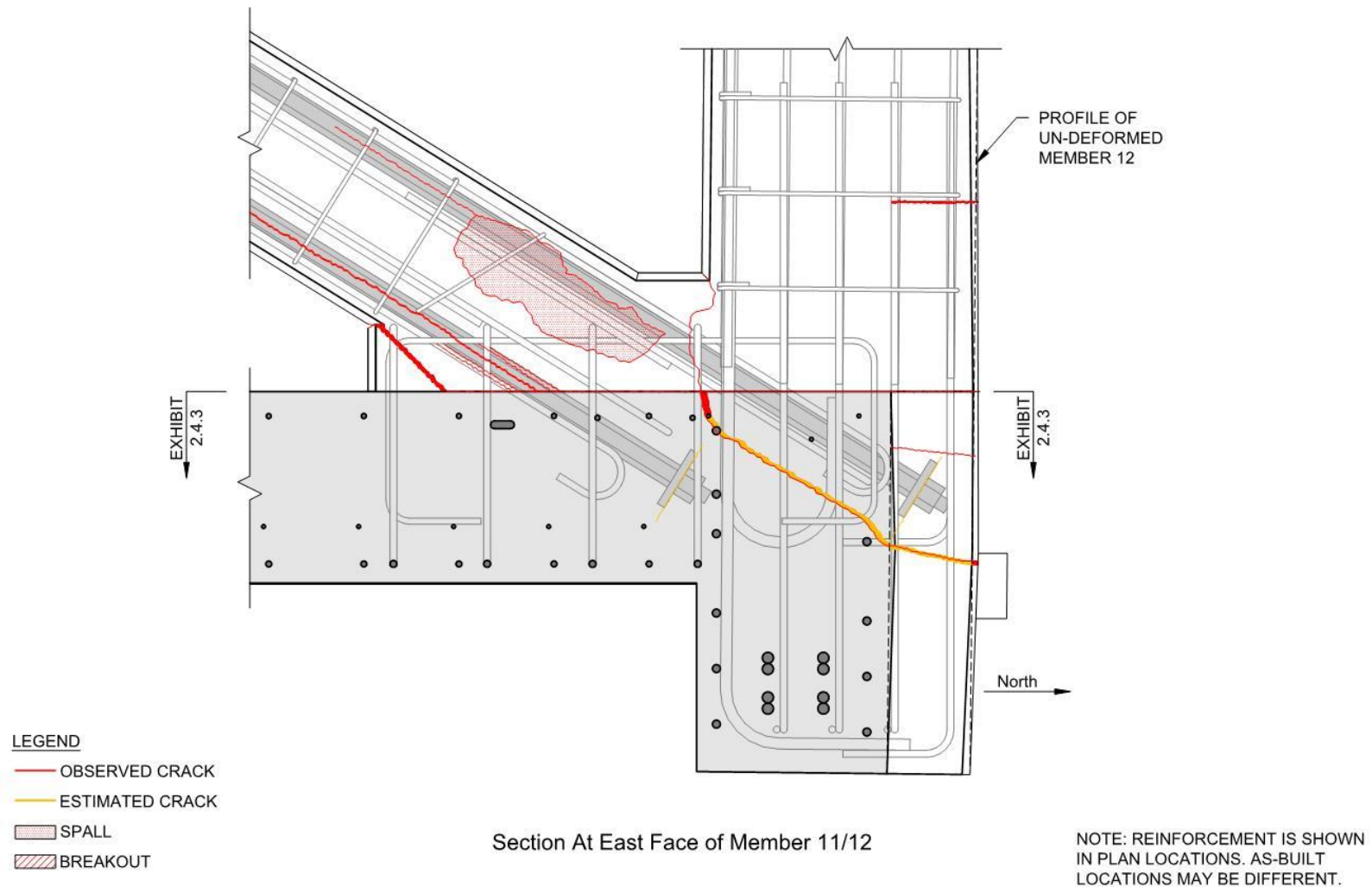


Exhibit 2.4.3
OBSERVED AND ESTIMATED CRACKS AT MEMBER 11/12 DECK CONNECTION
One Day Before Collapse (March 14, 2018)

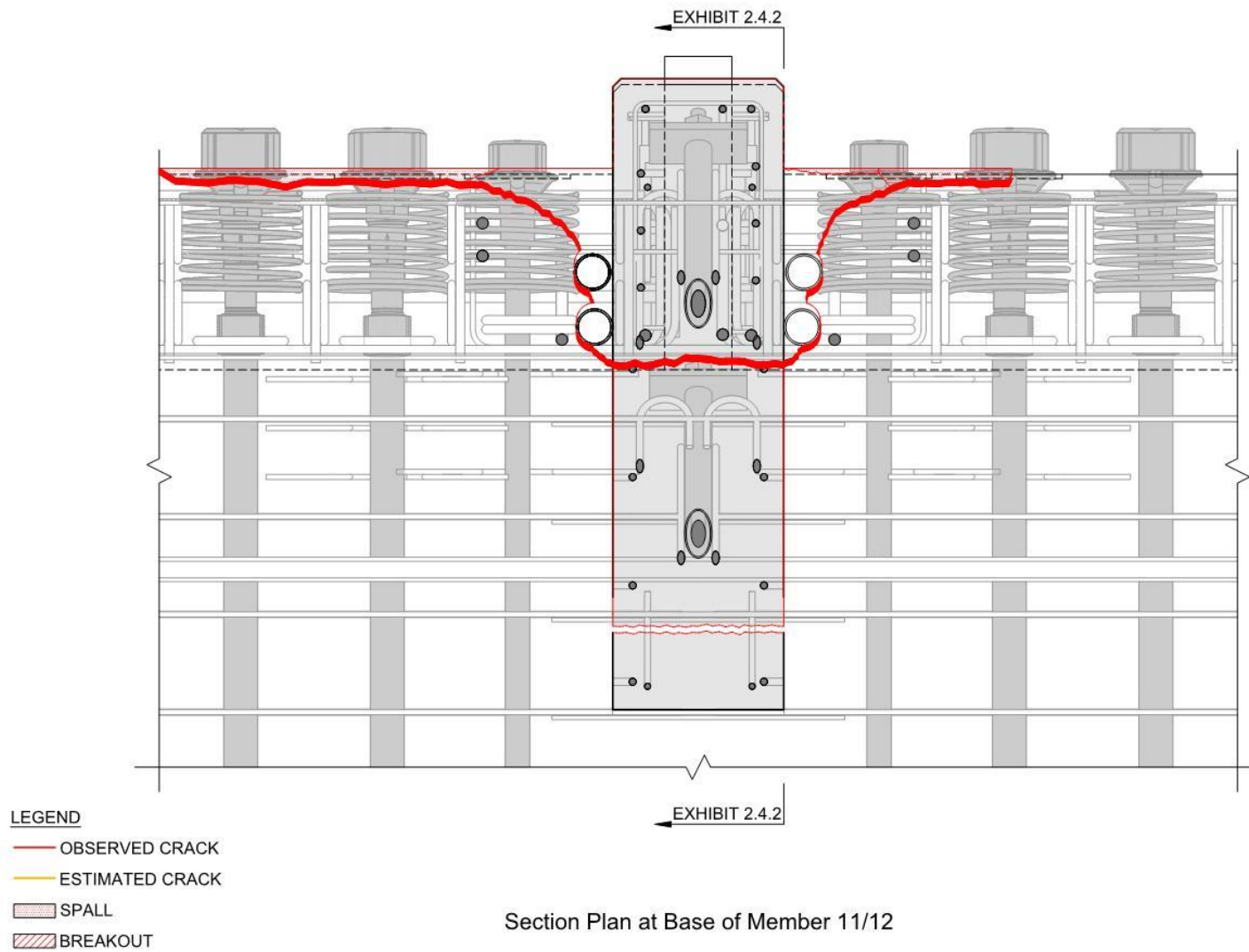
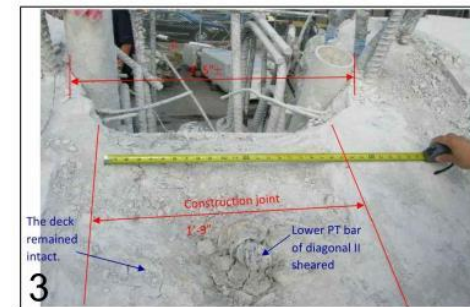
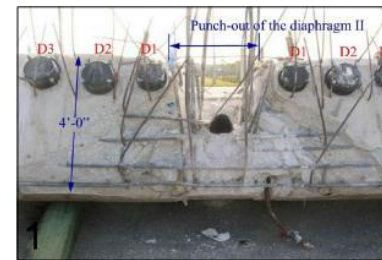
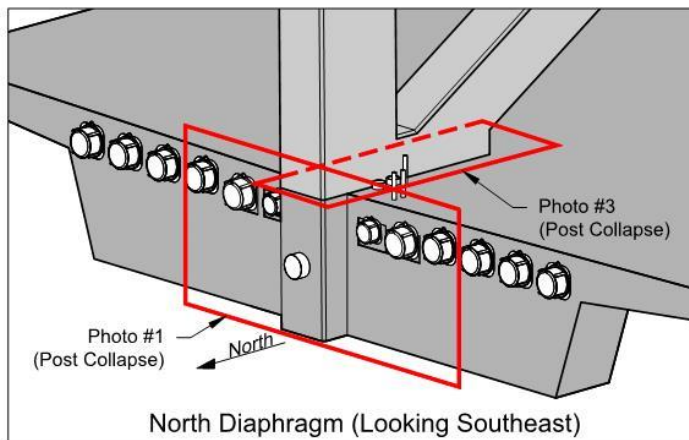
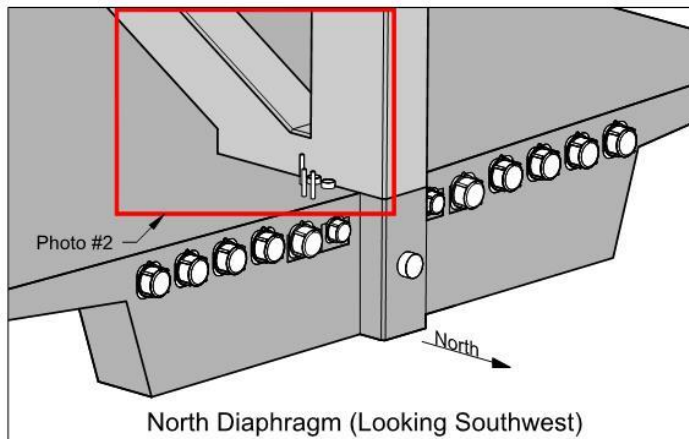


Exhibit 2.5.1

OBSERVED AND ESTIMATED CRACKS AT MEMBER 11/12 DECK CONNECTION After Collapse (March and April, 2018)



Photos

1. North end of deck end diaphragm II, post collapse. OSHA report figure 62, dated April 8, 2018.
2. East side of Member 11&12. Taken by WJE on March 19, 2018.
3. Topside of north deck under Member 11&12, post collapse. OSHA report figure 63, dated April 8, 2018.

Exhibit 2.5.2
OBSERVED AND ESTIMATED CRACKS AT MEMBER 11/12 DECK CONNECTION
After Collapse (March and April, 2018)

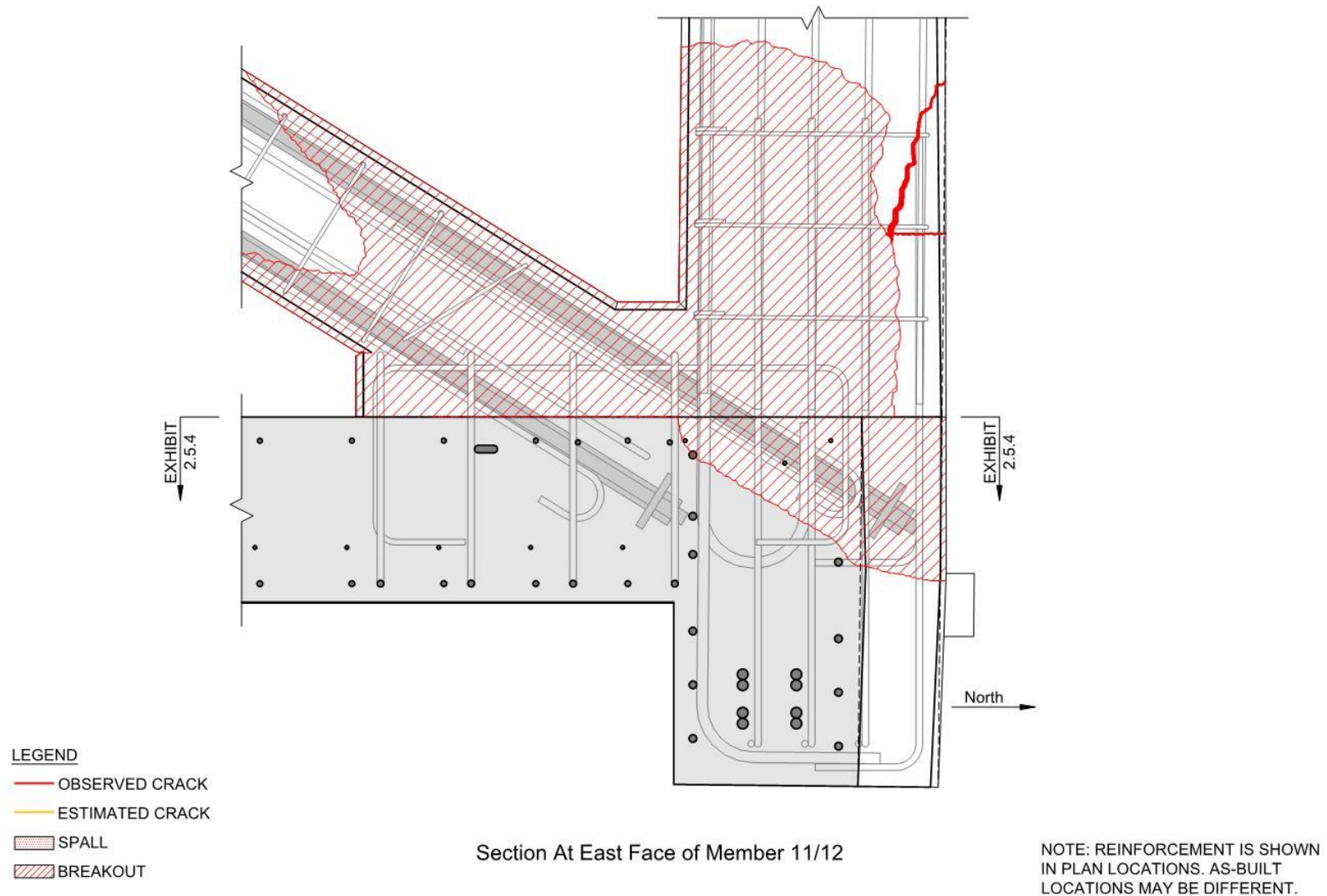


Exhibit 2.5.3
OBSERVED AND ESTIMATED CRACKS AT MEMBER 11/12 DECK CONNECTION
After Collapse (March and April, 2018)

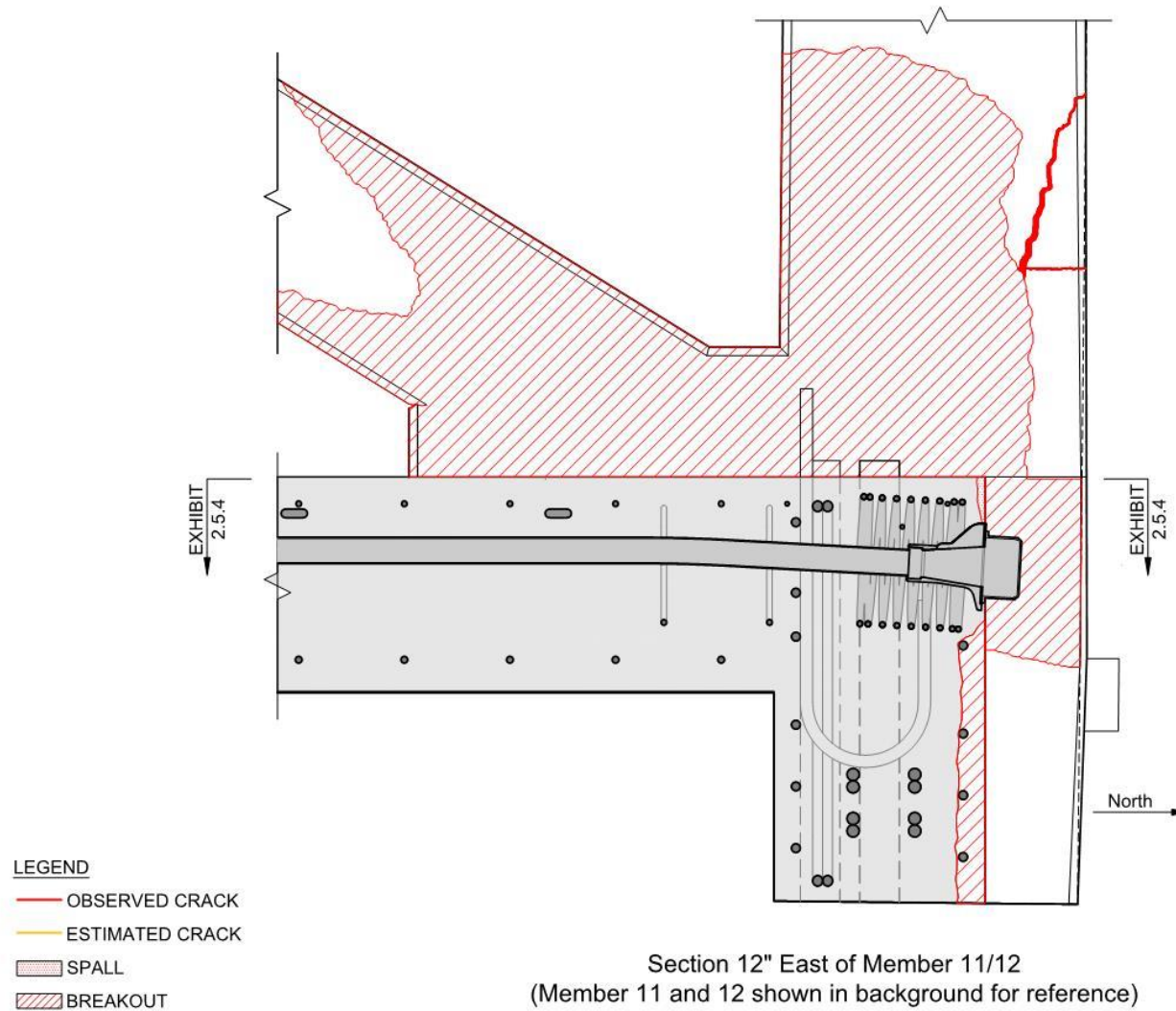
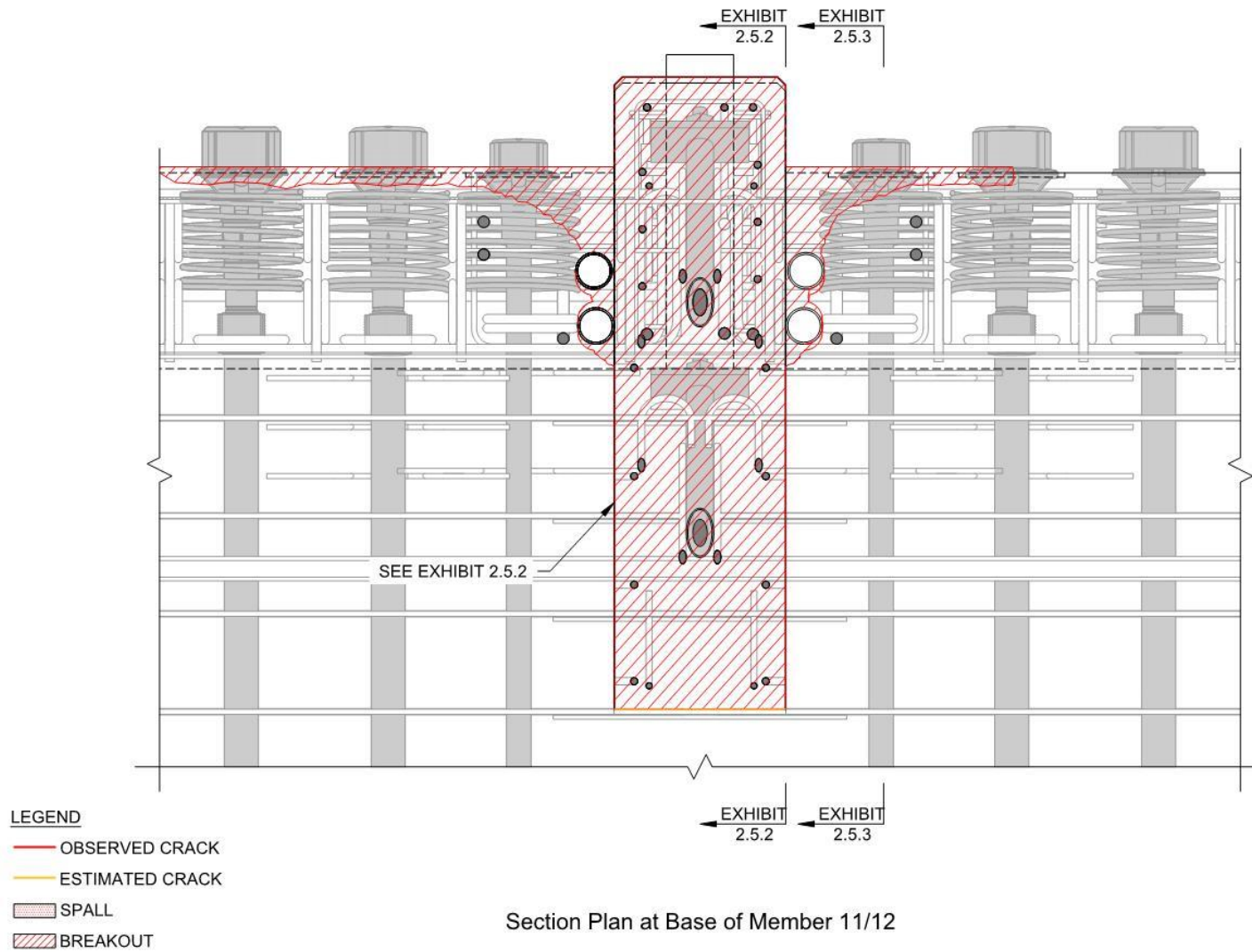


Exhibit 2.5.4
OBSERVED AND ESTIMATED CRACKS AT MEMBER 11/12 DECK CONNECTION
After Collapse (March and April, 2018)



3 EVALUATION OF CONSTRUCTION JOINT CONDITIONS

The objective of this study is to assess the condition of the construction joint between the deck and Members 11 and 12 relative to the project specifications. The assessment of the construction joint condition is primarily based on review of relevant and publicly available documents, including email correspondence, photos, videos, and photos in the OSHA report. The evaluation also includes comparisons to the construction joint condition of WJE's interface shear transfer test specimens, which are described in Section 4.

3.1 Document Review

Observations from review of key documents pertaining to the construction joint are provided in the following sections.

3.1.1 Construction Documents

The released-for-construction structural drawings comprise three subsets of drawings labeled *Foundation Plans*, *Substructure Plans*, and *Superstructure Plans*. Sheet No. 1 of the contract drawings cites FDOT standards as governance for the bridge. An extract from the cover page citing the FDOT specifications is shown in Figure 3.1.

GOVERNING STANDARDS AND SPECIFICATIONS: FLORIDA
DEPARTMENT OF TRANSPORTATION, DESIGN STANDARDS
DATED 2015, AND STANDARD SPECIFICATIONS FOR ROAD
AND BRIDGE CONSTRUCTION DATED 2015, AS AMENDED
BY CONTRACT DOCUMENTS.

APPLICABLE DESIGN STANDARDS MODIFICATIONS: 01-01-15

Figure 3.1. Text from Sheet No. 1

The general notes for the project, provided on Sheet B-2 (which was issued with the Foundation Plans subset), indicate additional specifications. The "CONSTRUCTION SPECIFICATIONS" in the general notes specify FDOT Standard Specifications. An excerpt from the general notes citing the FDOT specifications is shown in Figure 3.2. The FDOT specifications are considered to govern.

CONSTRUCTION SPECIFICATIONS:

1. FLORIDA DEPARTMENT OF TRANSPORTATION STANDARD SPECIFICATIONS
FOR ROAD AND BRIDGE CONSTRUCTION 2015.

Figure 3.2. Text from Sheet B-2

FDOT requirements for construction joints are addressed in Article 400-9 of the FDOT Standard Specifications. Preparations of surfaces is covered in Article 400-9.3:

400-9.3 Preparations of Surfaces: Before depositing new concrete on or against concrete which has hardened, re-tighten the forms. Roughen the surface of the hardened concrete in a manner that will not leave loosened particles, aggregate, or damaged concrete at the surface. Thoroughly clean the surface of foreign matter and laitance, and saturate it with water.

3.1.2 Pre-Construction Email Correspondence

WJE reviewed available emails produced before and during construction. Several emails between MCM, BPA, and FIGG discuss construction joint preparation. One email, sent on June 12, 2017, by Alan Ruiz (MCM) to entities of MCM, BPA, and FIGG, confirms that he spoke with FIGG regarding construction joint treatment, as shown in Figure 3.3.

From: Alan Ruiz, P.E. [REDACTED]
Sent: Monday, June 12, 2017 10:15 AM
To: Rafael Urdaneta [REDACTED]; Jose Morales [REDACTED]; Carlos Chapman [REDACTED]; Pedro Cortes [REDACTED]; Pedro Gomez, P.E. [REDACTED]; Ernie Hernandez [REDACTED]; Dwight Dempsey [REDACTED]
Cc: FIU-Field-Office [REDACTED]; Rodrigo Isaza (MCM) [REDACTED]
Subject: RE: Concrete Pour

Rafael,

FCA 19-1

I spoke with FIGG and they advised us to follow FDOT Specs which is as follows:

400-9.3 Preparations of Surfaces: Before depositing new concrete on or against concrete which has hardened, re-tighten the forms. Roughen the surface of the hardened concrete in a manner that will not leave loosened particles, aggregate, or damaged concrete at the surface. Thoroughly clean the surface of foreign matter and laitance, and saturate it with water.

The plan notes do not mention the use of a bonding agent so it is not required.

Thanks,

Figure 3.3. June 12th, 2017 email regarding surface preparation from MCM's project engineer to members of the construction and design teams

3.1.3 Concrete Placement Video

An initial attempt to place the concrete deck was made on September 1, 2017. The placement was aborted when it was learned that concrete could not be continuously supplied due to a problem at the ready-mix plant. Nevertheless, the video from this first placement attempt shows the placement methods, consistency of the concrete, and surface texture. Figure 3.4 is a screenshot from one of the videos showing concrete placement and internal vibration. At the time the video was taken, the concrete level had not yet reached the top reinforcing bar mat. Note that the surface texture is relatively smooth, especially in the vicinity of the vibrator, although the coarse aggregate occasionally protrudes above the surface. The surface texture appears comparable to the as-placed (non-roughened) surface texture of the WJE interface shear transfer Specimen 3 (Figure 3.4).



Figure 3.4. Screenshot of video of first deck concrete placement attempt.

3.1.4 OSHA Report

In their June 2019 report on the collapse, which was publicly released, OSHA included an annotated photograph of a portion of the construction joint below Member 11. This photograph is shown below in Figure 3.5. The area around and to the north of the lower PT bar was damaged due to the collapse. Elsewhere, within the limits of the construction joint shown, the deck remained intact and appears to be smooth, especially on the right hand (east) side of the joint where the deck has been cleared of debris.

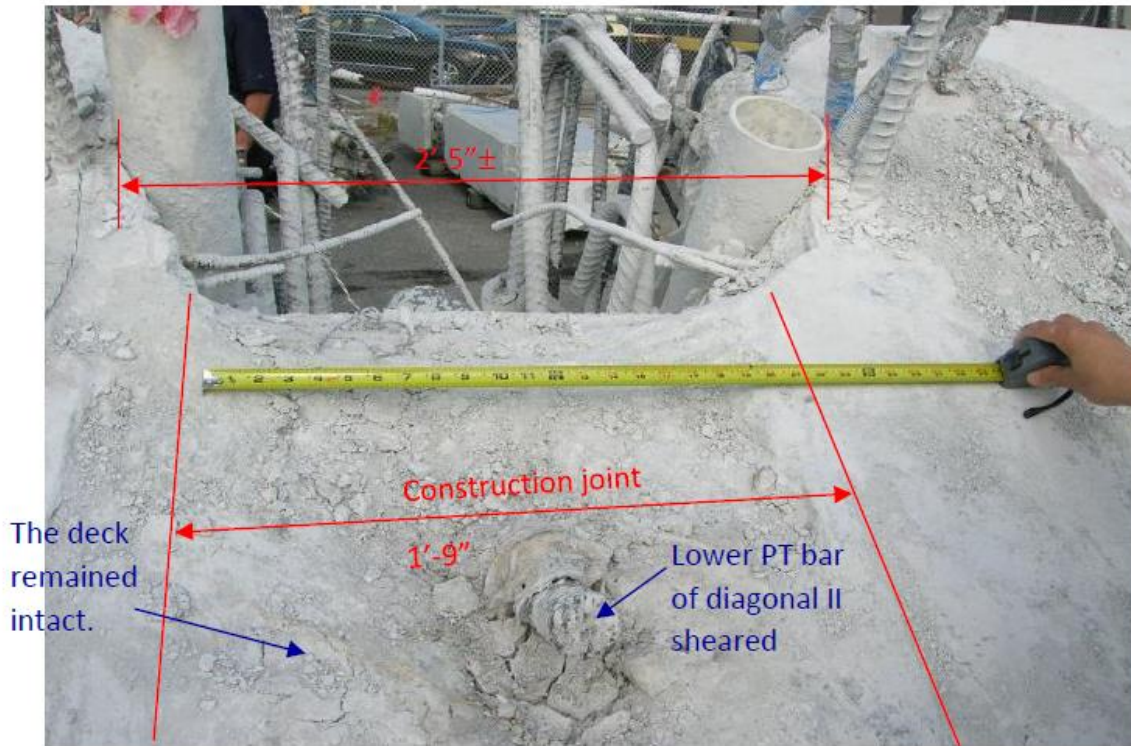


Figure 3.5. Construction joint below Member 11. (North is upward in the photograph.)

3.1.5 WJE Interface Shear Transfer Specimens

WJE conducted compression testing of column-like specimens with inclined construction joints to evaluate interface shear transfer at construction joints in the main span. The tests are described in Section 4. The mix design and slump of the specimen concrete was designed to match the concrete in the deck and diagonal members. Laser scan measurements of an as-placed (non-roughened) and roughened construction joint were made.

Figure 3.6 shows a photograph of the as-placed (non-roughened) surface of the Specimen 3 construction joint, and a laser scan of the same surface. The as-placed surface was created by internally vibrating the concrete during placement without further treatment. Note that the surface texture is similar to that shown in Figure 3.4, which is a screenshot of the first deck placement attempt.



Figure 3.6. Photograph and laser scan of Specimen 3 (as-placed). (Note: the mortar adhering to the reinforcing bars in the left photo was removed before scanning and placement of the upper lift.)

Table 3.1 provides the surface roughness parameters for Specimen 3.

Table 3.1. Surface Roughness Parameters (mm)

Parameter	Specimen 3 (as-placed)
Maximum Positive Deviation	5.29
Maximum Negative Deviation	-4.48
Average Positive Deviation	0.82
Average Negative Deviation	-0.64
Standard Deviation	0.94
RMS Estimate	0.94
Segment Length	775
Segment Width	320

3.2 Discussion

3.2.1 Project Records

Construction drawings by FIGG cite FDOT as the governing construction specifications. As indicated by the email correspondence, the FDOT specifications were considered to govern. The FDOT specifications include the following explicit instructions on the preparation of construction joints: “Roughen the surface of the hardened concrete in a manner that will not leave loosened particles, aggregate, or damaged concrete at the surface.” Furthermore, these specifications were re-iterated by MCM in an email to members of the design and construction team before the concrete for the main span of the superstructure was cast.

About half of the state DOT standard specifications require roughening of the hardened concrete at construction joints by mechanical means. Roughening the hardened concrete is preferable to creating a rough surface texture during finishing because roughening the hardened concrete also removes the surface laitance, which improves bond.

3.2.2 Photographs and Laser Scans

Comparison of the OSHA photograph to the WJE test specimens indicates that the construction joint below Members 11 and 12 was most likely left as-placed (non-roughened) after internal vibration; that is, the condition shown in the video of the first deck placement attempt (Figure 3.4). This observation is contrary to the project specifications, which were reconfirmed before the deck concrete was placed.

3.3 Findings

The following findings as to the construction joint below Members 11 and 12 are based on the reviews described above:

- Construction documents cite FDOT specifications. The FDOT specifications governed and required the contractor to “roughen the surface of the hardened concrete in a manner that will not leave loosened particles, aggregate, or damaged concrete at the surface.”
- In response to a question by MCM before the placement of the deck, FIGG confirmed that the FDOT construction joint requirements were to be followed. MCM reiterated these instructions by email correspondence to BPA and the MCM construction team, which included the relevant excerpt from the FDOT specifications.
- Photographic evidence indicates the construction joint below Members 11 and 12 was not intentionally roughened and appeared to be in an as-placed, relatively smooth condition.

In summary, despite FIGG’s confirmation to MCM that the FDOT specifications requiring roughening of the *hardened* concrete must be followed, the construction joint surface below Members 11 and 12 appeared to have been left in an as-placed, relatively smooth condition.

4 INTERFACE SHEAR TRANSFER TESTING

WJE has carried out independent testing to evaluate interface shear transfer at construction joints in the main span of the FIU UniversityCity Prosperity Pedestrian Bridge. The objective of the testing program was to assess the effect of surface condition on interface shear transfer at construction joints between the northernmost diagonal and deck.

4.1 Experimental Program

4.1.1 Introduction and Specimen Description

The experimental program features slant shear tests of column-like specimens with a diagonal construction joint. The specimens were designed to reasonably replicate shear transfer between Member 11 and the deck. Two construction joint interface conditions were tested: as-placed (non-roughened) and roughened.

In total, six specimens were fabricated and tested: three with an as-placed construction joint and three with a roughened construction joint in accordance with FDOT Standard Specifications. Additional details on the reinforcement, concrete mix design, placement methods, and construction joint treatment are provided in subsequent sections of this report.

4.1.2 Specimen Reinforcement

Figure 4.1 is an isometric view of a typical specimen showing the internal reinforcement. The detail of the connection of Members 11 and 12 to the deck taken from Sheet B-61 of the FIGG superstructure drawings is provided in Figure 4.2. The cross-sectional dimensions and longitudinal reinforcing bars in the test specimens are identical to those of Member 11, although the section does not include post-tensioning bars or ducts. The #4 ties above and below the construction joint are similar to the ties in Member 11. Three #7 stirrups are provided across the construction joint to replicate the effect of the three northernmost shear-friction reinforcement stirrups (identified as 7S01 bars in Figure 4.2). The southernmost #7 stirrup is not included because it did not contribute to shear-friction resistance. As explained in a Section 2, the concrete “wedge” between the deck and Member 11 remained attached to the deck when Member 11 slid to the north. Also, consistent with the design plans, #6 and #7 bars are provided across the top and bottom legs of the #7 stirrups, respectively.

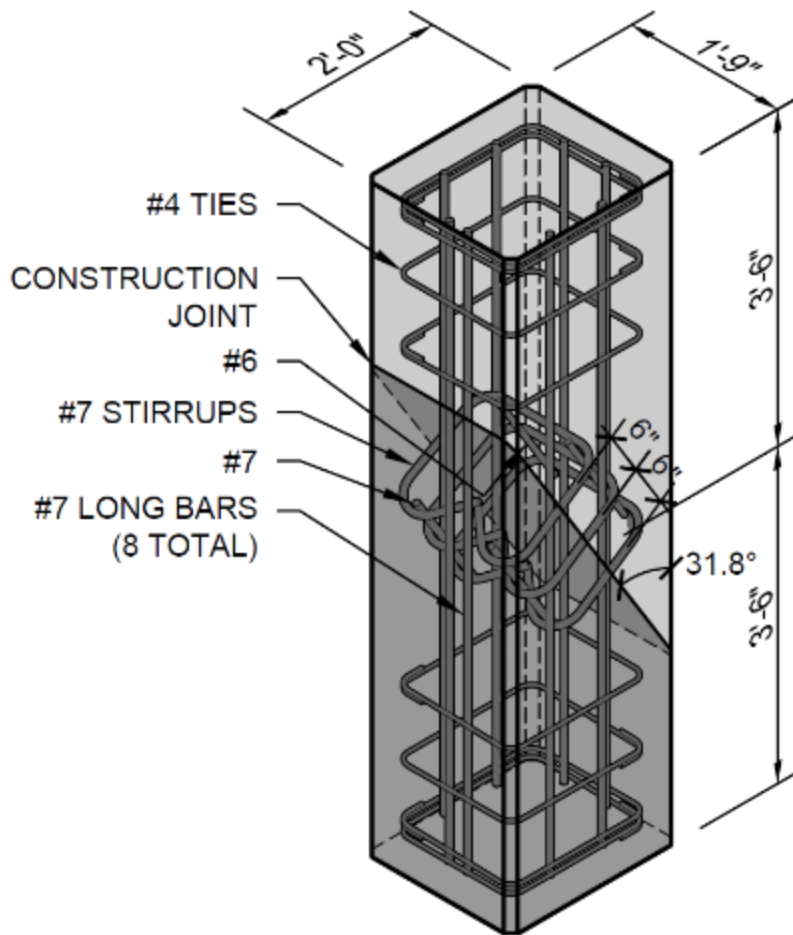


Figure 4.1. Isometric view of specimens

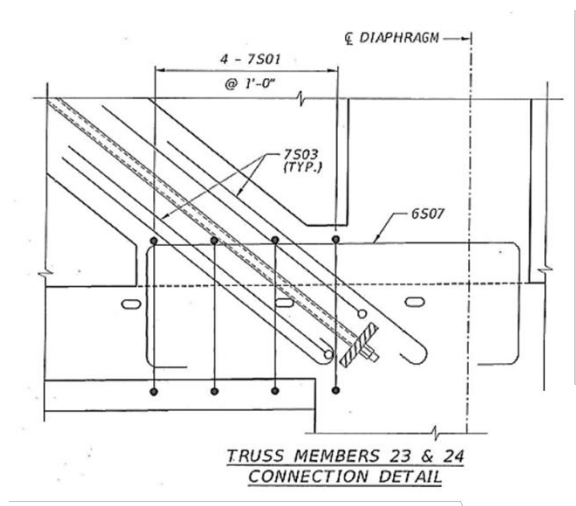


Figure 4.2. Detail of connection between deck and Members 11 & 12 from FIGG drawings

4.1.3 Concrete Mixture Proportions

For the fabrication of laboratory test specimens, WJE developed a mix to closely match the original mixture proportions (Class VI 8,500 psi) using materials available in the Chicago area¹. The original Class VI 8,500 psi mix had a target slump of 7 to 9 inches, an air content of 0 to 6.0 percent, and a 28-day design compressive strength of 8,500 psi. WJE developed a mix to closely match these properties, which is provided in Table 4.1. The following describes the developed mix as it relates to the original:

- The water to cementitious ratio was kept at 0.33.
- The total cementitious materials (cement, slag cement, fly ash, and metakaolin) was kept at 800 pounds per cubic yard (lb./yd³)
- The portland cement to slag cement ratio was increased in order to facilitate early strength development. The original mix had a portland cement to slag cement ratio of 0.76, and the mix developed had a ratio of 2.45.
- A different source of portland cement was used but of the same type (Type I). Gray portland cement was used and not white.
- A different source of fly ash was used but at the same dosage rate.
- A different source of slag cement was used but the same grade.
- A different source of metakaolin was used but at the same dosage rate.
- The same source of Titanium dioxide² was used at the same dosage rate.
- Chicago area coarse and fine aggregates were used in lieu of original Florida coarse (Cemex - Krome) and fine (CEMEX Krome and Palmdale) aggregates. Like the Krome coarse aggregates, the Chicago aggregates were crushed limestone.
- The combined aggregate gradations were designed to closely match the original.
- A high range water reducer (HRWR - Sika ViscoCrete 2100) and hydration stabilizer (SikaTard 440) were used to establish the target slump and setting properties of the original mix. The original mix used W.R. Grace chemical admixtures as opposed to the Sika products.

Table 4.1. Concrete Mixture Proportions

Constituent	Source	Quantity (lb./yd ³)
Cement	Type I-II, St. Mary's - Charlevoix	500
Slag Cement	Grade 100, Skyway Cement - Chicago	204
Fly Ash	Class C, LaFarge - Elm Road Unit 2	80
Metakolin	Burgess Optipozz	16
Titanium Dioxide	Ti-Pure R-103	5
Fine Aggregate	Hanson Materials - Romeoville	1400
3/4 Coarse Aggregate	Hanson Materials - Romeoville	1310
1/2" Coarse Aggregate	Hanson Materials - Thornton	303
Water		264
High Range Water Reducer (HRWR)	Sika ViscoCrete 2100	As Needed
Hydration Stabilizer	SikaTard 440	As Needed
W/cm		0.33
Target Slump		8-in.
Target Air Content		0 to 6 %

¹ Concrete mixes using locally available materials are routinely used in research and testing to replicate concrete mixes from other locales.

² Titanium dioxide was used in the original mix design for aesthetic purposes

A trial batch of this mix was performed on July 2, 2019, with ready mix concrete supplied by Prairie Material (Votorantim Cimentos). The metakaolin and titanium dioxide were added by WJE once the concrete was delivered to the laboratory. The concrete slump and air content of this trial batch were measured to be 9.0 inches and 1.8 percent, respectively. Both are consistent with the original mix. Compressive strength cylinders were fabricated and tested (ASTM C39) at 1, 3, 6, 7, 14, 17, and 28 days, and the results are presented in Table 4.2 and plotted in Figure 4.3. The measured 28-day compressive strength of 9,270 psi exceeded the design compressive strength of 8,500 psi and is consistent with measured 28-day strengths for the project. A Universal Engineering Sciences concrete testing report provided in the OSHA Report indicate 28-day strengths ranging from 8890 to 9380 psi.

Table 4.2. Compressive Strength Results*

Test Age (days)	July 2 - Trial Batch (psi)
1	2,850
3	4,770
6	6,710
7	7,300
14	8,780
17	8,850
28	9,270

*Each entry represents an average of two compressive strength cylinders (6 x 12-in.)

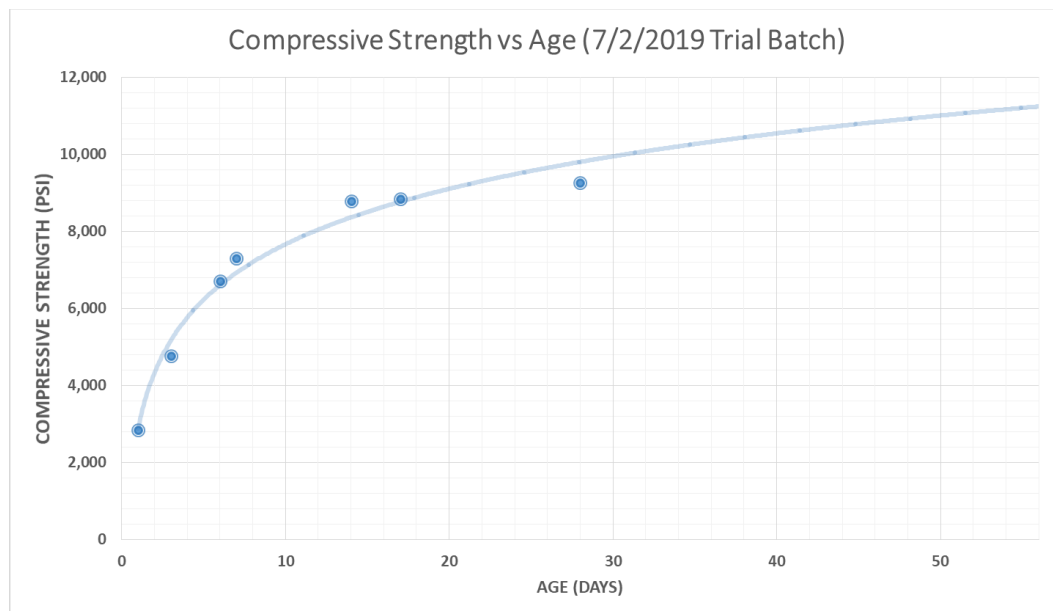


Figure 4.3. Concrete strength development of trial batched concrete, 7/2/2019

4.1.4 Concrete Placement

As illustrated in Figure 4.1, the specimens were cast in two lifts with a sloped construction joint at mid-height. The angle of the construction joint relative to the longitudinal axis of the specimens, 31.8 degrees, matched the angle between Member 11 and the concrete deck.

The lower lift was placed on July 9, 2019, and the upper lift was placed on July 16, 2019, using the mixture proportions in Table 4.1 supplied by ready mix concrete from Prairie Material (Votorantim Cimentos). Similar to the trial batch, the met kaolin and titanium dioxide were added by WJE once the concrete was delivered to the laboratory. Concrete slump, air content, unit weight, and temperature were measured on each of these placements and are summarized in Table 4.3. The concrete slump and air content of the two placements were both consistent with the original mix design. Compressive strength cylinders (6 x 12-in.) were fabricated from each placement and cured under standard conditions (ASTM C31) and match cured (cured alongside the replicate construction joint specimens). In addition to the 1, 7, and 14-day compressive strength testing (ASTM C39), strength testing was performed during the first replicate construction joint test and after completion of all joint tests. The testing of the replicated construction joints were started when the lower and upper lift were at an age of 27 and 20 days, respectively, with the completion of the testing at 28 and 21 days, respectively. The compressive strength results are presented in Table 4.4 and plotted in Figure 4.4 and Figure 4.5.

Table 4.3. Plastic Concrete Properties

Concrete Property	Lower Lift	Upper Lift
Slump (in.) - ASTM C143	8.5	8.5
Air Content (%) - ASTM C231	2.2	1.7
Unit Weight (lb./ft ³) - ASTM C138	148.0	149.4
Temperature (F) - ASTM C1064	87.0	84.0

Table 4.4. Compressive Strength Results (psi)*

Test Age (days)	Lower Lift		Upper Lift	
	Standard Cure ³	Match Cure ⁴	Standard Cure ³	Match Cure ⁴
1		2,860		2,760
7	7,080	7,090	6,640	6,860
14		8,020		8,260
During First Joint Test	9,410	8,680	8,930	8,360
After Testing	9,550	8,870	8,990	8,500

*Each entry represents the average compressive strength of two cylinders

³ Standard-cured cylinders are cured at specified temperature and humidity conditions in accordance with ASTM C511

⁴ Match-cured cylinders are cured in the same environment as the structure or specimen

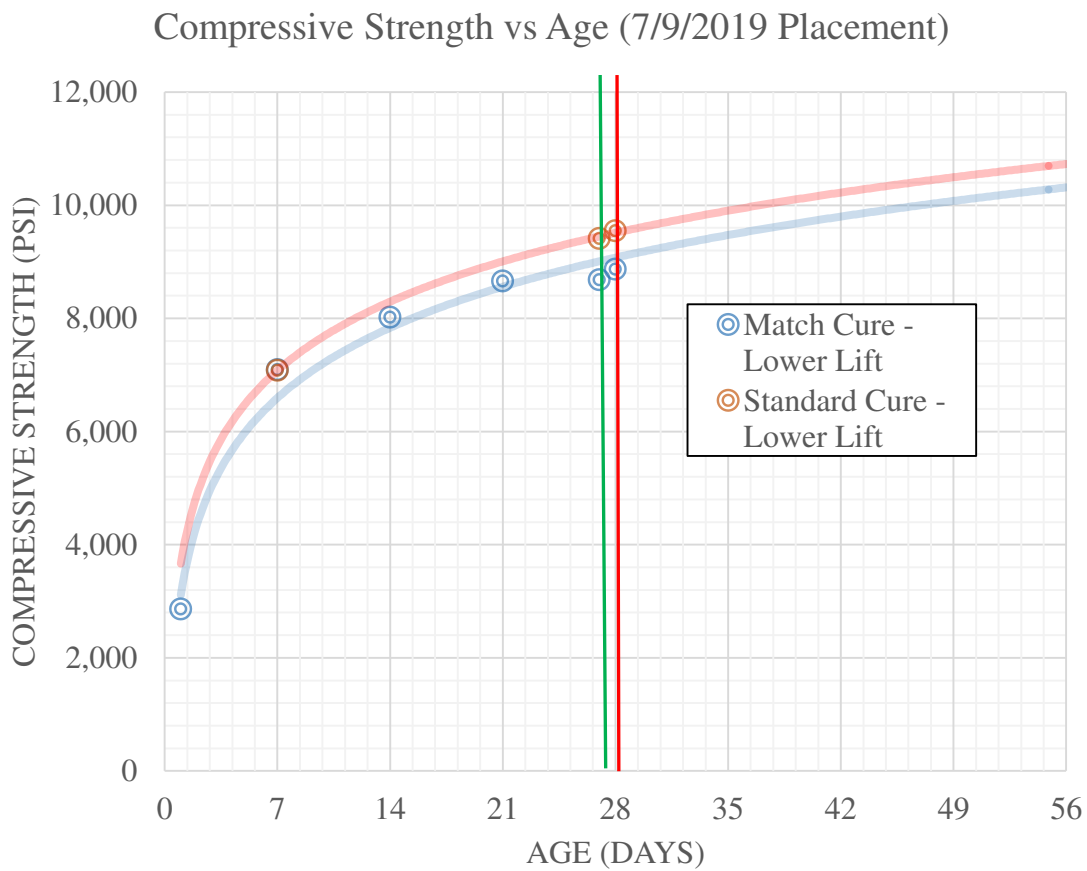


Figure 4.4. Strength development of lower lift fabricated on 7/9/2019. The vertical green and red lines represent the start and completion dates of the replicate construction joint tests, respectively.

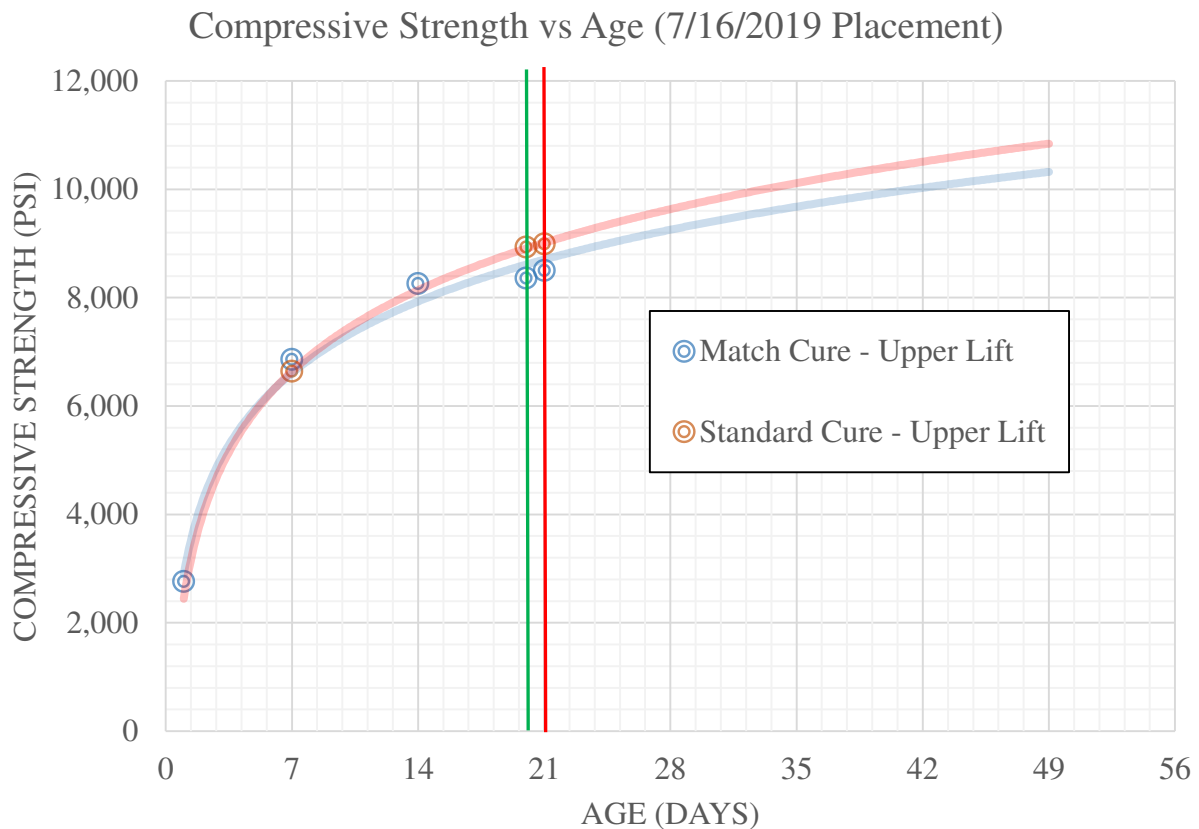


Figure 4.5. Strength development of upper lift fabricated on 7/16/2019. The vertical green and red lines represent the start and completion dates of the replicate construction joint tests, respectively.

4.1.5 Construction Joint Interface

To create the *as-placed* (non-roughened) condition, the concrete was placed using internal vibration without further treatment of the construction joint surface. Based on WJE’s review of the construction records and available photographs and videos, it appears the deck concrete below Members 11 and 12 was vibrated and left as-placed.

For the *roughened* condition, the hardened concrete was roughened one day after placement using an electric chipping hammer with amoil bit (a rectangular bit tapered to a sharp point). The roughening operation is shown in Figure 4.6.

This roughening method was considered the most practical means to meet the requirements of the FDOT Standard Specifications⁵. Article 400-9.3 on preparation of construction joint surfaces requires: “roughen the surface of the hardened concrete in a manner that will not leave loosened particles, aggregate, or damage concrete at the surface.” Note that this requirement does not permit roughening the concrete before

⁵ Florida Department of Transportation, *Standard Specifications for Road and Bridge Construction*, 2015.

hardening, while it is still in a plastic state. Removing the hardened concrete removes the surface laitance, which is also required by FDOT Standard Specifications. Use of a chipping hammer with amoil point was selected because this equipment is readily available and commonly used at construction sites. Also, themoil point can work around most interferences from reinforcement.



Figure 4.6. Roughening operation using an electric chipping hammer with amoil point (trial slab shown)

To determine the surface roughness, the surface of one as-placed (non-roughened) and one roughened construction joint surface was measured using a laser scanner. The laser scans were conducted by WJE's scanning consultant, Khan Consultants. The Khan report is provided in Exhibit 4.1.

Figure 4.7 compares a photograph of the Specimen 3 construction joint surface (as-placed) to a laser scan of the same surface. Figure 4.8 provides a similar comparison for Specimen 4 (roughened).



Figure 4.7. Photograph and laser scan of Specimen 3 (as-placed). (Note: the mortar adhering to the reinforcing bars in the left photo was removed before scanning and placement of the upper lift.)



Figure 4.8. Photograph and laser scan of Specimen 4 (roughened in accordance with FDOT Standard Specifications). (Note: the mortar adhering to the reinforcing bars in the left photo was removed before scanning and placement of the upper lift.)

Table 4.5 compares the surface roughness parameters for the as-placed (non-roughened) and roughened test specimens. Using the standard deviation for comparison purposes, Specimen 4 (roughened) is more than twice as rough as Specimen 3 (as-placed). Comparison using the sum of average positive and negative deviations indicates that the roughened surface is about 2.2 times as rough as the as-placed surface.

Table 4.5. Surface Roughness Parameters (mm)

Parameter	Specimen 3 (as-placed)	Specimen 4 (roughened)	<u>Specimen 4</u> <u>Specimen 3</u>
Maximum Positive Deviation	5.29	6.72	1.27
Maximum Negative Deviation	-4.48	-10.03	2.24
Average Positive Deviation	0.82	1.31	1.60
Average Negative Deviation	-0.64	-1.91	2.98
Standard Deviation	0.94	2.03	2.16
RMS Estimate	0.94	2.04	2.17
Segment Length	775	778	1.00
Segment Width	320	321	1.00

To simulate the condition of the construction joint between Member 11 and the deck prior to moving the main span, two as-placed specimens (Specimens 1 and 2) and two roughened specimens (Specimens 4 and 5) were intentionally cracked at the construction joint. Unbonded and initially cracked specimens are primarily used in shear-friction research because a crack at the interface between concrete cast at different times should be assumed.

The construction joints at the remaining two specimens (Specimens 3 and 6) remained bonded. However, after Specimen 6 (roughened) sustained the maximum test load of 3 million pounds, the interface was then cracked, and the specimen was re-tested.

Stone-splitting wedge sets in drilled holes were used to create the cracks at the construction joint. Figure 4.9 is a photograph of the cracking operation at Specimen 6. Machined measurement points and a digital caliper were used to detect and monitor the width of the crack at the surface. The wedge sets were driven until the surface crack width was approximately 0.012 to 0.014 inches. In WJE's laboratory, an ultrasonic pulse velocity meter was used to verify that this surface crack width was sufficient for propagation of the crack across the width of the specimen. The wedge sets were removed after cracking.



Figure 4.9. Stone-splitting wedge sets being used to create a crack across the construction joint of Specimen 6

4.1.6 Test Set-up and Instrumentation

Testing of specimens was performed at the University of Illinois at Urbana-Champaign in the Talbot Laboratory using the Southwark-Emery universal test machine. The test machine uses manually controlled hydraulics and has a load capacity of 3,000,000 lbs. (Figure 4.10).



Figure 4.10. University of Illinois Southwark-Emery test machine

Linear variable displacement transducers (LVDT) were attached on either side of each test specimen and positioned to measure sliding and separation of the interface shear joint (Figure 4.11) during testing. The transducers have a maximum displacement range of 0.5-in.

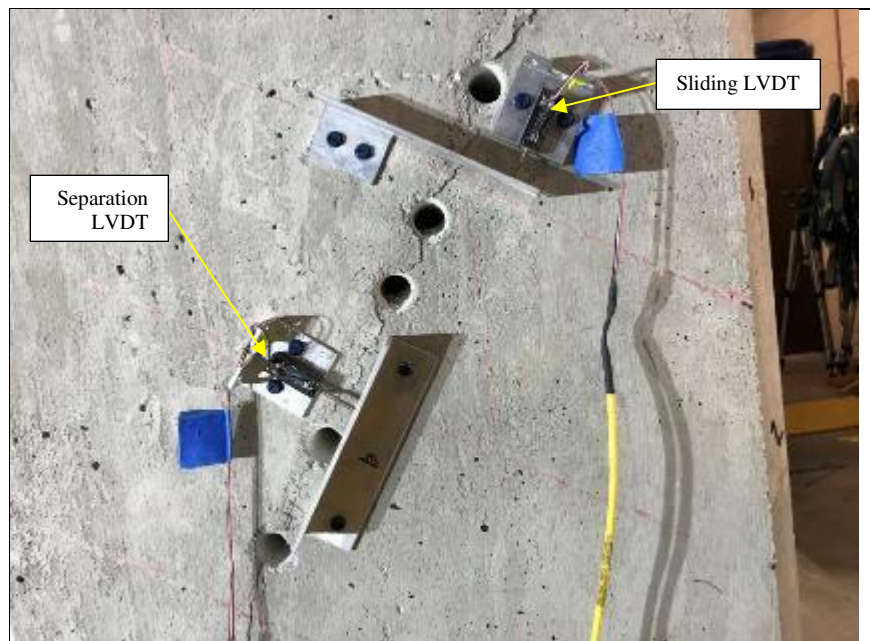


Figure 4.11. Linear displacement transducers across interface shear joint

Load and displacement data were continuously collected using a computer controlled data acquisition system to capture load and corresponding sliding and separation values.

4.1.7 Loading Protocol

A loading protocol was developed to simulate the axial force in Member 11 from shoring removal in the casting yard through re-stressing. The loading protocol is presented in Table 4.6⁶.

Table 4.6. Loading Protocol

Stage	Field Condition	Loading	Force (kips)	
			Start	Final
1	Shoring removal in casting yard	Dead + PT	0	1680
2	<i>Lifting by transporter</i>	<i>Dead + PT</i>	<i>1680</i>	<i>0</i>
3	Placement on piers	Dead + PT	0	1680
4	<i>De-stressing Member 11</i>	<i>Dead</i>	<i>1680</i>	<i>1227</i>
5	Re-stressing Member 11	Dead + PT + CLL	1230	1743
6	NA	To 3000 kips or failure	1743	3000 or Failure

Note: *Italic* type indicates unloading stage

⁶ Forces are based on finite element model of main span. See Section 5.1.1.

4.1.8 Interface Shear Transfer Results

The interface shear transfer results are summarized in Table 4.7. Both axial load and shear stress along the construction joint are reported. Sliding and separation at peak load are also reported.

Table 4.7. Summary of Shear Transfer Test Results

Specimen	Construction Joint Condition	Peak Load (kip)	Maximum Shear Force (kip)	Sliding at Peak Load (in.)	Separation at Peak Load (in.)	Failure Mode
1	As-placed cracked	1296*	1101	0.0023	None measured	Shear-friction
2	As-placed cracked	1614	1372	0.0070	None measured	Shear-friction
3	As-placed bonded	2775	2358	0.0024	0.0006	Shear-friction
4	Roughened cracked	2516	2138	0.0120	None measured	Shear-friction
5	Roughened cracked	2551	2168	0.0145	-0.0008	Shear-friction
6	Roughened bonded	3000	2550	0.0025	0.0014	Did not fail; specimen retested
6	Roughened cracked	2714	2307	0.0120	None measured	Shear-friction
Average	Roughened cracked	2594	2204	0.0128		
Average	As-placed cracked	1455	1237	0.0047		

*Because Specimen 1 was not severely damaged in the initial test, the specimen was reloaded after the first failure. The peak load in the retest was 737 kips.

Most failures were similar. Except for Specimen 1, the specimens failed suddenly at peak load. A typical specimen after failure is shown in Figure 4.12. The wedges of concrete at the top and bottom of the construction joint broke away and the underlying #7 longitudinal reinforcement bars buckled. Also, the side faces typically delaminated or spalled along the joint, apparently due to deformation of the #7 stirrups at the side faces.

Although measured sliding at peak load is very small (0.0025 inches or less), the specimens continued to slide along the construction joint after failure due to strain energy in the sample and testing machine. The crack specimens began sliding early, usually after a load of a few hundred kips. The residual sliding after failure was typically about 0.5 inches, as can be seen in Figure 4.12.



Figure 4.12. Specimen 5 after failure: overall view looking southwest (left); close-up of sliding on east side (right)



Figure 4.13. Screenshots from slow-motion video showing instant of failure: Specimen 3 (left) and Specimen 6 (right)

The images in Figure 4.13 are screenshots from slow-motion video recordings and show Specimen 3 (as placed, bonded) and 6 (roughened, cracked) at the instant of failure. As can be seen, both specimens slid suddenly along the construction joint with a concentration of damage near the top and bottom of the joint. The spalling and delamination described above is secondary damage, which occurred with continued sliding.

The behavior of Specimen 1 was atypical. At an axial load of 1296 kips, the specimen slid along the construction joint without spalling or delamination, which is similar to the sliding failure observed in the actual structure. Because Specimen 1 was not severely damaged, the specimen was reloaded after the initial failure. The peak load in the retest was 737 kips.

Figure 4.14 is a close-up of the interface of Specimen 5 (roughened, cracked) after failure. Numerous fractured aggregate are evident, but these fractures may have occurred when the specimen was intentionally cracked. The circled areas show corresponding fractured aggregate on each side of interface. Figure 4.15 is

a similar photo from Specimen 1 (as-placed, cracked). Relatively few fractured aggregate are evident at the construction joint.



Figure 4.14. Construction joint interface of Specimen 5 (roughened, cracked) after failure. Circled areas show corresponding fractured aggregate on each side of interface.



Figure 4.15. Construction joint interface of Specimen 1 (as-placed, cracked) after failure.

4.1.9 Slant Shear Tests

The Chicago coarse aggregates used in the testing of the replicate construction joints were of higher specific gravity than the Florida (Krome) aggregate used in the actual construction, with the specific gravity of the Chicago aggregates equal to 2.69 to 2.71 and the Florida aggregates equal to 2.43. Some research has shown that the interface shear transfer across roughened specimens is affected by the density of the aggregates.^{7, 8} In order to assess this effect, slant shear tests were performed using a modified version of ASTM C882. A total of 20 slant shear specimens, 10 with Chicago aggregates (2 specimens were rejected as outliers) and 10 with the Florida aggregates, were fabricated using the mixture proportions in Table 4.1 and tested with the following modifications to ASTM C882:

- The bottom halves of the slant shear specimens were cast using an angle of incidence of 38.9 degrees in 6 x 12-inch cylinder molds.
- The bottom halves were removed from the cylinder molds and roughened, within 48 hours after fabrication, in the same fashion as the replicated construction joints by use of a chipping hammer. In order to avoid chipping and spalling of the edges of bottom halves of the cylinders, the roughened surface was limited to the inner portion, leaving approximately 1 inch along the perimeter smooth.
- The outside perimeter was coated with form release agent to prevent any bond (for the subsequent top half concrete placement) in the smooth (unroughened) area.

⁷ AlMosawi, F.H., "Effect of Coarse Aggregate Type on Shear Transfer Strength. International Journal of Scientific & Engineering Research", Volume 8, Issue 3, March 2017.

⁸ Krc, K., "An Investigation of Shear-Friction of Lightweight Aggregate Concretes", University of Missouri Science and Technology, 2015.

- The prepared bottom halves were placed back into 6 x 12-in. cylinder molds, and the top halves of the cylinders were cast directly onto the bottom halves, with the top and bottom halves having the same aggregate source.
- Similar to the replicated construction joint testing, all slant shear specimens were pre-cracked within 48 hours after fabrication. Cracking along the top and bottom half interface was achieved by cutting an approximately 3/4-inch groove along the interface, inserting a thin steel plate in the groove, and loading the specimen parallel to the interface plane.

Concrete was made and specimens were cast in general accordance with ASTM C192. The compressive strength and slant shear specimens were demolded at 1 day cured in the concrete laboratory until loading, in accordance with ASTM C31 Field Curing, with the following exception. The Florida aggregates specimens were placed in water and cured at 100 °F for 6 days (from 36 to 42 days for the top halves and age of 49 to 55 days for the bottom halves) in order to increase the compressive strength of the top halves to be similar to Chicago aggregate top half concrete. For the bottom and top concrete, compressive strength specimens were fabricated and tested according to ASTM C31 and ASTM C39 (Table 4.8).

Table 4.8. Compressive Strength of Slant Shear Concrete (psi)

Test Age (days)	Chicago Aggregates		Florida Aggregates		
	Bottom Half (CB)	Top Half (CT)	Bottom Half (FB)	Top Half - Batch 1 (FT1)	Top Half - Batch 2 (FT2)
1	4,570	2,610	4,150	1,510	2,050
2		3,960		2,520	2,800
7		6,250		4,740	5,620
14	11,860	7,280	9,290		
15		7,250			
23				5,810	6,640
28	13,260				
35				5,870	6,770
43				5,770	7,340
56			10,150		
Strength at testing	13,260	7,250	10,150	5,770	7,340

The slant shear testing of all specimens were tested per ASTM C882 when the upper halves of both aggregate sources achieved similar compressive strengths. In the case of the Florida aggregate specimens the replicate batches of concrete for the top half of slant shear cylinders had significantly different compressive strengths at the time of the slant shear testing. The replicate batches for the other mixtures (bottom half Chicago aggregate, bottom half Florida aggregate, top half Chicago aggregate) had typical variance between batches and the results shown are the average of the replicate batches. The results for the Chicago and Florida aggregate are summarized in Table 4.9 and Table 4.10, respectively.

Table 4.9. Slant Shear Test Results: Chicago Aggregate

Specimen	Mix	Test Load (lbs)	Shear Stress (psi)	Normalized to Top Compressive Strength	Normalized to Average Compressive Strength
C1	CT/CB	163,700	2,829	0.390	0.276
C2	CT/CB	179,760	3,107	0.429	0.303
C3	CT/CB	150,150	2,595	0.358	0.253
C4	CT/CB	164,330	2,840	0.392	0.277
C5	CT/CB	145,970	2,523	0.348	0.246
C6	CT/CB	174,640	3,019	0.416	0.294
C7	CT/CB	166,260	2,874	0.396	0.280
C8	CT/CB	162,230	2,804	0.387	0.273
Average		163,380	2,824	0.390	0.275
Standard Deviation		9,910	171	0.024	0.017

- Notes
1. Shear stress divided by compressive strength of top half
 2. Shear stress divided by average compressive strength of both halves

Table 4.10. Slant Shear Test Results: Florida Krome Aggregate

Specimen	Mix	Test Load (lbs)	Shear Stress (psi)	Normalized to Top Compressive Strength	Normalized to Average Compressive Strength
F1	FT1/FB	144,810	2,503	0.434	0.314
F2	FT1/FB	96,660	1,671	0.290	0.210
F3	FT1/FB	156,640	2,707	0.469	0.340
F4	FT1/FB	89,980	1,555	0.270	0.195
F5	FT1/FB	91,170	1,576	0.273	0.198
F6	FT1/FB	107,470	1,858	0.322	0.233
F7	FT2/FB	126,550	2,187	0.298	0.250
F8	FT2/FB	134,420	2,323	0.317	0.266
F9	FT2/FB	158,040	2,732	0.372	0.312
F10	FT2/FB	142,800	2,468	0.336	0.282
Average		124,854	2,158	0.338	0.260
Std. Dev.		24,072	416	0.061	0.047

- Notes
1. Shear stress divided by compressive strength of top half
 2. Shear stress divided by average compressive strength of both halves

4.2 Discussion

4.2.1 Results Relative to AASHTO Code

All test specimens exhibited capacities greater than predicted by the AASHTO Code⁹. To at least some degree, these results are expected because the Code equations provide a lower-bound to expected capacity.

⁹ See Section 5.2.3 for discussion of AASHTO Code provisions for interface shear.

For all samples, the peak load was reached when measured sliding was 0.0025 inches or less. The measured separation, if any, was typically much less. This behavior is not indicative of true shear-friction behavior where sliding causes separation that strains the shear-friction reinforcement, increasing the normal force. In this case, most of the normal force resulted from the component of the axial force acting perpendicular to the construction joint. Thus, capacity was apparently limited by shear stress rather than yield strength of the shear-friction reinforcement.

The observed shear stress limit on capacity is consistent with the AASHTO Code prediction. As described in Section 5.2.3, capacity is limited by maximum shear stress: 1.5 ksi for concrete roughened to an amplitude of 0.25 inches and 0.8 ksi for a surface that is not intentionally roughened. However, the observed shear stresses at failure were much higher: 2.30 ksi average for a roughened cracked interface, and 1.29 ksi for the as-placed (non-roughened) cracked interface. The maximum shear stress in the bonded specimens was even greater.

The AASHTO Code specifically calls for a roughness amplitude of 0.25 inches, but this criterion is not included in the FDOT Specifications. The test results indicate that intentionally roughening the *hardened* concrete, as required by FDOT specifications, achieves the roughness required by the AASHTO Code — in effectiveness, if not actual amplitude.¹⁰ Therefore, these calculations use the friction parameters for intentional roughness found in the AASHTO Code.

4.2.2 Florida Krome vs Chicago Limestone

As can be seen in Table 4.9 and Table 4.10, the slant shear test results were normalized by dividing the shear stress by the compressive strength of the top half of the time of testing. Using this method, the average shear stress at failure of the Florida aggregate slant shear specimens was 13.3 percent less than that of the Chicago area specimens. This approach is based on the assumption that shear stress is controlled by the lesser of the two concrete strengths.

The results were also normalized by dividing the shear stress by the average compressive strength of both halves. This approach is based on the assumption that the failure shear stress is influenced by the compressive strength of the bottom half as well as the top half. Normalizing with respect to the average compressive strength, the average failure shear stress Florida aggregate specimens was just 5.5 percent less than that of the Chicago aggregate specimens. The slant shear test results do not apply to the as-placed (non-roughened) specimens because interface shear transfer does not depend on aggregate interlock across the relatively smooth surface.

Arguments for either normalization approach can be made, and there is no available research on interface shear transfer between concretes of significantly different strengths. As such, reductions of both 13.3 percent and 5.5 percent are considered for adjusting the results of the full-sized interface shear strength specimens with roughened, cracked surfaces.

Based on the above, Table 4.11 summarizes the unadjusted and adjusted capacities of the specimens with roughened, cracked surfaces.

¹⁰ Neither the AASHTO Code nor ACI 318-19 provide detailed criteria for measuring amplitude. In WJE's experience, 1/4-inch amplitude is generally taken as the typical peak-to-valley heights over short distances.

Table 4.11. Capacities of Roughened, Cracked Specimens Adjusted for Florida Aggregate

Adjustment for Florida Aggregate Based on Slant Shear Tests	Florida Aggregate Adjustment	Adjusted Average Capacity (kip)	<u>Roughened</u> <u>As-Placed</u>
None	No Adjustment	2594	1.78
Normalized to average compressive strength of both halves	5.5% reduction	2451	1.68
Normalized to lower compressive strength of top half	13.3% reduction	2246	1.54

4.2.3 Roughened vs As-Placed (Non-Roughened) Interface

Roughening the construction joint surface in accordance with FDOT Standard Specifications greatly improved performance. On average, the roughened cracked interface was 1.78 times as strong as the as-placed (non-roughened) cracked interface. The relative difference according to the AASHTO Code is similar: the maximum allowable shear stress for a roughened surface (1.5 ksi) is 1.88 times that for a non-roughened surface (0.8 ksi). However, the observed maximum shear stresses are at least 50 percent greater than the Code values. As previously noted, Code values represent the lower-bound to research data.

The bonded roughened specimen was also stronger than the bonded as-placed (non-roughened) specimen. The actual difference is not known because the bonded roughened specimen did not fail at the maximum testing machine capacity of 3000 kips.

Also, it is noteworthy that the tested capacity of the as-placed (non-roughened) cracked interface (average of 1455 kips) is less than the calculated force in Member 11 after the shoring was removed (1680 kips, see Table 4.6). This result explains the initial cracking and horizontal movement when the shoring was removed and suggests that the construction joint was at least partially debonded when the shoring was removed. It is also possible that the bond between Member 11 and the deck was weaker than that of Specimen 3 (as-placed, bonded), which failed at an axial force of 2775 kips (see Table 4.7).

4.3 Findings

The primary finding from the experimental program described above is that intentional roughening of the construction joint following FDOT Standard Specifications improved the shear capacity of the cracked interface by a factor of 1.78. This factor reduces somewhat if adjustment for Florida aggregate is made. The Florida aggregate reduction does not apply to as-placed (non-roughened) specimens because friction across the relatively smooth surface does not depend on aggregate interlock.

Comparison of observed axial strengths of the as-placed (non-roughened) specimens to the calculated force in Member 11 after the shoring was removed suggests that the construction joint was weakened or at least partially debonded when the shoring was removed.

More significantly, the axial capacities of the roughened specimens, before or after adjustment for Florida aggregate, substantially exceed the calculated force in Member 11 at the time of the collapse. As such, if the construction joint were roughened as required by the project specifications, the collapse would not have occurred. See Section 5.3 for evaluation of the observed performance of the Member 11 and 12 deck connection relative to the expected resistance based on test results. Also see Sections 7 and 8 for evaluation of other factors contributing to the collapse.



KHAN CONSULTANTS



The following report of data is the result of calculation from data gathered via 3D scanning of physical concrete blocks as provided to Khan Consultants. The analysis of the data in a pre-determined manner to elicit certain mathematical characteristics is submitted purely as a report of mathematical results from the data and is not warranted to be findings or conclusions of any kind or representative of any physical behavior. The accuracy of the scan data is only as defined by the manufacturer of the HDI ADVANCE 3D scanner in publicly available information.

Exhibit 4.1



Summary of Deviations - Numerical

The values calculated by the system for the segments studied from each block are as follows (in millimeters):

	3-As Placed	4-Roughened
Max Pos Deviation	5.29	6.72
Max Neg Deviation	-4.48	-10.03
Avg Pos Deviation	0.82	1.31
Avg Neg Deviation	-0.64	-1.91
Standard Deviation	0.94	2.03
RMS Estimate	0.94	2.04
Segment Length	775.01	778.33
Segment Width	320.57	321.73

Exhibit 4.1



Isometric and Top of view of Full Block - Original Scan Data with Rebar members:

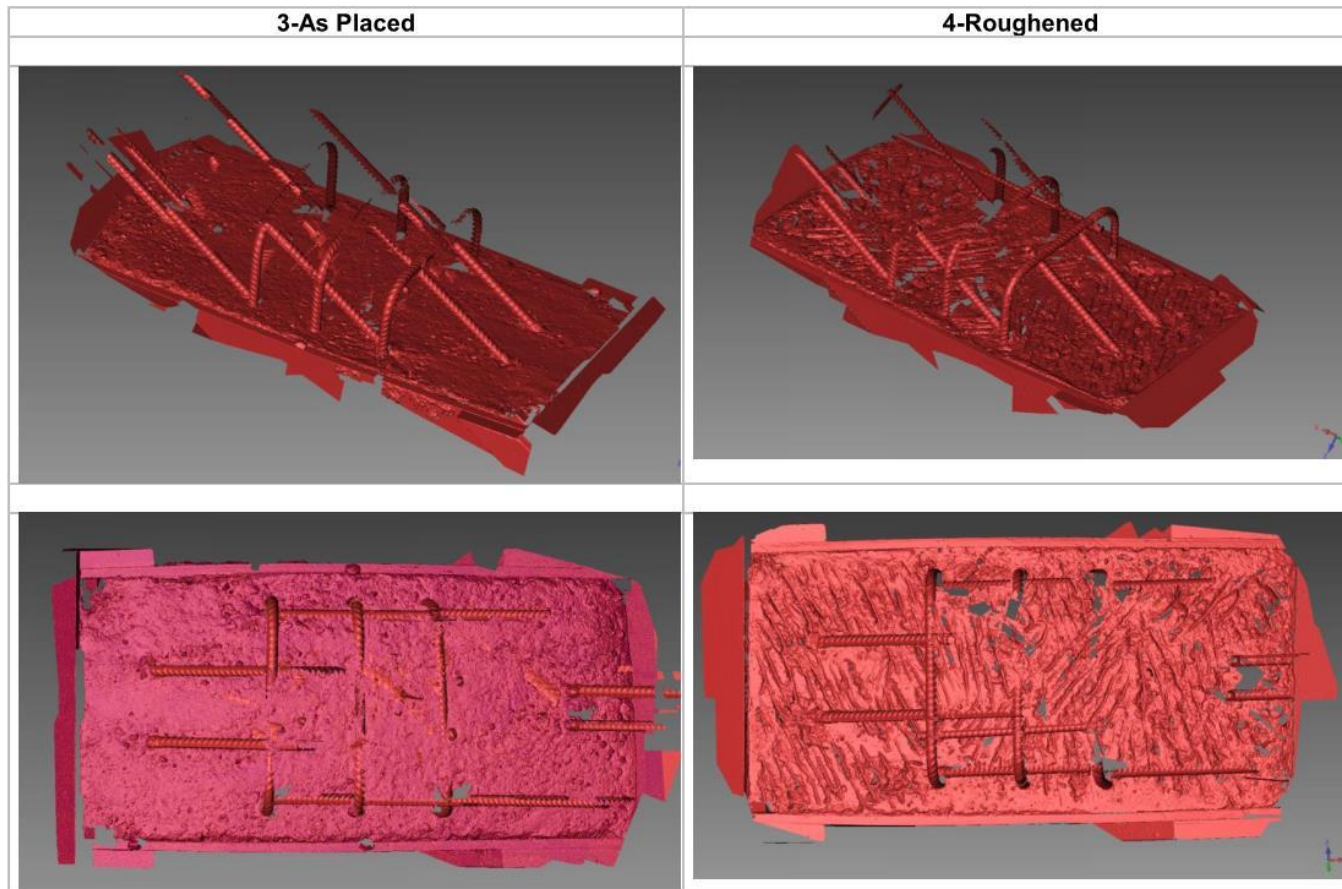


Exhibit 4.1



Isometric view of Scan Data Used (in red) for concrete section:

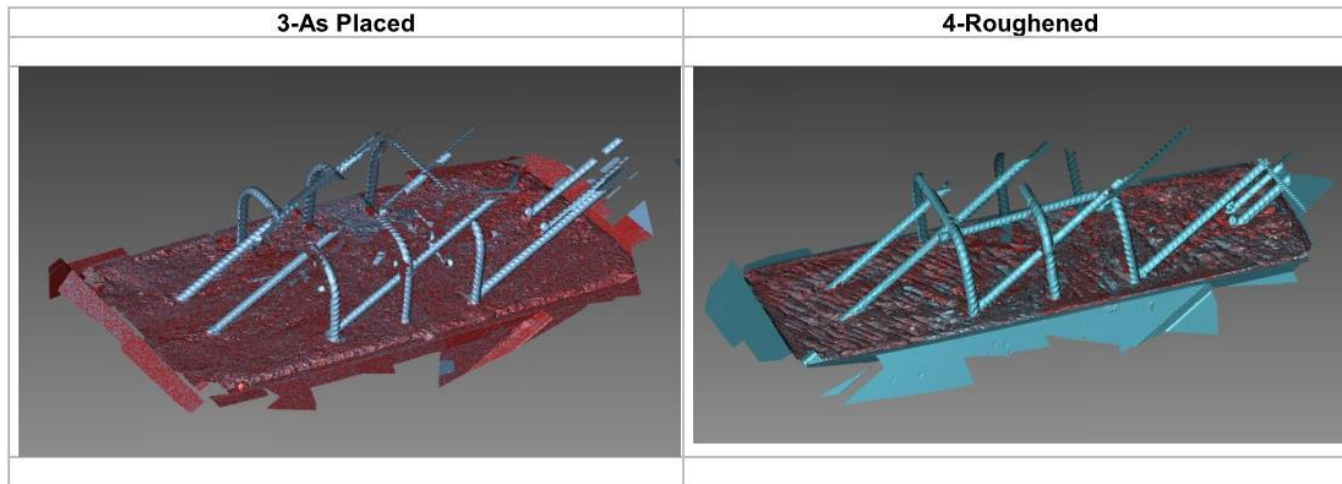


Exhibit 4.1



Top of view of Full Block and Colormap showing deviations to best-fit plane:

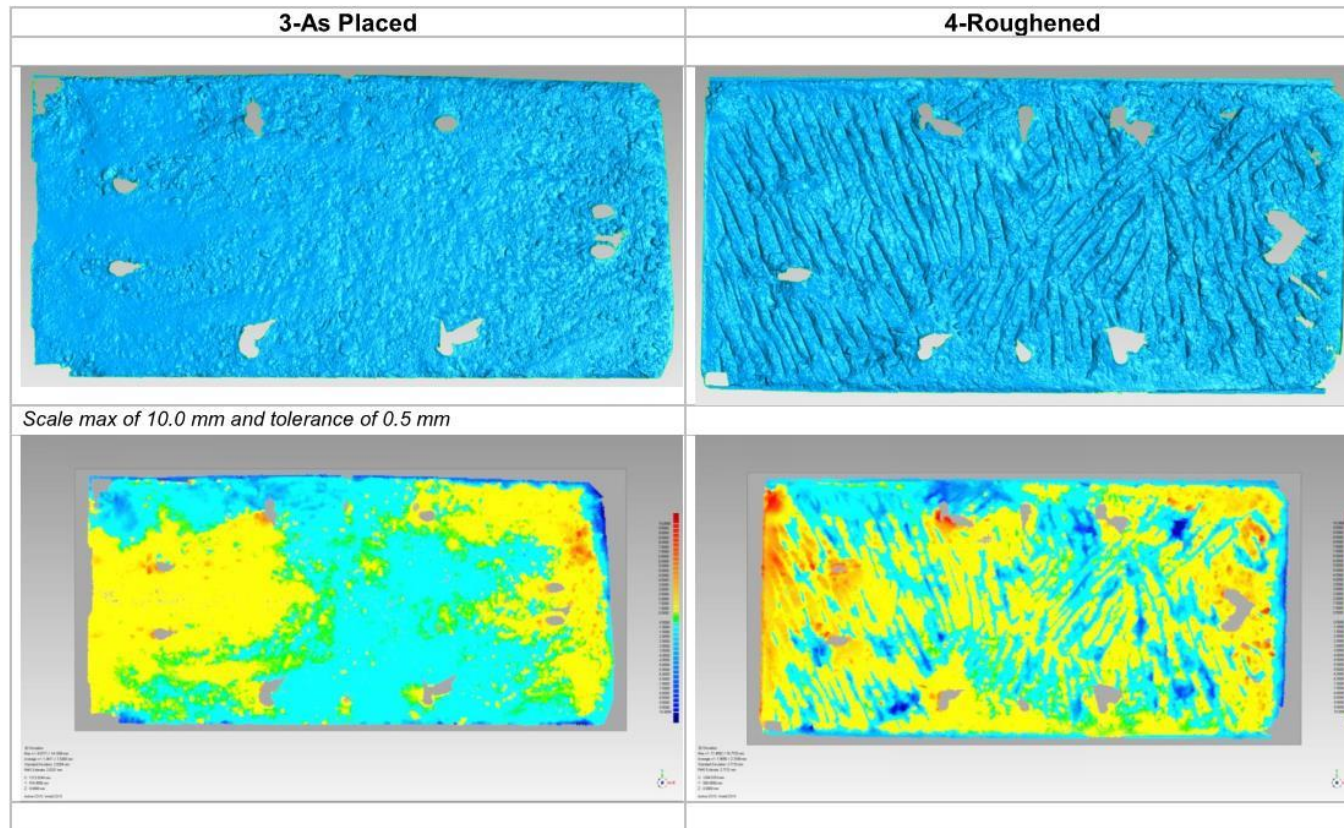


Exhibit 4.1



Top of view of Data Segment and Colormap showing deviations to best-fit plane:

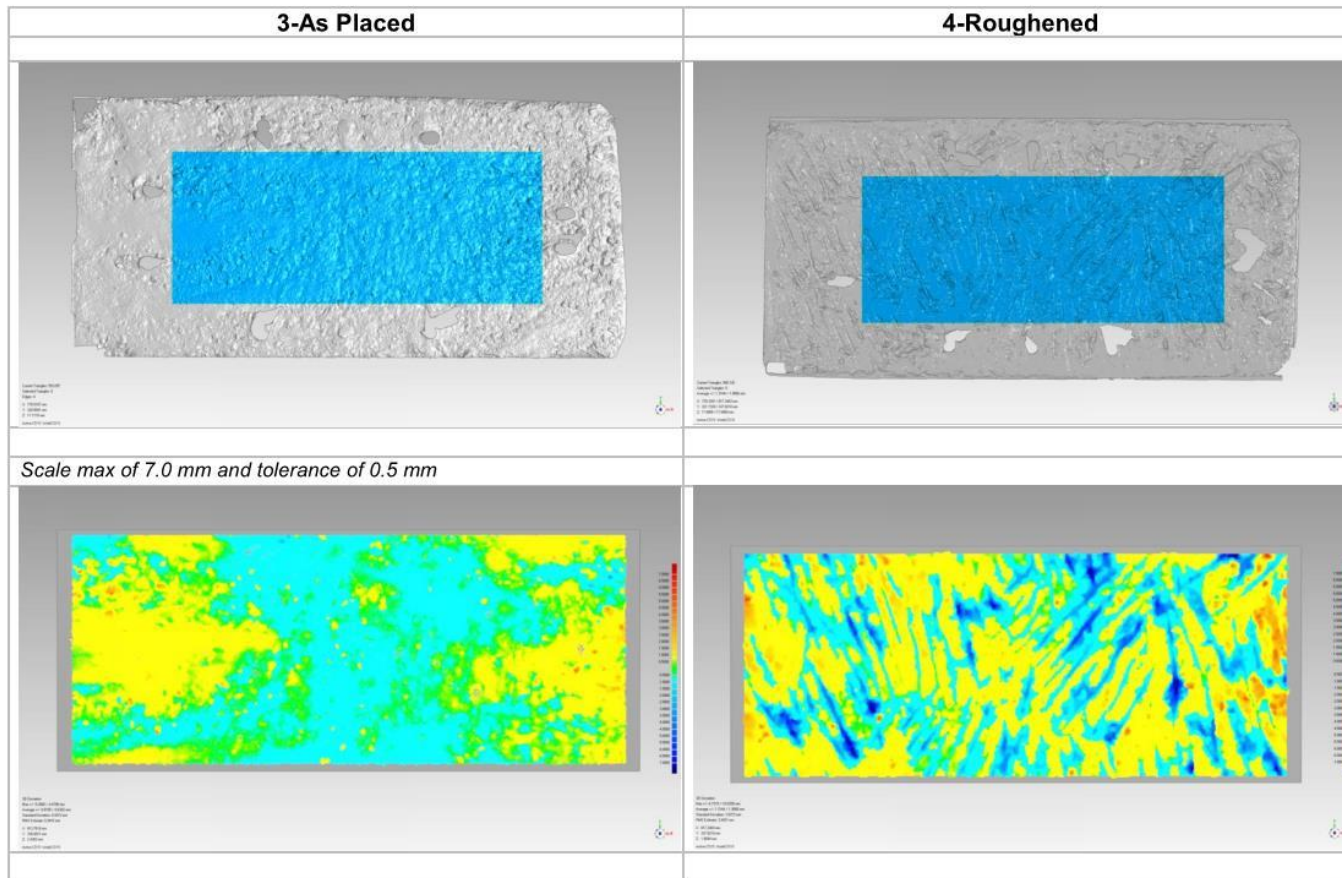


Exhibit 4.1



Isometric view of Data Segment and Colormap showing deviations to best-fit plane:

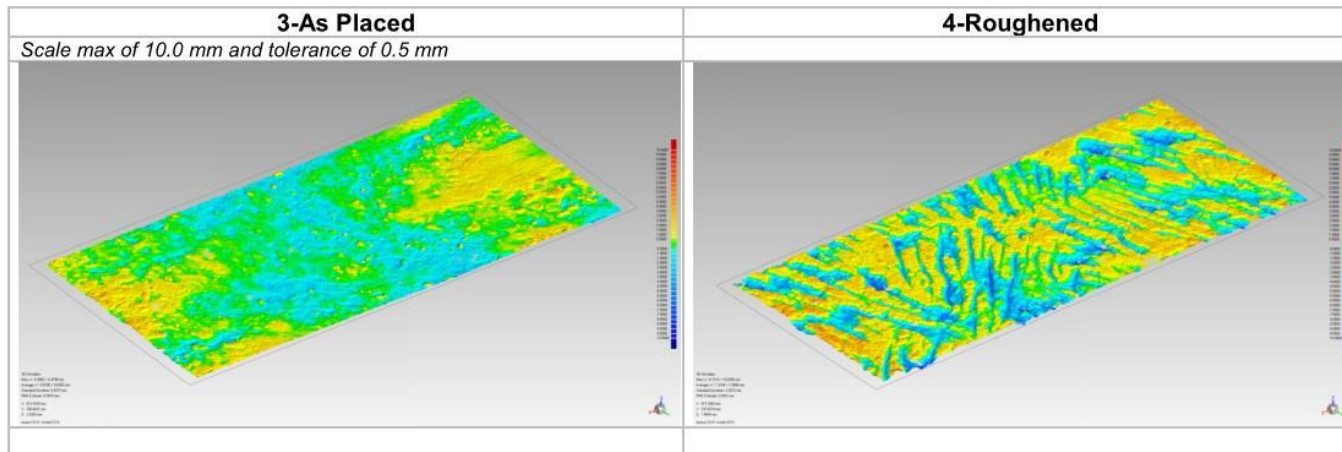


Exhibit 4.1



Isometric view of Colormap showing deviations to best-fit plane (different tolerance thresholds):

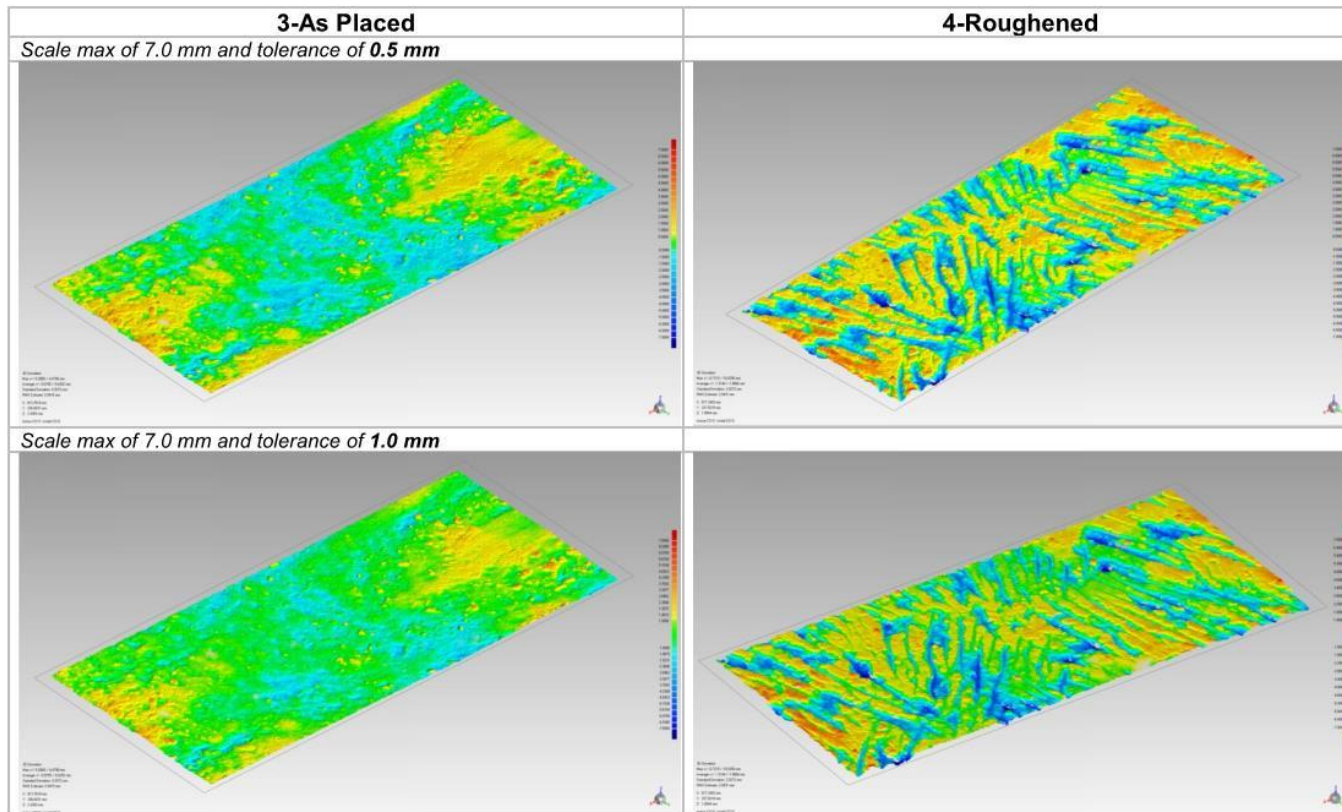
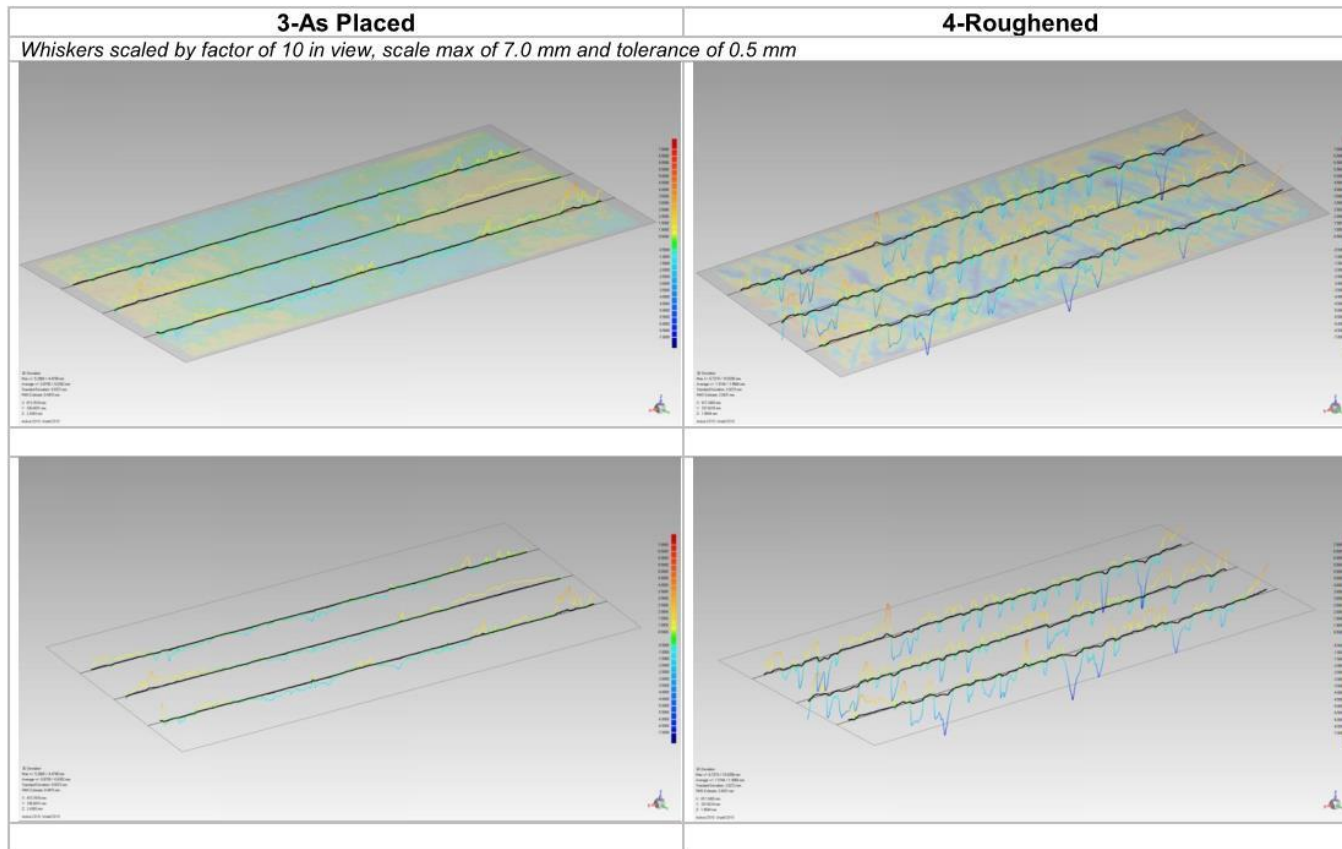


Exhibit 4.1



Sectional Deviations (whiskers scaled by factor of 10 in view, scale max of 7.0 mm and tolerance of 0.5 mm):



5 STRUCTURAL ANALYSES

WJE carried out independent structural analyses of the main span. The analyses included the following:

- Development of a finite element models to independently determine the forces and bending moments in the truss members during construction.
- AASHTO Code evaluation of the Member 11/12 deck connection for loading during construction when the main span was placed on its final supports.
- Evaluation of the Member 11/12 deck connection for the conditions at the time of the collapse based on test results.

5.1 Finite Element Analysis

5.1.1 Model Description and Assumptions

A finite element model of the main span was developed and analyzed using Abaqus, general purpose commercial finite element software for structural analysis of complex systems. The model was used to determine truss forces and bending moments during construction. The concrete elements were modeled using approximately 800,000 solid hexahedral elements. Diagonal and horizontal post-tensioning bars were modeled with beam and truss elements, respectively. An overview of the model is shown in Figure 5.1.

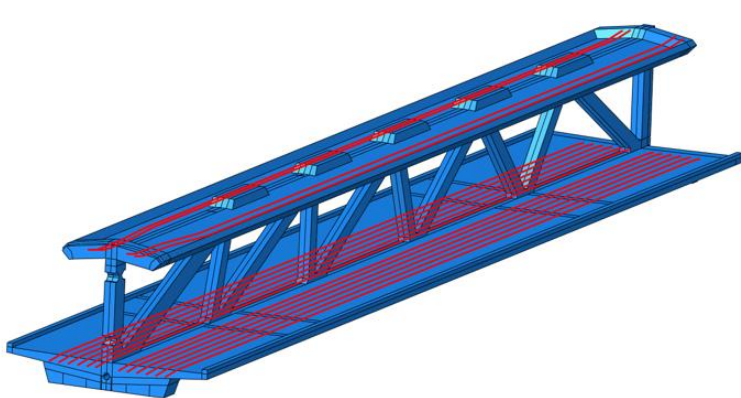


Figure 5.1. Abacus model of main span (Blue elements are concrete; red elements are post-tensioning tendons.)

Two versions of the model were developed:

- *Model 1 – Design Conditions.* A model representing the conditions required for design of the main span after it was placed in its final position between the south pier and central pier.
- *Model 2 – As-Built Conditions.* A model representing as-built conditions at the time of the collapse.

The materials properties for each of these models are summarized in the following table.

Table 5.1. Materials Properties for Finite Element Models

Property	Model	Value	Source
Concrete compressive strength	1	8,500 psi	Project General Notes
	2	10,200 psi	Estimate based on concrete testing information in the OSHA Report
Concrete unit weight	1	148.5 pcf	AASHTO ¹¹ Table 3.5.1-1 based on specified compressive strength. Unit weight was increased 5 pcf to account for mild reinforcement.
	2	138.7 pcf	Estimate from WJE replication of project mix design, not including 5 pcf allowance for weight of mild reinforcement.
Concrete modulus of elasticity	1	5255 ksi	AASHTO Equation 5.4.2.4-1
	2	4584 ksi	Estimate for project mix design
PT modulus of elasticity	1 and 2	29,700 ksi	DSI DYWIDAG Post-tensioning Systems brochure (page 25)

5.1.2 Loading

The loadings for each of these models are summarized in the following table. Load factors are not included. The weight of the concrete curb is not included in the design conditions model because the project drawings show it being constructed after the back span is placed. The weight of the curb is included in the as-built conditions model because it was constructed in the casting yard.

Table 5.2. Loadings for Finite Element Models

Loading	Model	Loading
Dead load	1	Specified dimensions and AASHTO unit weight of 148.5 pcf increased by 5 pcf for mild reinforcement. Concrete curb not included.
	2	Specified dimensions and unit weight of 138.7 pcf increased by 5 pcf for mild reinforcement. Concrete curb included.
Construction load	1	20 psf on deck walking surface, the minimum construction load required by Section 4.10 of the project design criteria (April 2015 revision).
	2	Calculated weight of temporary railing (3 plf) plus the estimated weight of the workers and hydraulic jack on the canopy at the time of the collapse (1.5 kips at blister above Member 11).

5.1.3 Post-Tensioning Force in Member 11

The specified post-tension force of 280 kips in each post-tensioning bar was applied as an imposed strain. The construction sequence was considered. For the design conditions model, the post-tensioning was applied before shoring below the main span was removed. In this way, the post-tensioning force decreased due to shortening of Member 11 as the self-weight was applied in the final, simply-supported condition.

For the as-built conditions model, the specified post-tensioning force was applied when the span was supported in its final position between the south pier and central pier to simulate the re-tensioning. Consistent with review of the time of collapse video, it was assumed that the final post-tensioning step was being applied when the collapse occurred. In this case, the specified post-tensioning force was not reduced

¹¹ AASHTO LRFD Bridge Design Specifications, Seventh Edition

due to elastic shortening of Member 11 due to self-weight. Therefore, the Member 11 post-tensioning force in the as-built conditions model is slightly greater than that in the design conditions model.

5.1.4 Results

The results are summarized in Table 5.3. Finite Element Model Results. These results are considered in the evaluations of the Member 11/12 Deck Connection in Sections 6 and 7.

Table 5.3. Finite Element Model Results

Member	Model	Axial Force (kips)			Bending Moment (kip-ft)		
		DL	CL	PT	D	CL	PT
Member 11	1	-1236	-68	-589	217	9.8	-11
	2	-1166	-3	-574	207	0.4	-9
Member 12	1	-67	-1	-15	57	5	210
	2	-63	0	-14	55	0.2	197

Notes:

DC = Dead load of structural components

CL = Construction live load

PT = Post-tensioning force

Negative axial force indicates compressive force

For design, the forces and bending moments listed in Table 5.3. Finite Element Model Results must be multiplied by the appropriate load factor for the controlling load combination.

5.2 Code Evaluation of Member 11/12 Deck Connection (As-built Condition)

The objective of the evaluation was to independently determine the capacity of the northernmost truss web member's connection to the deck per the governing design code¹² (AASHTO Code). The loading configuration considered was the main span placed in its final position between the south pier and central pier before the post-tensioning in Member 11 was released.

5.2.1 Limit State

The main span was constructed in three primary casting operations: the deck, the diagonal and vertical web members, and the canopy. Figure 5.2 shows an elevation view of the M11/M12 joint and the deck with the construction joint between the deck and web members is highlighted. This evaluation focuses on the horizontal shear transfer across this interface to resist the horizontal component of the compressive axial force in Member 11. The most obvious load transfer mechanism is shear-friction, which uses surface roughness and reinforcement crossing the interface to transfer shear with a combination of dowel action, cohesion, and friction. If the interface is not cracked, shear along an interface is resisted by cohesion from cementitious bond. After cracking, cementitious bond is lost and load is resisted by aggregate interlock, friction, and dowel action.¹³ The friction component relies on the reinforcement and applied loading to develop a normal force.

¹² AASHTO LRFD Bridge Design Specifications, Seventh Edition

¹³ Hofbeck, J. A., Ibrahim, I. O., & Mattock, A. H. (1969, February). Shear transfer in reinforced concrete. In Journal Proceedings (Vol. 66, No. 2, pp. 119-128).

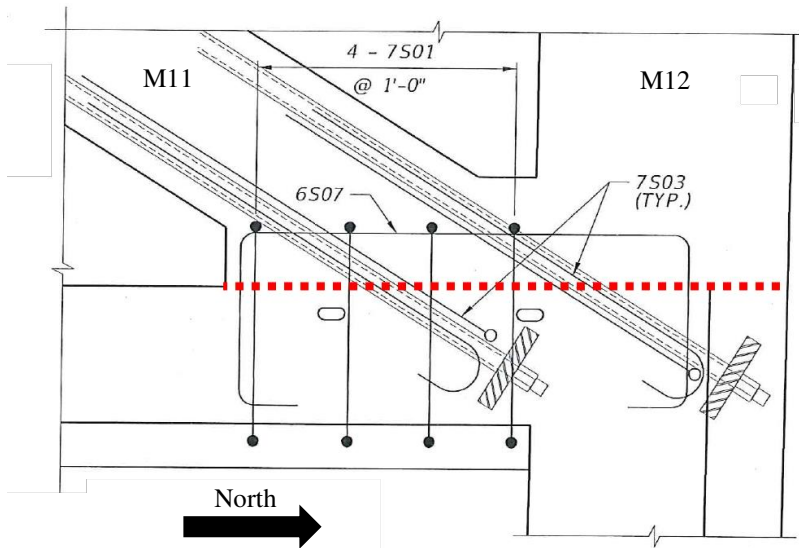


Figure 5.2. Excerpt from Design Drawings showing configuration of joint area. Construction joint indicated by dotted line.

At the time of collapse, the bridge was in a temporary condition with only the main span in place. In the final configuration, Member 12 and the north diaphragm would have been incorporated into the pylon, and Span 2 would have been placed against the north end of the main span. These changes would have made the truss continuous and prevented any horizontal displacement at the joint.

5.2.2 Demand

The structural demands at the joint were due to dead load, construction live load, and post-tensioning force in Members 11 and 12 (see Table 5.3). To determine the factored load effect, the controlling load combination was evaluated. Per the AASHTO Code Strength I load combination, load factors of 1.25, 1.5, and 1.0 apply to the dead load, construction live load, and post-tensioning load, respectively.

Section 1.3.2.1 of the AASHTO Code requires consideration of load modifiers greater than 1.0 for the strength limit state in certain circumstances. Specifically, Section 1.3.3 specifies a load modifier of 1.05 for non-ductile components and connections, and Section 1.3.4 specifies the load modifier of 1.05 for non-redundant members. However, the AASHTO Code lacks specific guidance on when to apply these factors, apparently leaving it to the judgment of the engineer. Also, the AASHTO Code makes no mention of the applicability of these factors to temporary construction stages, nor does it exempt construction activities from their applicability. However, as a practical matter, even highly-redundant multi-girder bridges are often non-redundant when the first beam is erected.

The results are summarized in Table 5.4 in terms of the northward force at the M11/M12 interface with the deck. The northward force includes horizontal force components from both Members 11 and 12.

**Table 5.4. Calculated Horizontal Shear Force at Connection of M11/M12 to Deck
(Finite Element Model 1: Design Conditions)**

Load	Northward Force at M11/M12 (kips)		
	Un-Factored	Factored	Factored with Load Modifiers
Dead Load	1089	1361	1501
Construction Live Load*	59	89	98
Post-tensioning	529	529	583
Total	1677	1979	2182

*20 psf on deck walking surface as required by Section 4.10 the Project Design Criteria

5.2.3 Capacity

The capacity of the connection between Member 11/12 and the deck is shear-friction at the construction joint below Members 11 and 12, the dashed red line in Figure 5.2.

Shear-Friction in AASHTO. A pure shear-friction model assumes interface shear resistance is a product of the net normal clamping force and the friction coefficient. The normal force is usually provided by reinforcement crossing the interface and axial load. The AASHTO Code uses a modified shear-friction model accounting for a contribution from cohesion and/or aggregate interlock, which is evident in the experimental data. In this way, the AASHTO Code shear-friction model is analogous to the vertical shear resistance expression of $V_c + V_s$.¹⁴

The nominal shear resistance of the interface plane is given by AASHTO Code Equation 5.8.4.1-3:

$$V_{ni} = cA_{cv} + \mu(A_{vf}f_y + P_c)$$

where:

- V_{ni} = nominal interface shear resistance (kip)
- c = cohesion coefficient (ksi)
- A_{cv} = area of concrete section resisting shear transfer (in.²)
- μ = coefficient of friction
- A_{vf} = area of shear-friction reinforcement (in.²)
- f_y = yield strength of shear-friction reinforcement (ksi)
- P_c = permanent compressive force (kip)

As can be seen in the above equation, the resistance provided by cohesion is taken as a cohesion factor times the interface area under consideration. For simplicity, a “cohesion factor” is used in the AASHTO Code to capture the effects of cohesion and/or aggregate interlock. However, cohesion provided by cementitious bond and the shear-friction contribution of reinforcement cannot co-exist because the latter requires separation across the interface to develop strain in the shear-friction reinforcement. Thus, when friction from a normal force provided by reinforcement is combined with the “cohesion” contribution, the latter is actually the contribution of aggregate interlock or other effects related to the concrete area. For concrete that is roughened to amplitude of 0.25 inches, the cohesion coefficient is 0.24 ksi and the friction

¹⁴ Commentary to AASHTO Code, Section C5.8.4.1

coefficient is 1.0. For concrete that is not intentionally roughened, the cohesion coefficient is 0.075 ksi and the friction coefficient is 0.6.

In the above resistance equation, P_c is defined as the permanent compressive force. While an argument could be made that this refers to dead load, P_c was interpreted to mean force that is coincident by necessity with the design interface shear; that is, forces that are present by virtue of the presence of the shear demand. Vertical components of truss compressive force meet this criterion.

These shear-friction parameters are based on research in which the interfaces of most specimens were intentionally unbonded or initially cracked.¹⁵ Unbonded and initially cracked specimens were primarily used because a crack at the interface between concrete cast at different times should be assumed.

In addition, the AASHTO Code includes two maximum shear stress limits. The first limit is the concrete compressive strength multiplied by a surface preparation coefficient: 0.25 for concrete roughened to an amplitude of 0.25 inches and 0.2 for a surface that is not intentionally roughened. The second shear stress limit depends only on surface roughness: 1.5 ksi for concrete roughened to an amplitude of 0.25 inches and 0.8 ksi for a surface that is not intentionally roughened.

Construction Joint. One of the primary factors in evaluating the shear-friction capacity is the roughness of the construction joint when the web members were cast against it. In correspondence between FIGG and MCM during construction, FIGG confirmed that the FDOT Standard Specifications¹⁶ were to be followed. These include instructions for preparations of construction joints before casting new concrete against hardened concrete including direction to “roughen the surface of the hardened concrete.” Despite this, the joint appeared to be left in an as-placed (non-roughened) condition, as described in Section 3.

For the assumption of a roughened surface, the AASHTO Code specifically calls for a roughness amplitude of 1/4 inch, but this criterion is not included in the FDOT Specifications. However, AASHTO does not provide specifics on preparation of the construction joint (including intentional roughening of hardened concrete) or how roughness amplitude is measured. The FDOT Standard Specifications, as proven by the tests described in Section 4, achieves the requirements of the AASHTO Code. Therefore, these calculations use the friction parameters for intentional roughness found in the AASHTO Code.

Shear-Friction Assumptions. Although inconsistent with the failure mode described in Section 2, which involved a combination of shear-friction below Member 11 and breakout below Member 12, shear-friction was evaluated across the entire construction joint shown in Figure 5.2. The AASHTO Code does not require or even address evaluation of a combined shear-friction and breakout resistance. As such, the assumption of shear-friction resistance across the entire construction joint is considered to be a likely choice in design.

Section 5.8.4.1 of the AASHTO Code requires reinforcement for interface shear transfer to be developed on both sides of the interface to develop the design yield stress. At mid-length, there are three #11 bars on the south face of Member 12. However, only two of three #11 bars on the north face are fully developed across the construction joint and considered to contribute to shear-friction resistance.

¹⁵ Mattock, A., "Shear Transfer under Monotonic Loading, across an Interface between Concrete Cast at Different Times," Report SM 76-3, University of Washington Department of Civil Engineering, 1976.

¹⁶ Florida Department of Transportation. (July 2015). *Standard Specifications for Road and Bridge Construction, Division II - Construction Details*.

The #6 and #7 stirrups shown in Figure 5.3 were not fully developed above the interface in accordance with the AASHTO Code requirement for development of hooked bars in tension (AASHTO 5.11.2.4). However, the vertical legs of the #6 and #7 stirrups are connected across the top. The vertical legs of these bars are fully developed based on the AASHTO requirements for strut-and-tie models in Section 5.6.3. The strut-and-tie model for the #7 stirrups is shown in Figure 5.3. As such, these bars were considered to contribute to shear-friction resistance.

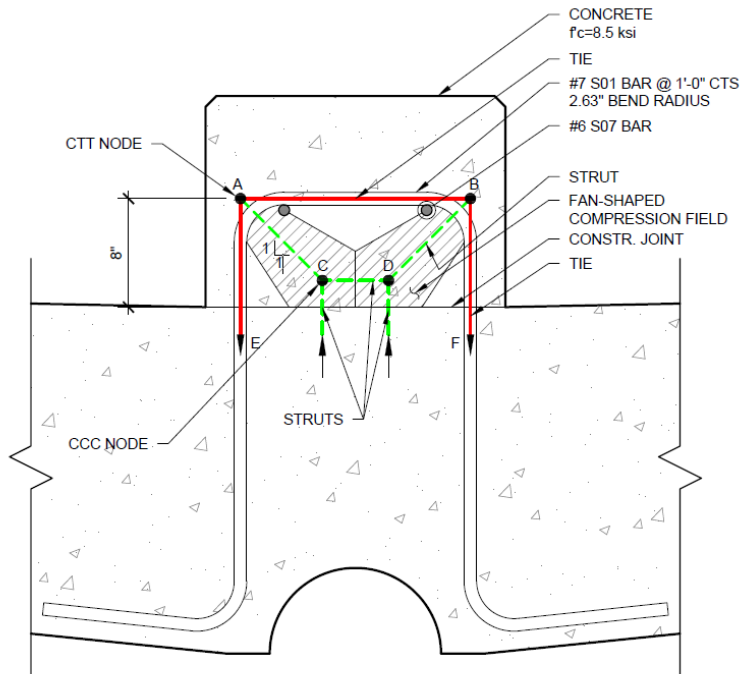


Figure 5.3. Strut-and-tie model of #7 stirrups across construction joint

The inclined #7 bars in Member 11 crossing the interface were not considered to contribute to shear-friction capacity because northward sliding produces compression in the inclined bars, as explained in Section R22.9.4.3 of ACI 318-14.¹⁷

5.2.4 Findings: Design Conditions

The findings with respect to shear-friction design capacity are summarized in Table 5.5, both in terms of factored shear-friction resistance and the ratio factored load effects to factored resistance, capacity-demand ratio (CDR). As described above, a roughened surface is assumed in accordance with the FDOT Standard Specifications. In light of the uncertainty as to their applicability to as-built conditions, Factored resistance and CDRs excluding and including the load modifiers are provided. Design strengths include the strength reduction factor, ϕ , for shear of 0.9.

¹⁷ ACI 318-14. "Building Code Requirements for Structural Concrete and Commentary." American Concrete Institute.

Table 5.5. Summary of Shear-Friction Resistance and CDRs

Factored Northward Force (kips)		Factored Shear-Friction Resistance, ϕV_n (kips)	CDR	
Load Modifiers			Load Modifiers	
Excluded	Included		Excluded	Included
1979	2182	2150	1.09	0.99

These results indicate compliance with the AASHTO Code for shear-friction along the construction joint below Members 11 and 12.

If a combined shear-friction and breakout failure similar to that observed were to be evaluated assuming a roughened surface, a somewhat lower resistance would be calculated than that assuming resistance by shear friction across the entire construction joint. Such a combined failure is not likely to be envisioned in design and is not addressed by the AASHTO Code. Regardless of which of the two failure mechanisms is assumed, the connection would not have failed if the joint was prepared in accordance with FDOT Standard Specifications.

5.2.5 Findings: Design Conditions (Non-Roughened Surface)

The CDRs for shear-friction are much lower if a non-roughened surface is assumed, as summarized in Table 5.6.

Table 5.6. Summary of Shear-Friction Resistance and CDRs

Factored Northward Force (kips)		Factored Shear-Friction Resistance, ϕV_n (kips)	CDR	
Load Modifiers			Load Modifiers	
Excluded	Included		Excluded	Included
1979	2182	1157	0.58	0.53

5.3 Test-based Evaluation of Member 11/12 Deck Connection for As-built conditions

The objective of this study is to evaluate the observed performance of the connection relative to the expected resistance based on test results and advanced analyses. The determination of loading and resistance is based on actual conditions at the time of the failure, when the main span was supported between the south pier and central pier. The resistance is based on calculations as well as the results of tests of specimens that replicate shear transfer between the northernmost diagonal of the main span (Member 11) and the deck.

5.3.1 Failure Sequence and Pattern

The failure pattern and sequences described in Section 2. The physical evidence indicates extreme northward deformation of the Member 11/12 deck connection due to shear-friction failure at the construction joint below Member 11 in combination with breakout failure of the north end diaphragm below Member 12. The movement caused sudden crushing of Member 11 near its base, which in turn triggered the collapse.

5.3.2 Calculated Forces at Time of Collapse

The structural demands at the joint were due to dead load, construction live load, and post-tensioning. Construction loading included the calculated weight of the temporary railing plus the estimated weight of

the workers and hydraulic jack on the canopy at the time of the collapse. The calculated axial force in Member 11 and the calculated northward force at the M11/M12 interface with the deck are based on the finite element model of the main span and are provided in Table 5.7. Note that the northward force includes force components from both Members 11 and 12.

Table 5.7. Calculated Forces in Member 11 and Connection of M11/M12 to Deck

Load	Axial Force in Member 11 (kips)	Northward Force at M11/M12 (kips)
Dead Load	1166	1028
Construction Live Load*	3	3
Post-tensioning	574	527
Total	1743	1677

5.3.3 Connection Strength (As-Built)

Based on the observed failure pattern, the resistance of the connection to horizontal movement comes primarily from two mechanisms: 1) horizontal shear-friction below Member 11, and 2) horizontal break-out of the north and diaphragm below Member 12. Apparently, the # 11 bars extending from the diaphragm into Member 12 precluded continued sliding; that is, north of the #11 bars, the observed behavior indicates breakout resistance was less than shear-friction resistance.

The following sections discuss these two primary resistance mechanisms as well as other factors affecting resistance of the connection to horizontal force.

Shear-Friction Resistance. Shear-Friction resistance depends on the area and roughness of the interface, the reinforcement crossing the interface, as well as any external normal force across the interface. As described in Section 3, the concrete on the deck surface below Members 11 and 12 was apparently left in an as-placed (non-roughened) condition. Photographs indicate that the surface texture is relatively smooth, although coarse aggregate occasionally protrudes above the surface. Longitudinal reinforcement and stirrups cross the interface. The axial force in Member 11 creates both a normal force and sliding force at the interface.

Given the unique interface conditions, shear-friction resistance was evaluated based on tests of specimens that replicate shear transfer between the Member 11 and the deck. As described in Section 4, six specimens were tested: three with an as-placed (non-roughened) interface and three with a roughened interface. Two of the three as-placed and roughened specimens were cracked at the bond line prior to testing. The specimens with an as-placed, cracked interface (Specimens 1 and 2) best reflect the field conditions at the time of the failure. The results are summarized in Table 4.7.

Because Specimen 1 was not severely damaged in the initial test, the specimen was reloaded after the first failure to get a sense of residual strength. After the initial failure, displacement along the construction joint was about 0.5 inches. The peak axial load in the retest was 737 kips, 43 percent less than the axial load at the initial failure.

The performance of the as-placed (non-roughened) cracked specimens described in Section 4 indicate that the vast majority of the shear force at the connection was resisted through shear-friction below Member 11. Based on results of Specimens 1 and 2, 66 to 82 percent of the calculated horizontal force (1677 kips) is

resisted by shear-friction. The remainder, roughly 400 kips, must be resisted by breakout or other mechanisms.

Breakout Resistance. The physical evidence indicates breakout of the north end diaphragm below Member 12 contributed to resistance to the horizontal force at the Member 11/12 deck connection. The total breakout resistance was calculated to be 440 kips. This calculated resistance was determined by modifying the code-based breakout capacity for breakout angle and the expected difference between experimental results and lower-bound code resistance equations.

To evaluate the breakout capacity of the north end diaphragm, the #11 column bars in the south face of Member 12 were treated as anchors loaded in shear. The AASHTO Code does not include provisions for breakout and instead refers to ACI 318. Section 17.5 of ACI 318-14 was applied to the joint geometry. This approach produced a calculated resistance of 161 kips. Reinforcement crossing the breakout plan, which may enhance breakout resistance, was not considered. Likewise, the vertical PVC pipes and the drainpipe, which may reduce breakout resistance, were also not considered.

However, the interior post-tensioning tendons forced a narrow breakout cone. The angle between the outermost #11 bars and the interior post-tensioning tendons is about 55 degrees relative to an east-west line, as illustrated in Figure 5.4. In contrast, the breakout angle on which the ACI 318 resistance model is based is 35 degrees¹⁸.

Shear resistance increases with increasing crack angle, which is reflected in research¹⁹ as well as ACI 318 provisions for shear in discontinuity regions²⁰. In ACI 318-19 Eq. 23.4.4, which applies to one-way shear in discontinuity regions, shear strength is proportional to the tangent of the crack angle. Applying this rationale to breakout strength, the observed narrow breakout cone would double the breakout resistance ($\tan 55 / \tan 35 = 2.04$).

Furthermore, the basic ACI 318 expression for breakout²¹ is based on the lower-bound of test results. The design equation is partly derived from research by Eligehausen, et al²². The coefficient of variation for the underlying test results is 19 percent. The Eligehausen expression for the mean value of the test data gives results that are 34 percent greater than the ACI 318 expression.

¹⁸ ACI 318-19, Figure R17.5.1.

¹⁹ Zsutty, T. C., 1971, "Shear Strength Prediction for Separate Categories of Simple Beams Tests," ACI Journal, Proceedings V. 68, No. 2, Feb., pp. 138-143

²⁰ ACI 318-19, 23.4.4

²¹ ACI 318-19, Eq. (17.6.2.2.1)

²² Eligehausen, R.; Fuchs, W.; and Mayer, B., 1987, "Load Bearing Behavior of Anchor Fastenings in Tension," Betonwerk + Fertigteiltechnik, V. 12, pp. 826-832, and 1988, V. 1, pp. 29-35.

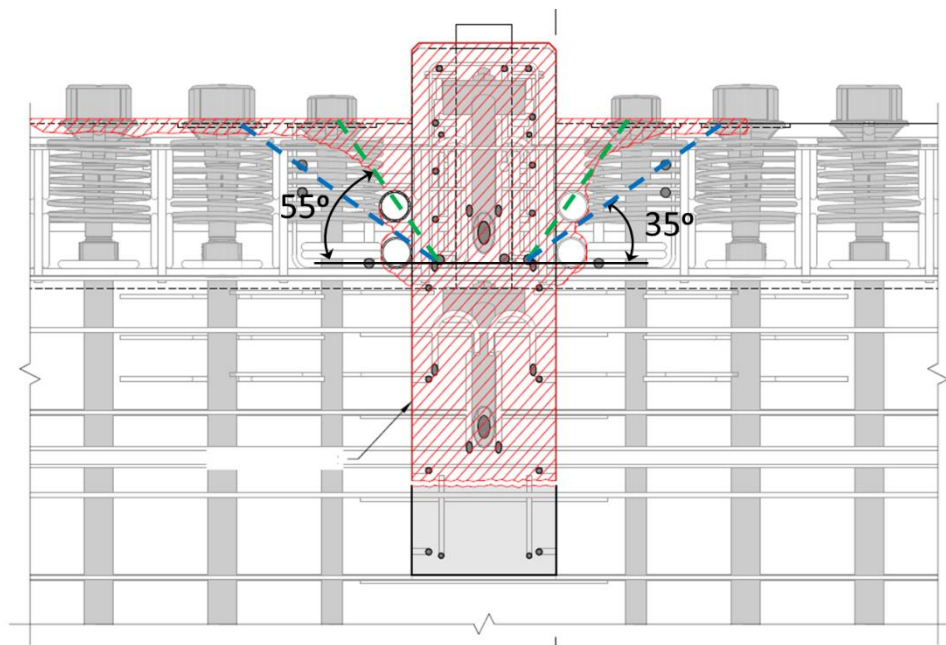


Figure 5.4. Plan view at north end showing breakout angle

Adjusting for both breakout angle and the conservatism of the ACI expression, a breakout resistance of 440 kips would be expected ($161 \times 2.04 \times 1.34 = 440$ kips).

The maximum measured shear forces for the as-placed (non-roughened), cracked specimens were 1101 kips and 1372 kips (see Table 4.7). Thus, the shear-friction resistance from testing plus the adjusted calculation of the breakout resistance (440 kips) ranges from 1541 kips to 1812 kips. The calculated shear force, 1677 kips (see Table 5.7), is in the middle of this range.

5.3.4 Discussion

The test results and calculations described above indicate the potential resistance of shear-friction and breakout is consistent with the calculated horizontal force at the Member 11/12 connection to the deck and the observed cracking and sliding shortly after the shoring was removed.

However, both shear-friction and breakout reach peak resistance with very little deformation. In the case of the interface shear tests, peak shear-friction resistance occurs at a deformation of approximately 0.02 inches. Deformations at breakout failure are about twice this amount, 0.04 inches. Before collapse occurred, the total horizontal deformation exceeded 0.5 inches. Therefore, other mechanisms must have taken over as shear-friction and breakout resistance dropped off. Recall that the shear-friction capacity of Specimen 1 was reduced by more than 40 percent when the specimen was retested after the initial failure and displacement of about 0.5 inches.

In WJE's opinion, the most likely source of supplemental resistance is the numerous reinforcing bars that cross the shear-friction interface and breakout cone. More than 20 square inches of reinforcement with a combined yield strength exceeding 1200 kips cross the perimeter of the shear-friction and breakout planes. With significant north-south movement, this reinforcement would offer resistance that increases with increasing displacement through dowel action as well as the north-south component of tension in the

deformed reinforcement²³. The resistance from shear-friction and breakout together with the resistance from the deformed reinforcement explains why resistance was maintained even though northward displacement exceeded 0.5 inches.

5.3.5 Findings

The studies described in this section indicate that the combined shear-friction and breakout resistance is consistent with the calculated horizontal force at the Member 11/12 deck connection. The estimated actual resistance of the Member 11/12 connection to the as-placed (un-roughened) deck surface is roughly equal to the estimated northward force of 1677 kips at failure.

²³ With large displacement, reinforcement crossing the interface would bend into an S-shaped curve, the north-south component of which would add to shear resistance.

6 EVALUATION OF PEER REVIEW

WJE evaluated the peer review of the structural design Louis Berger²⁴ for FIGG. The objective of the independent evaluation is to assess the quality and completeness of the peer review relative to the requirements of Berger's contract, applicable standards, and the standard of care for peer review services.

6.1 Document Review

Observations from review of key documents pertaining to the Berger peer review are provided in the following sections.

6.1.1 Request for Proposals (RFP)

With respect to the peer review, the Florida Department of Transportation, working through FIU, required the following:

“Prior to submittal to the OWNER, bridge plans shall have a peer review analysis by an independent engineering firm not involved with the production of the design or plans, prequalified in accordance with Chapter 14-75²⁵. The peer review shall consist of an independent design check, a check of the plans, and a verification that the design is in accordance with AASHTO, FDOT, and other criteria as herein referenced. The cost of the peer review shall be incurred by the Design-Build Firm. The independent peer review engineer's comments and comment responses shall be included in the 90% plans submittal. At the final plans submittal, the independent peer review engineer shall sign and seal a cover letter certifying the final design and stating that all comments have been addressed and resolved.”

6.1.2 Berger Agreement with FIGG

An excerpt from the scope of services in Berger's agreement with FIGG is shown below in Figure 6.1. The agreement required an independent peer review of the pedestrian bridge plans (foundation, substructure, and superstructure plans) as well as independent estimation of demands on all elements due to different load combinations based on a finite element model. The peer review was to be carried out in accordance with project and RFP requirements as well as Chapter 26 of the FDOT Plans Preparation Manual.

²⁴ Since conducting the peer review in 2016, Louis Berger has become part of WSP Global Inc. Louis Berger is referred to herein as Berger.

²⁵ Refers to Chapter 14-75 of the Florida Administrative Code

<u>Independent Peer Review Scope</u>											
1.	Louis Berger will perform Independent Peer Review for the concrete pedestrian bridge plans in accordance with the project and RFP requirements and FDOT Plans Preparation Manual (Chapter 26).										
2.	The Independent Peer Review will include the following activities:										
	<table border="1"> <thead> <tr> <th>Item #</th><th>Item Description</th></tr> </thead> <tbody> <tr> <td>1</td><td>Develop finite element model for the bridge and estimation of demands on all elements due to different load combinations</td></tr> <tr> <td>2</td><td>Peer review of foundation plans</td></tr> <tr> <td>3</td><td>Peer review of substructure plans</td></tr> <tr> <td>4</td><td>Peer review of superstructure plans</td></tr> </tbody> </table>	Item #	Item Description	1	Develop finite element model for the bridge and estimation of demands on all elements due to different load combinations	2	Peer review of foundation plans	3	Peer review of substructure plans	4	Peer review of superstructure plans
Item #	Item Description										
1	Develop finite element model for the bridge and estimation of demands on all elements due to different load combinations										
2	Peer review of foundation plans										
3	Peer review of substructure plans										
4	Peer review of superstructure plans										
3.	The Independent Peer Review will be performed for the following submittals:										
	<ul style="list-style-type: none"> a) Final Foundation and Substructure Plan Submittals b) Final Superstructure Plan Submittals 										
4.	This Independent Peer Review scope of work is for the pedestrian bridge structure components only. The elevator structures and stairways/landings are not included in this scope of work.										

Figure 6.1. Excerpt from FIGG agreement with Berger (Scope of Services)

Referring to Figure 6.1, note that the agreement requires peer review of the superstructure plans and references the RFP requirements as well as Chapter 26 of the FDOT Plans Preparation Manual.

6.1.3 FDOT Plans Preparation Manual: Chapter 26

Section 26.12 of the FDOT Plans Preparation Manual²⁶ (2015 Edition) addresses independent peer review of Category 2 bridges. The FIU pedestrian bridge is a Category 2 bridge in accordance with Section 26.3.2 because it includes post-tension components and design concepts, components, details, and construction techniques not normally used by the Florida DOT. Section 26.12 includes the following statements and requirements:

- “An independent peer review ... is an independent verification of the design using different programs and independent processes than what was used by the EOR.”
- “All independent peer review shall include... 4. Compliance with AASHTO, Department and FHWA design requirements... 7. Design results/recommendations (independent verification of design)... 10. Constructibility assessment limited to looking at fatal flaws in design approach.”

²⁶ Excerpts are from the 2015 edition, which is believed to be applicable. However, the quoted requirements are not substantially changed in subsequent editions through 2017.

6.1.4 Released for Construction (RFC) Plans

Sheet B-109 of the Superstructure Plans, which are included within the scope of the peer review, illustrate and describe the construction sequence. Figure 6.2 is an excerpt from Sheet B-109 showing erection of the main span in Stage 3. Step 2 of Stage 3 calls for “move main span from the staging area to final position.” At this stage of construction, the main span functions as a simply supported concrete truss and must carry its own weight plus any construction live load without the benefit of the back span or stay pipes, which are constructed in subsequent stages.

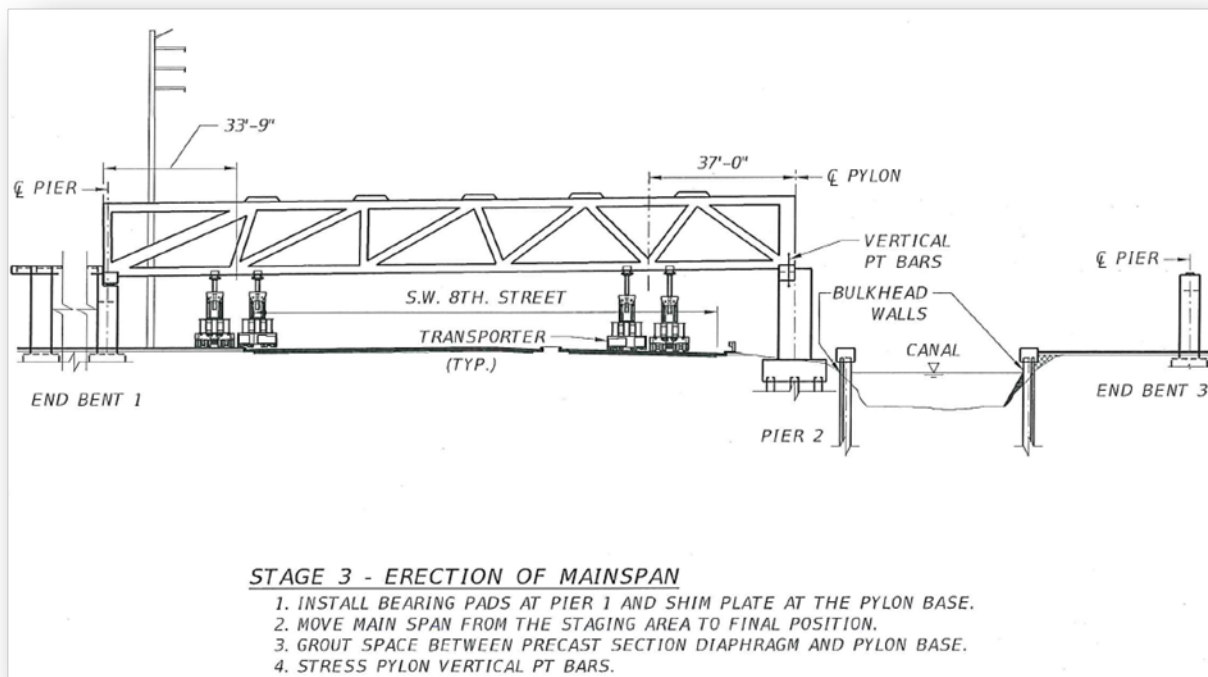


Figure 6.2. Illustration and description of Stage 3 of construction sequence from Superstructure Plan Sheet B-109

6.1.5 Berger Peer Review Comments

Under the Design Quality Management Plan for the project, review comments from all parties were submitted using the Review Comment Form, which included numbered comments and responses. Based on WJE’s review of documents produced by Berger, Berger submitted only one Review Comment Form, which pertained to the Foundation Plans (attached hereto as Exhibit 6.1.1 and 6.1.2). All but one comment pertained to foundation issues. The exception is Comment 2, which expresses concern that the first vertical vibration frequency calculated by Berger was just under the AASHTO minimum of 3 Hertz. FIGG responded that their calculations indicate a natural frequency of 3.1 Hertz. Accordingly, the comment was closed.

6.1.6 Email Correspondence

Only a few email messages were found in the Berger file. Two emails are considered noteworthy:

1. Ayman Shama, the lead peer reviewer for Berger, emailed Jamey Barbas, Berger Senior VP, on July 25, 2016. The email is provided in Figure 6.3. The message describes Mr. Shama's understanding of the bridge's structural behavior, indicating that "While the bridge is not a cable stayed bridge, but all the steps followed in analyzing and reviewing a cable stayed bridge will be followed."
2. Nick Ivanoff, Berger Executive VP, emailed Jeff D'Agosta, also with Berger, on March 15, 2018, at 3:38 p.m., less than two hours after the collapse. The email states that "Louis Berger had provided a review of the design but had nothing to do with the constructibility review or issues."

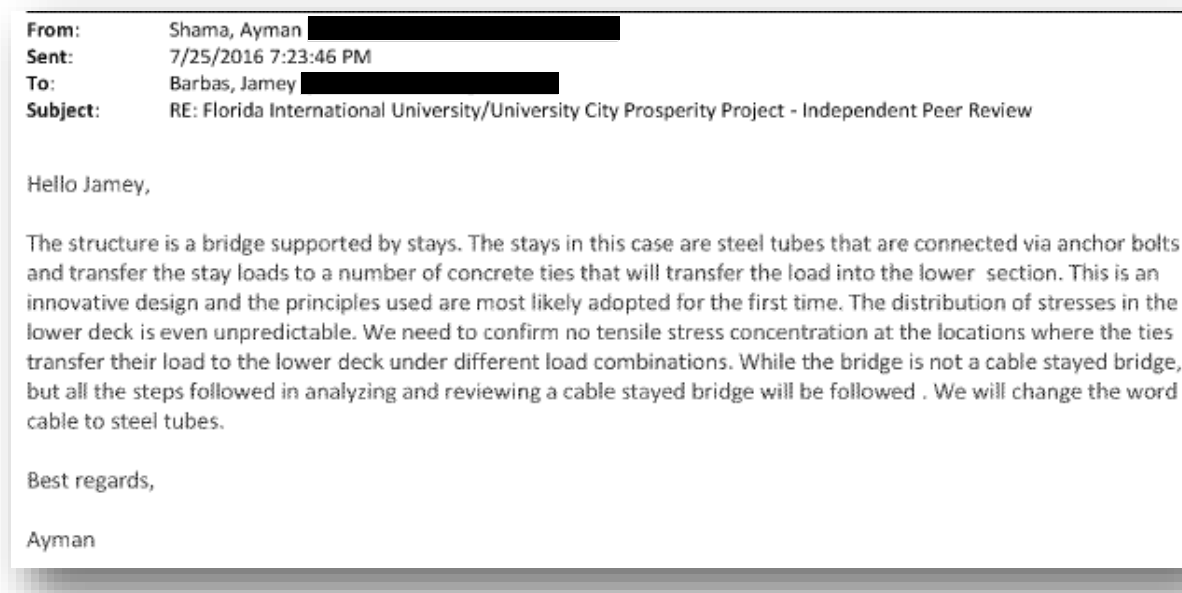


Figure 6.3. July 25, 2016, email from Ayman Shama, lead peer reviewer for Berger, to Jamey Barbas, Berger Senior VP

6.1.7 Berger Analytical Model

Berger developed an analytical model of the bridge using Adina, a finite element analysis program for linear and nonlinear analysis of solids and structures in statics and dynamics. Berger's input and output files were provided after the collapse and reviewed by WJE. WJE re-created the model using Berger's input file. Figure 6.4 shows Berger's model of the bridge.

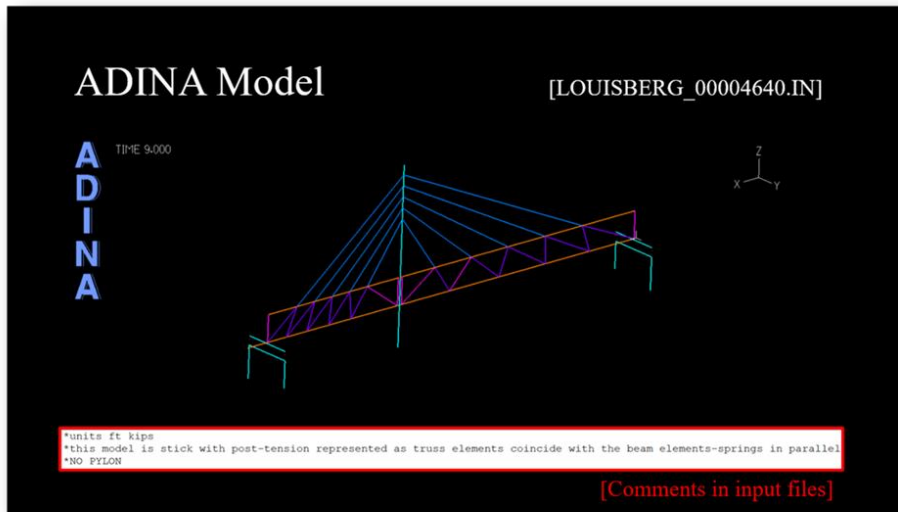


Figure 6.4. Adina finite element model of the bridge re-created from the Berger input file

As can be seen in Figure 6.4, the model includes the stay pipes as well as the concrete truss members in the main span and back span. Figure 6.5 shows the deformed shape under dead load according to Berger's model. In this model, the stay pipes work with the truss members to resist dead load from the concrete structure. However, according to the construction sequence, the concrete structure must support itself before the stay pipes are installed. As previously noted, the stay pipes are intended only to increase bridge stiffness and mitigate vibration. As such, the Berger model could not have been used to reasonably estimate the forces in the concrete truss members, which was required by their peer review contract.

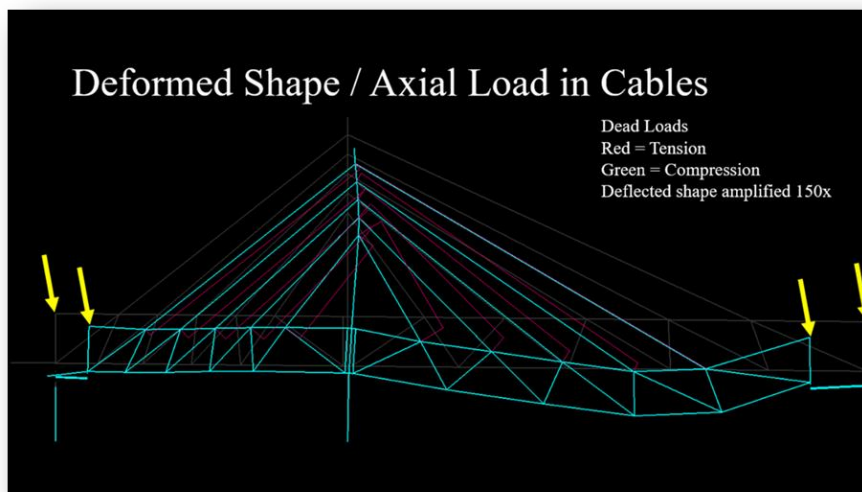


Figure 6.5. Deformed shape according to Berger model

6.1.8 Berger Web Member Checks

Although no comprehensive calculation package was found in the file, it was apparent that Berger analyzed the capacity of the web members. The web members were evaluated by Berger using *pcaColumn*, software for design and investigation of reinforced cross-sections subject to axial and flexural loads.

Berger's *pcaColumn* files included analysis of the northernmost diagonal in the main span (Member 11), a 24-inch by 21-inch rectangular member with 2-#7 bars on each face. WJE used the Berger input file to re-create their *pcaColumn* analysis in accordance with the Seventh Edition of the AASHTO LRFD Code. The graphical output, including axial forces determined by Berger, is provided in Exhibit 6.2. Their analysis consider a factored axial force of 1760 kips. Presumably, this value was based on their Adina model.

The factored axial force considering construction staging is 2365 kips, 34 percent more than the value considered by Berger. The discrepancy is apparently due to the unconservative Adina model in which the stay pipes are incorrectly assumed to work with the truss members to resist dead load of the concrete structure. As noted in the previous section, the Berger model could not have been used to reasonably estimate the forces in the concrete truss members, which was required by their peer review contract.

6.1.9 Certification Letters

Berger provided certification letters, signed and sealed by their review engineer for the foundation, substructure and superstructure final plans, stating that they conducted an independent peer review in accordance with FDOT requirements.

6.2 Expected and Provided Peer Review Documents

Based on review of the Berger file, WJE compared the peer review documents produced by Berger to those expected based on Berger's contractual requirements and the standard of care for a structural peer review of a Category 2 bridge.

WJE's findings are summarized in Exhibit 6.3.1 to 6.3.3.

6.3 Discussion

6.3.1 Quality and Completeness of Berger Peer Review.

Berger's contractual obligations are defined by their agreement with FIGG, which incorporated referenced standards for peer review, including the RFP and Chapter 26 of the FDOT Plans Preparation Manual.

The language in the agreement itself required an independent peer review of the foundation, substructure, and superstructure plans, as well as development of a finite element model for estimating demands on all elements due to different load combinations. Chapter 26 of the FDOT Plans Preparation Manual clarifies that the peer review must be independent and in compliance with AASHTO, FDOT and FHWA design requirements. Furthermore, Berger was obligated to assess the design at critical stages of the construction because construction staging was explicitly shown in the superstructure plans and because Chapter 26 requires "constructibility assessment limited to looking at fatal flaws in design approach."

As described under *Expected and Provided Peer Review Documents*, Berger's file included only a fraction of the documents expected to meet their contractual obligation and the standard of care. In particular, only

a few comments on the foundation plans were provided in the file. There were no written comments or questions whatsoever on the substructure and superstructure plans.

Berger did not attempt to assess the design at critical stages of the construction, as admitted by Berger VP Nick Ivanoff in his March 15, 2018 email. Furthermore, Berger incorrectly modeled the stay pipes in their finite element model to carry the dead weight of the concrete trusses. Therefore, the Berger model could not have been used to reasonably estimate the forces in the concrete truss members during construction or in the structure's final configuration. As such, Berger's evaluation of the capacity of Member 11 considered a factored axial force that was much less than the factored force required by the project design criteria and the AASHTO Code.


6.4 Findings

The following conclusions are based on the review described above:

- The Berger agreement with FIGG required an independent peer review of the superstructure, including review of structural integrity during construction.
- As admitted in Nick Ivanoff's email of March 15, 2018, Berger failed to consider structural integrity during construction.
- Numerous documents that would be expected based on contractual requirements and standard peer review practice were missing from the file, most notably:
 - An analytical model of the main span during and after transport
 - Verification of connection strength
 - Listing of review comments for substructure and superstructure plans (if any)
- Berger's analytical model of the completed structure was incorrect and unconservative because the stay pipes were modeled to resist dead load.


In summary, contrary to the certification letters they provided, Berger's peer review fell far short of their contractual obligations. In particular, by their own admission, Berger did not even attempt to assess the conditions at the construction stages shown in the plans (including the stage of construction at the time of collapse), which was required by their contract. Furthermore, the Berger finite element model could not have been used to reasonably estimate the forces in the concrete truss members during construction or in the structure's final configuration.

Exhibit 6.1.1. Berger peer review comments on foundation plans (page 1 of 2)

		UniversityCity Prosperity Project DESIGN QUALITY MANAGEMENT PLAN	
Doc. No.: DQP104FA	Rev. 0	07.27.16	Page DQP104FA - 1 of 3

REVIEW COMMENT FORM						
DESIGNER	1. PACKAGE: 100% Foundation Plans					
	2. SUBMITTAL: <input type="checkbox"/> FIU OVERSIGHT REVIEW <input type="checkbox"/> EARLY START OF CONSTRUCTION <input checked="" type="checkbox"/> 100% Foundation Plans <input type="checkbox"/> RELEASED FOR CONSTRUCTION <input type="checkbox"/> INTERNAL					
	3. REVIEW TYPE: <input type="checkbox"/> DCR <input type="checkbox"/> ITR <input type="checkbox"/> CR <input checked="" type="checkbox"/> IPR					
	4. DISCIPLINES: <input checked="" type="checkbox"/> Structural <input type="checkbox"/> Drainage <input type="checkbox"/> Aesthetics <input type="checkbox"/> Utilities <input type="checkbox"/> Roadway <input type="checkbox"/> Traffic <input type="checkbox"/> Geotechnical					
	5. DATE: 9/9/16		6. COMMENTS DUE DATE: 9/9/16		7. RETURN COMMENTS TO: M. Feliciano	
	8. RESOLUTION MEETING DATE & TIME: 9/12/2016		9. RESOLUTION MEETING LOCATION: Conf. Call		10. Concurrent Review? Checked for overlap by Design Manager: <input type="checkbox"/> Yes <input type="checkbox"/> No (DM initials)	
	11. REVIEWER: Ayman Shama		12. ORGANIZATION: <input type="checkbox"/> FIU <input type="checkbox"/> MCM <input type="checkbox"/> FIGG <input checked="" type="checkbox"/> Louis Berger			
No.	Dwg. / Pg.	Comment	Disp.	Response	Disp.	Ver.
1	B-2	Please remove the statement about scour since no scour analysis was performed.	D	The scour analysis was performed for the bulkhead wall on the north side of the project. Therefore, drawing B-2 makes reference to scour since the design of the wall accounts for it.	closed	
2		Under vibrations: based on the analysis done by LB the structure satisfied the horizontal vibration criteria. AASHTO requires the first vertical natural frequency to be higher than 3 Hz. The value obtained is 2.9. We recommend reducing the thicknesses of the pipe stays to achieve higher natural vertical frequency	D	According to our analysis, the natural frequency of the bridge is approximately 3.1 Hz.	closed	
3	B-9	The table shows that scour and down drag are not accounted for. Nevertheless, the equation in the LHS shows that they are included. Please change the equation so that it reflects the factor design load only.	D	For FDOT projects, it is customary to show the entire equation even though the values for the net scour and downdrag are equal to zero or N/A. It is understood that the nominal bearing resistance is equal to the factored design load divided by the resistance factor.	closed	
4		It is not clear if the minimum tip elevation is the value started with in the FB-Deep analysis or this is the anticipated tip elevation of the pile. This tip elevation is inconsistent with the pile length of 32 ft in the table. The 32 ft pile length is consistent with the results from FB-Deep.	D	The Pile Order Length in the Pile Data Table is what is necessary in order to satisfy the required design axial loading. Length of the pile will be confirmed during construction with PDA.	closed	
RESOLUTION MEETING FINAL CONCURRENCE		13. DESIGNER Sign & Date:		14. REVIEWER Sign & Date:		
INITIAL DISPOSITION CODES:		C = Will Comply F = Further Clarify		D = Delete Comment N = Incorporate Next Submittal		FINAL DISPOSITION CODES: C D N
Written by: ADH		Revised by:		Approved by:		
Date: 07.27.16		Date:		Date:		

Exhibit 6.1.2. Berger peer review comments on foundation plans (page 2 of 2)

		UniversityCity Prosperity Project DESIGN QUALITY MANAGEMENT PLAN	
Doc. No.: DQP104FA	Rev. 0	07.27.16	Page DQP104FA - 2 of 3

No.	Dwg. / Pg.	Comment	Disp.	Response	Disp.	Ver.
5		The geotechnical report states that it is anticipated that the required compression capacity of about 433 kips will be achieved at -15 ft. At this time we recommend adhering to the results of FB-Deep as it is the most reliable tool to evaluate the capacity until the real capacity is validated during construction by PDA. The 433 nominal capacity in the table is consistent with a tip elevation at -30 ft.	D	See response to comment 4.	closed	
6		The lateral capacity of the 24 inch pile was checked against the case of the extreme-2 load using simple hand calculations and moment curvature analysis. The capacity was found adequate.	C	Agree.	closed	
7	B-7,B-11, B-13	Please locate foundations Type-1 and Type-3 at the same bearing strata to avoid the likelihood of differential settlement effects at the south pier. Currently elevations of the bottom of foundations for the two footings are 4.00 and 0.50. Try to locate the bottom of foundations directly on top of the hard limestone, or at least use elevation 0.50 for the two footings	D	It is our opinion that the contact pressures at these foundation locations are well below the recommended bearing capacity values. Both Type 1 and Type 3 footings are bearing on top of the limestone layer and no dissimilar materials were observed at these bearing elevations based on the boring performed. Furthermore, currently, the estimated settlements at these footing locations are about 1/4 inches, or significantly less than 1 inch and adequate. Hence, differential settlement is not a concern.	closed	
8	B-7,B-15, B-16	Please locate foundations Type-6 and Type-7 at the same bearing strata to avoid the likelihood of differential settlement effects at the north pier. Currently elevations of the bottom of foundations for the two footings are 4.00 and 0.50. Try to locate the bottom of foundations directly on top of the hard limestone, or at least use elevation 0.50 for the two footings	D	It is our opinion that the contact pressures at these foundation locations are well below the recommended bearing capacity values. Both Type 6 and Type 7 footings are bearing on top of the limestone layer and no dissimilar materials were observed at these bearing elevations based on the boring performed. Furthermore, currently, the estimated settlements at these footing locations are about 1/4 inches, or significantly less than 1 inch and adequate. Hence, differential settlement is not a concern.	closed	
9	B-11	It seems that the bottom foundation reinforcement is governed by the minimum reinforcement ratio. It was expected for the square foundation to have the same number and size of bars in the two perpendicular directions. Currently there are 14-9F01 in one side and 14-7F01 for the other side.	D	For the Type I footing, the bottom flexural reinforcement is sized based on the bending moment at the face of the column. Although the design pressure is the same in both directions, the bending moment is larger in the transverse direction because the column is rectangular and the lever arm is longer than in the longitudinal direction. Therefore, more reinforcing steel was provided in the transverse direction.	closed	
10	B-26 through B-28	It is recommended for bar schedules to add one more column for the bar shape.	D	The bar lists are produced with an FDOT application; therefore, the layout of the table cannot be modified. Bar shape is shown in the 5th column (TYP BAR) and references the FDOT Standard Bar Bending Details (Index No. 21300).	closed	

RESOLUTION MEETING FINAL CONCURRENCE	13. DESIGNER Sign & Date:	14. REVIEWER Sign & Date:
INITIAL DISPOSITION CODES:	C = Will Comply D = Delete Comment F = Further Clarify N = Incorporate Next Submittal	FINAL DISPOSITION CODES: C D N QC VERIFY: Incorporation of C or N comments and agreement with D comments. (Design Task Mgr. Initials)
Written by: ADH	Revised by:	Approved by:
Date: 07.27.16	Date:	Date:

**Exhibit 6.2. pcaCOL
interaction diagram for
Member 11 per AASHTO
LRFD 7th Edition**

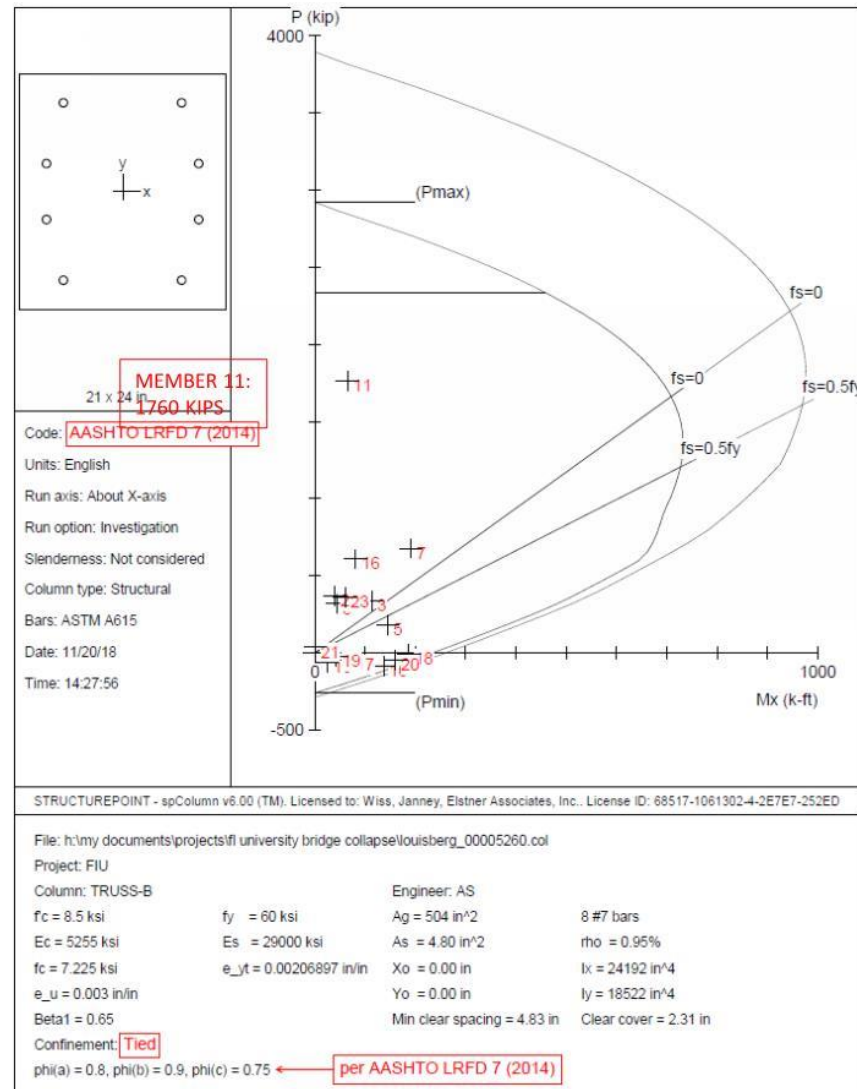


Exhibit 6.3.1

WJE EVALUATION OF EXPECTED AND PROVIDED PEER REVIEW DOCUMENTS

Items shown in **blue type** in the Expected Document(s) column were not found in the peer review file

Category	Expected Document(s)	Document(s) Provided by Berger
1. Design Criteria	Document identifying relevant FDOT, AASHTO, and FHWA criteria for structural design and peer review.	Relevant criteria were found in the file.
2. Input Calculations for Analytical Model	Calculation of loads, including wind loads. Calculation of truss geometry, material properties, and section properties used for input into the analytical model by hand calculation, Mathcad, Excel, proprietary software or other means.	None found in file
3. Analytical Model	Analytical models for all relevant construction stages, including, but not necessarily limited to the following: 1. Main span simply supported (with and without prestressing of exterior diagonals) 2. Transport with SPMTs 3. Two-span configuration (without stay pipes) 4. Final configuration The model should be consistent with the construction sequence shown on the drawings. Include all relevant load combinations (construction and in-service).	Only an analytical model in the final configuration was provided (using ADINA). The model was not consistent with the construction sequence. In-service load combinations were considered for the final configuration.
4. Verification of Analytical Modeling	Peer review verification of analytical modeling would include calculations confirming model geometry, loads, units, and assumptions. Verification is done to ensure no errors were made during the modeling and the model is behaving as expected. Verification of analytical models typically is performed by hand calculation, Mathcad, or Excel and at a minimum would include the following: 1. Confirmation the analytical model is calculating the weight of the bridge correctly 2. Confirmation external loads were applied to the bridge properly and the analytical model is distributing correctly.	No files verifying the analytical model were found in the file.

Exhibit 6.3.2

WJE EVALUATION OF EXPECTED AND PROVIDED PEER REVIEW DOCUMENTS

Items shown in **blue type** in the Expected Document(s) column were not found in the peer review file

Category	Expected Document(s)	Document(s) Provided by Berger
5. Verification of Sectional Strength of Bridge Elements	<p>Calculation of axial, flexural, shear and torsional sectional strength of main members by hand calculation, Mathcad, Excel, proprietary software or other means. Sectional strength is to be calculated in accordance with AASHTO specifications using appropriate strength reduction factors.</p> <p>Primary members include footings, pier columns, deck elements, truss diagonals, canopy elements, pylon, and stay pipes.</p> <p>Results are compared to calculated forces from analytical model including appropriate load factors.</p>	<p>PCACOL was used to verify the combined flexural and actual strength of strength of selected substructure and truss members. The strength reduction factor used in PCACOL appears to be from ACI 318 rather than AASHTO, which is conservative but incorrect. Otherwise, no sectional strength calculations were found in the file.</p> <p>No calculations of shear or torsional strength for any members were found in the file. Examples of members in which shear or torsional strength is important include footings, pier columns, and deck diaphragms.</p>
6. Verification of Strength of Connections	<p>Calculation of connection strength by hand calculation, Mathcad, Excel, proprietary software or other means. Connection strength is to be calculated in accordance with AASHTO specifications using appropriate strength reduction factors.</p> <p>Primary connections include pier column/footing connection, superstructure bearings, connections of diagonal web members to canopy and deck, post-tensioning anchorage zones, and connection of stay pipes to pylon and canopy.</p>	<p>A Mathcad calculation of the connection strength for the connection of the stay pipes to the pylon was provided. The calculation was performed in accordance with ACI 318 criteria, which is permitted by AASHTO.</p> <p>Otherwise, no calculations of connection strength were found in the file.</p>
7. Verification of Serviceability	<p>Calculations for serviceability criteria:</p> <ul style="list-style-type: none"> Deflection Cracking at Service Load Vibration <p>Such checks Please say that again re the bridge is serviceable.</p>	<p>Comment 3 on the Foundation Plans indicated that the horizontal vibration frequency met AASHTO criteria but expressed concern about the frequency of vertical vibration. Otherwise, no serviceability-related calculations were found in the file.</p>

Exhibit 6.3.3

WJE EVALUATION OF EXPECTED AND PROVIDED PEER REVIEW DOCUMENTS

Items shown in **blue type** in the Expected Document(s) column were not found in the peer review file

Category	Expected Document(s)	Document(s) Provided by Berger
8. Verification of Foundation strength	Calculation of vertical and lateral forces acting on the pile foundations relative to the resistance determined by the geotechnical report.	The expected documents were found in the file.
9. Review of Drawings for Completeness and Compliance with Design Criteria	<p>Listing of comments, questions, and/or drawing markups identifying concerns or comments relating to completeness or compliance with design criteria for each portion of the drawings included in the scope:</p> <ul style="list-style-type: none"> Foundation Plans Substructure Plans Superstructure Plans 	No drawing markups were found in the file. Only a few comments on the foundation plans were provided in the file. There were no comments or questions whatsoever on the substructure and superstructure plans.
10. Constructability Assessment	Listing of comments and/or drawing markups identifying concerns or comments relating to constructability.	No drawing markups or comments relating to constructability were from the file.

7 EVALUATION OF TILT EXCEEDANCES DURING MAIN SPAN TRANSPORT

WJE studied twist exceedances during transport of the main span. The objective was to assess the possible effect of exceeding the maximum allowable transverse twist on damage to the web members at the north end of the main span.

7.1 Background on Transport of Main Span

The design drawings prepared by FIGG called for the main span to be precast. MCM set up a casting yard just south of SW 8th Street and moved the precast span into its final position using self-propelled mobile transporters (SPMTs). After an initial lift and roll test on the evening of March 9, 2018, the move started at 4:20 a.m. on March 10, and the span was set into position at 12:27 p.m. As a subcontractor to MCM, Barnhart Crane & Rigging Company (Barnhart) was responsible for transport of the main span, including design and operation of the transporter system. Barnhart subcontracted to Bridge Diagnostics, Inc. (BDI) for monitoring of strain, tilt, and twist during the move.

7.2 Document Review

Observations from review of key documents pertaining to distress in the north end and transverse tilt during the move are provided in the following sections.

7.2.1 Photos of North-End Distress before and After Move

As described in the following paragraphs, photographic evidence indicates that cracks in the north end were much worse several hours after the move than they were before. The widened cracks were observed shortly before the posttensioning bars in Member 11 were de-stressed.

Exhibit 7.1.1 and 7.1.2. Barnhart provided a close-up photograph of the west side of the north-end diaphragm taken on March 8, 2018, prior to the move. As shown in Exhibit 7.1.1, a narrow diagonal crack can be seen on top of the diaphragm. Corradino provided a photograph (also shown in Exhibit 7.1.1) of the same area taken on March 10 at 3:14 p.m., after the move but before de-stressing of Member 11. After the move and placement of the main span in its final location, the narrow crack widened by more than 0.5 inches and was accompanied by spalling of the north face of the diaphragm. Exhibit 7.1.2 provides a similar comparison for cracks on the east side of the north end diaphragm.

Exhibit 7.1.3. A photograph taken on February 24, 2018 by BPA shows a diagonal crack along the bottom of Member 11 on the east face. The crack width appears to be approximately 0.03 inches in width at that time. Shortly after the move, at 12:30 p.m., a photo by FIGG shows the crack to be about the same width, although it is difficult to be certain because the member was apparently painted by the contractor prior to the move. However, less than three hours after the move, the crack widened more than tenfold to approximately 0.50 inches, based on a photograph taken by Corradino at 3:14 p.m.

7.2.2 SPMT Bridge Movement Monitoring Plan

The SPMT Bridge Movement Monitoring Plan is Submittal #00400-6.A. Page 4 of the plan indicates a 0.5-degree tolerance for the difference in rotation angle between Nodes 2 and 4, the points at which the main span is supported during the move. These points are illustrated on Figure 7.1. The difference in rotation between the north and south supports is referred to as twist.

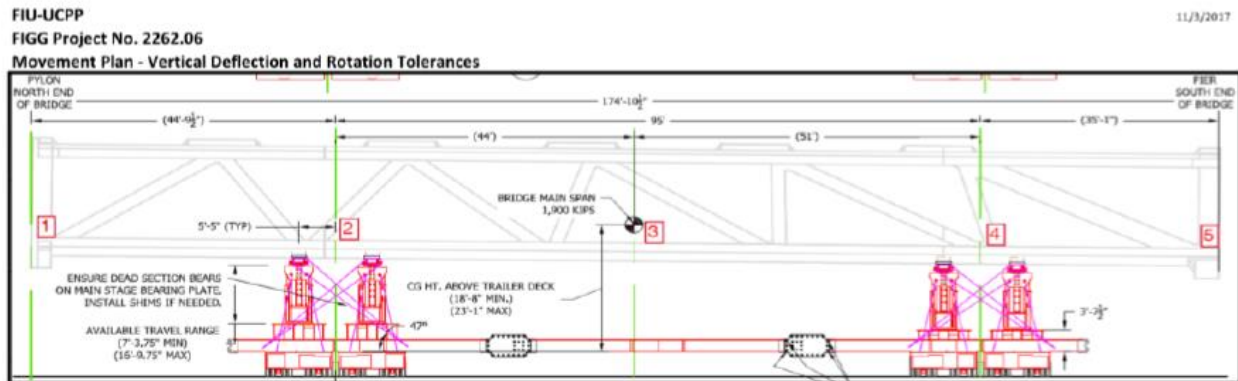


Figure 7.1. Schematic of movement plan from SPMT Bridge Movement Monitoring Plan

Submittal #00400-6.A includes the following discussion regarding the relationship between twist and cracking:

“Maximum limit for twist/torque that is achievable by Barnhart’s current equipment and methods where there likely would be temporary cracks observed on selected areas of certain struts (localized) for the temporary conditions during the bridge movements once the span is in the final position and the torque/twist is removed, any cracks that may have occurred during the movement would likely close and would be small in width, if measurable at all. There may be selected nonstructural cracks in select areas, if any, that may need to be sealed (Per FDOT Standard Specifications for Roadway Bridge Construction, 2015 – Section 400 Concrete Structures) once the span is in the final position...”

In summary, this statement acknowledges that the twisting during the main span move is likely to cause small cracks, which would close after the main span is supported in his final location. Apparently the 0.5-degree limit for the difference in rotation between support points (twist) was chosen because Barnhart believed that twist within that limit was achievable using their proposed methods and equipment²⁷.

7.2.3 BDI Monitoring Report

The BDI Monitoring Report is entitled “Florida International University Pedestrian Bridge – Monitoring of Lift and Move Procedures.” The final version is dated April 4, 2018 (20 days after the collapse), and was submitted to Barnhart. The executive summary on page 1 includes the following statements regarding monitoring of twist during the move:

- “The primary goal of the project was to monitor twist of the truss-girder span during the move and at final span placement. Vertical displacements and concrete surface strains were also measured at specified locations for the record.”
- “Measurements were recorded on a continuous basis during the initial lift and during a relatively short roll test. The roll test was done to verify twist measurement sensitivity during actual operations and BCR’s²⁸ ability to control adjustment of twist.”

²⁷ FIGG originally requested a much smaller tolerance.

²⁸ BCR refers to Barnhart Crane & Rigging

- “BCR was in charge of all rigging and moving operations while BDI’s role was to provide on-site feedback on the twist of the girder during movement and placement. BDI personnel operating the monitoring system were in direct contact with BCR’s transport operators and were authorized to stop movement at any time. Any time the girder twist approached the limit, transport movement was stopped and BCR adjusted the alignment.”

The 0.5-degree twist tolerance is acknowledged on page 9:

- “A BCR representative was with the BDI monitoring system operator and viewing the screen while tilt and rotation readouts displayed. Any time that twist data plot approached ± 0.5 degrees, an ‘All Stop’ command was given, transport movement was halted, and adjustments to the trailers were performed.”

The 0.5-degree twist limit was exceeded on at least two occasions during the move. These two points are indicated with red arrows in Exhibit 7.2.1²⁹, which is a plot of twist between support points versus time. As shown in Exhibit 7.2.1, a maximum twist of 0.84 degrees (168 percent of the maximum limit) occurred at 4:48 a.m. on March 10.

Most of the excessive twist is due to rotation of the north support. As can be seen in Exhibit 7.2.2³⁰, rotation at the north support was 0.97 degrees at 4:48 a.m. on March 10, when the maximum twist occurred. At the same moment, the south support point was rotated in the same direction (canopy rotated to the west). As shown in Exhibit 7.2.3³¹, the rotation at the south support was 0.13 degrees. Thus, the difference in rotation was $0.97 - 0.13 = 0.84$ degrees.

The BDI report discusses this tilt exceedance. Specifically, BDI points to Figure 7 in their report, which is reproduced herein as Exhibit 7.2.4. The figure shows spikes in the rotation and twist data. In particular, there is a significant spike at 4:48 a.m. on March 10 that is not matched in the strain measurements, although there is a smaller peak in the strain measurement at that time. BDI indicates that the spike “was observed to be an artifact of the tilt sensor dynamics.” However, BDI acknowledges that the “peak static twist value” at this time was approximately 0.65 degrees, which exceeds the 0.5 degree limit. Also, there is concurrent peak in strain readings at 4:48 a.m., indicating that the actual peak static twist value is greater than 0.65 degrees.

As previously described, twisting causes stresses between the support points, which may cause cracking. However, the north end of the main span is free to rotate, and cracking is not caused by twisting per se. Rather, the concern with respect to damage at the north end is transverse bending of the web members due to the rotation, which is addressed in Section 7.3 below.

7.3 Structural Analyses

A finite element model of the main span was developed and analyzed using Abacus, finite element software for structural analysis of complex systems (see Section 5.1.1). An overview of the model is shown in Exhibit 7.3.1.

²⁹ From BDI monitoring report Figure 32. Red arrows and dashed lines indicating tilt exceedances added by WJE.

³⁰ From BDI monitoring report Figure 29. Red lines and boxed note added by WJE.

³¹ From BDI monitoring report Figure 21. Red lines and boxed note added by WJE.

To evaluate stresses, the maximum observed rotation angles described above were imposed on the model. A plot of the deformed shape is shown in Exhibit 7.3.2. As can be seen in this exhibit, the rotation at the north transporter system support causes an even greater rotation at the north end. The resulting westward deformation at the north end of the canopy is 4.26 inches.

The tilt of the canopy causes transverse bending stress near the base of the web members at the north end — in the same way that tilting a patio umbrella causes bending of the support pole. A second-order³² analysis was used to capture the effect of the tilt. To isolate the effect of the canopy tilt, the effects of self-weight and post-tensioning were subtracted from the combined effects of self-weight, post-tensioning, and tilt. A plot of the tilt-induced stresses at the base of the north support members is shown in Exhibit 7.3.3. The green color indicates that the tilt causes a tensile stress of more than 500 psi on the east face of the northernmost vertical web member (Member 12), which is in the region where cracks were observed prior to the collapse. This peak stress would reduce to about 400 psi if the maximum rotation readings are reduced to account for spikes in rotation readings due to sensor dynamics.

7.4 Discussion

A 0.5-degree twist limit was established to control cracking. However, this limit was exceeded. The full degree of the exceedance is somewhat uncertain due to “spikes” in the rotation and twist readings.

Cracks in the north-end diaphragm and Member 11 were evident prior to the move and widened greatly after the move, although not immediately afterward. Obviously, the cracks occurring before the move were unrelated to the move. The nature and cause of these cracks is discussed in Section 2. There are four possible contributors to widening of the cracks:

1. The rotation associated with the twist exceedances caused high transverse bending stress near the base of the northernmost vertical. Although the calculated stress is somewhat less than that needed to initiate cracking, the stress from the tilt would tend to exacerbate cracking in the region.
2. Prior to the move, the north end diaphragm was supported on shoring at close intervals. After the move, the diaphragm was supported on temporary shims. The shims were nearly continuous except for a 38-inch gap at the centerline. The truss reaction at the center of the north-end diaphragm spanned the gap, increasing shear and bending stresses in the north-end diaphragm relative to the diaphragm stresses in the casting yard.
3. Prior to the move, the north-end diaphragm and Member 11 exhibited distress related to the northward sliding of Members 11 and 12. Immediately prior to the bridge being lifted by the transporter, the force in Member 11 would have been approximately equal to the force at the time of the failure. The horizontal force was temporarily relieved when the transport assembly lifted the main span from the casting yard and was then reapplied when the span was set in its final location. Thus, the move applied an additional load cycle to a connection that was near its strength limit. Damage can increase significantly due to even one additional load cycle when the load is near the strength limit.
4. For the reasons described in item 3, after the move, the north diagonal connection was near its strength limit. Cracks can widen over time due to sustained load near the strength limit.

There is not enough information to assess the degree to which each of these factors contributed to the increase in distress after the move. In WJE’s opinion, all of these factors could have contributed to the damage at the north end and ultimately the collapse.

³² Second-order analysis, also known as P-delta analysis, captures the effect of deformations on stress

Finally, it should be noted that the OSHA report³³ claims that cracks began to appear “as they began to de-stress the PT bars of Member 11.” For reasons explained in Section 8, WJE does not agree with this finding. In particular, the cracking shown in the right photo in Exhibit 7.1.1 occurred before de-stressing. The OSHA report also maintains that lateral bracing in the casting yard provided “considerable lateral support to diaphragm II.” Based on review of the OSHA photographs, it is WJE’s opinion that the location and stiffness of the support connected to the north diaphragm was insufficient to significantly reduce the pattern of distress.

7.5 Findings

In summary, this study shows that cracks in the region of the connection of Members 11 and 12 to the deck increased dramatically after the move from the casting yard to the final location. The tilt associated with exceeding the established twist limits caused high stresses in the region. Along with other factors, this stress may have contributed to damage in the region and ultimately to the collapse.

³³ Occupational Safety and Health Administration, "Investigation of March 15, 2018 Pedestrian Bridge Collapse at Florida International University, Miami, FL," June 2019.

Exhibit 7.1.1. Crack in west side of north end diaphragm before and after move



Photo 12 from BPA crack inspection after formwork/scaffolding removal. February 28. Crack is indicated by blue arrows. Crack width ruler appears to indicate 0.014 inches.



March 10 photo by Corradino showing same crack after move at 3:14 p.m. The yellow arrow points to the west side of the same #11 bar in each photograph.

Exhibit 7.1.2. Crack in east side of north end diaphragm before and after move



Photo 13 from BPA crack inspection after formwork/scaffolding removal. February 28.



March 10 photo by Corradino showing same crack after move at 3:14 p.m.

Exhibit 7.1.3. Diagonal “wedge” crack at Member 11 before and after move



Diagonal “wedge” crack along the bottom of Diagonal 11 on the east face. Photo taken by BPA prior to the move on February 24, 2018.



Same diagonal “wedge” crack shortly after the move. Photo taken by FIGG at about 12:30 p.m. on March 10.



Same diagonal “wedge” crack 3 hours after the move. Photo taken by Molina at about 3 p.m. on March 10.

Exhibit 7.2.1. Twist rotation between support points versus time

(From BDI monitoring report Figure 32. Red arrows and dashed lines indicating tilt exceedances added by WJE.)

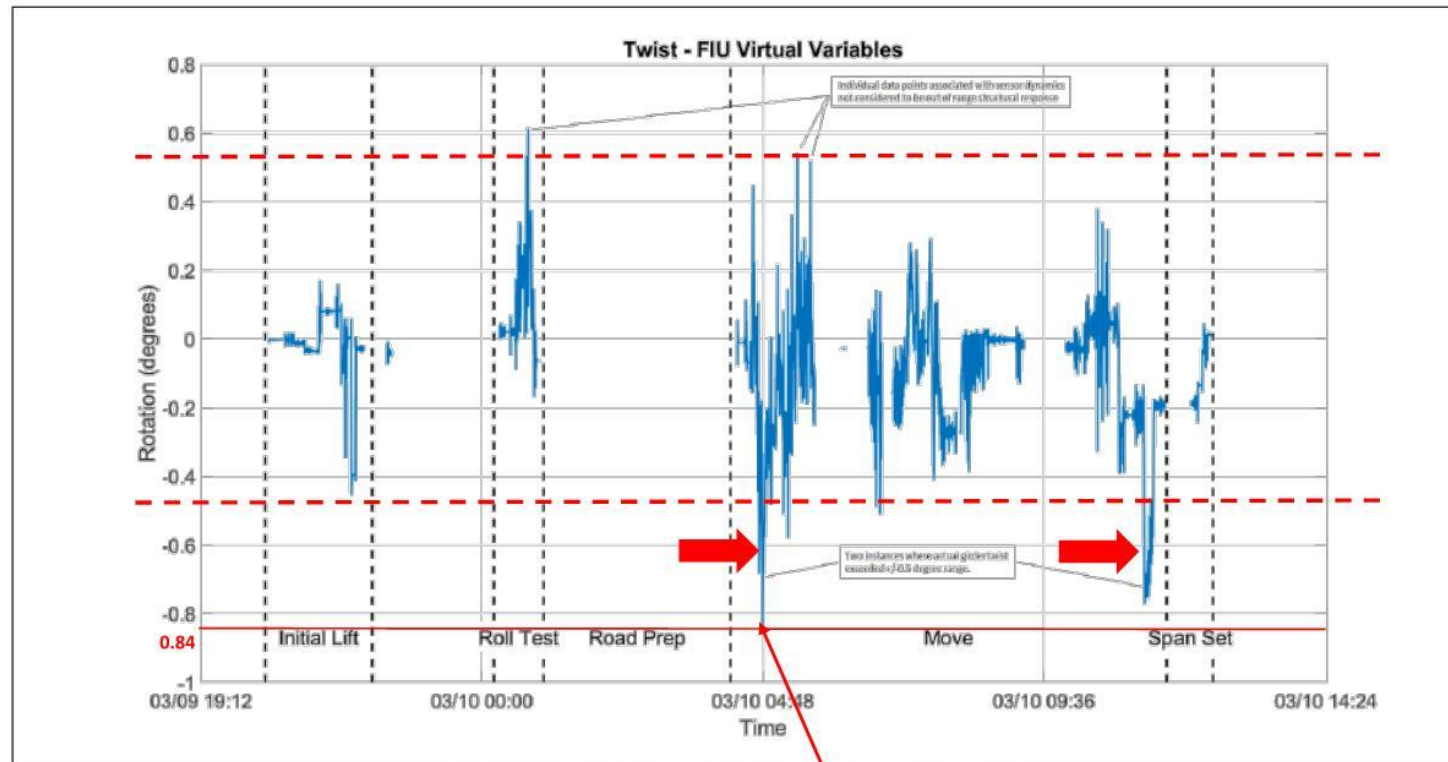


Figure 32 – Girder Twist – Difference in angle between Sections J & L

Difference in rotation between north and south supports: 0.84°

Exhibit 7.2.2. Tilt meter readings at north support versus time
(From BDI monitoring report Figure 29. Red lines and boxed note added by WJE.)

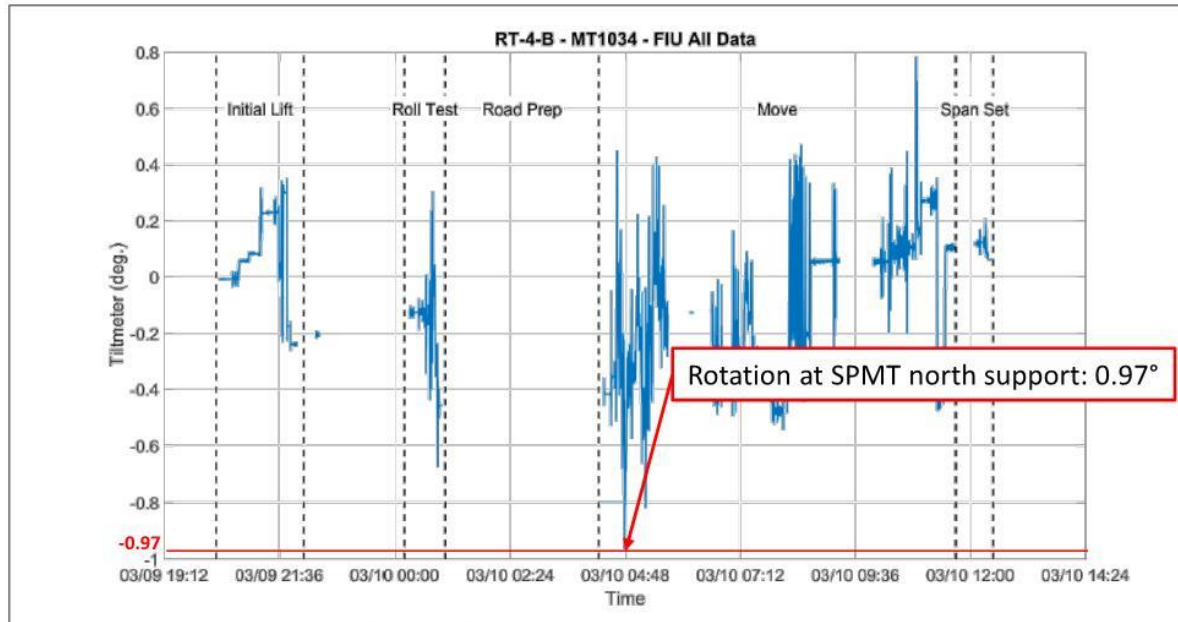


Figure 29 – Transverse rotation at Cross-Section 4 – Transverse Position B

Exhibit 7.2.3. Tilt meter readings versus time

(From BDI monitoring report Figure 21. Red lines and boxed note added by WJE.)

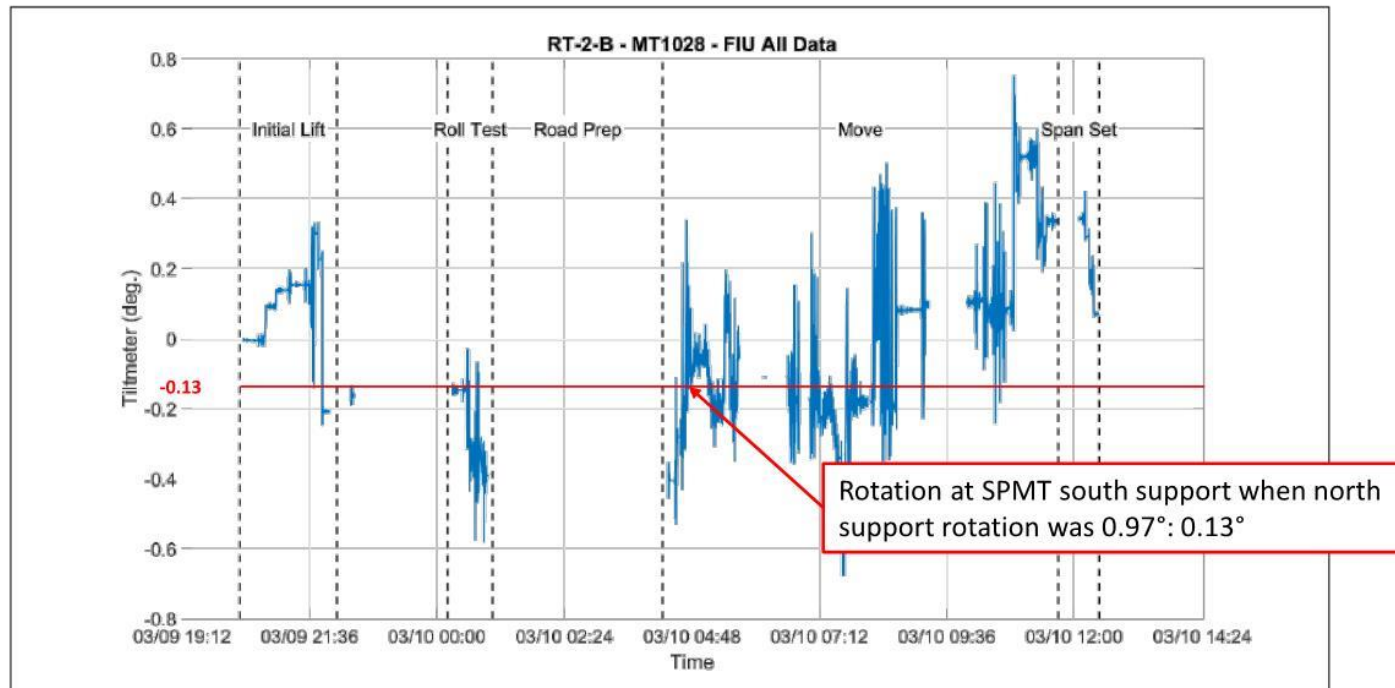


Figure 21 – Transverse rotation at Cross-Section J – Transverse Position B.

Exhibit 7.2.4. Twist, rotation and strain readings versus time

(From BDI monitoring report Figure 21. Boxed note added by WJE.)

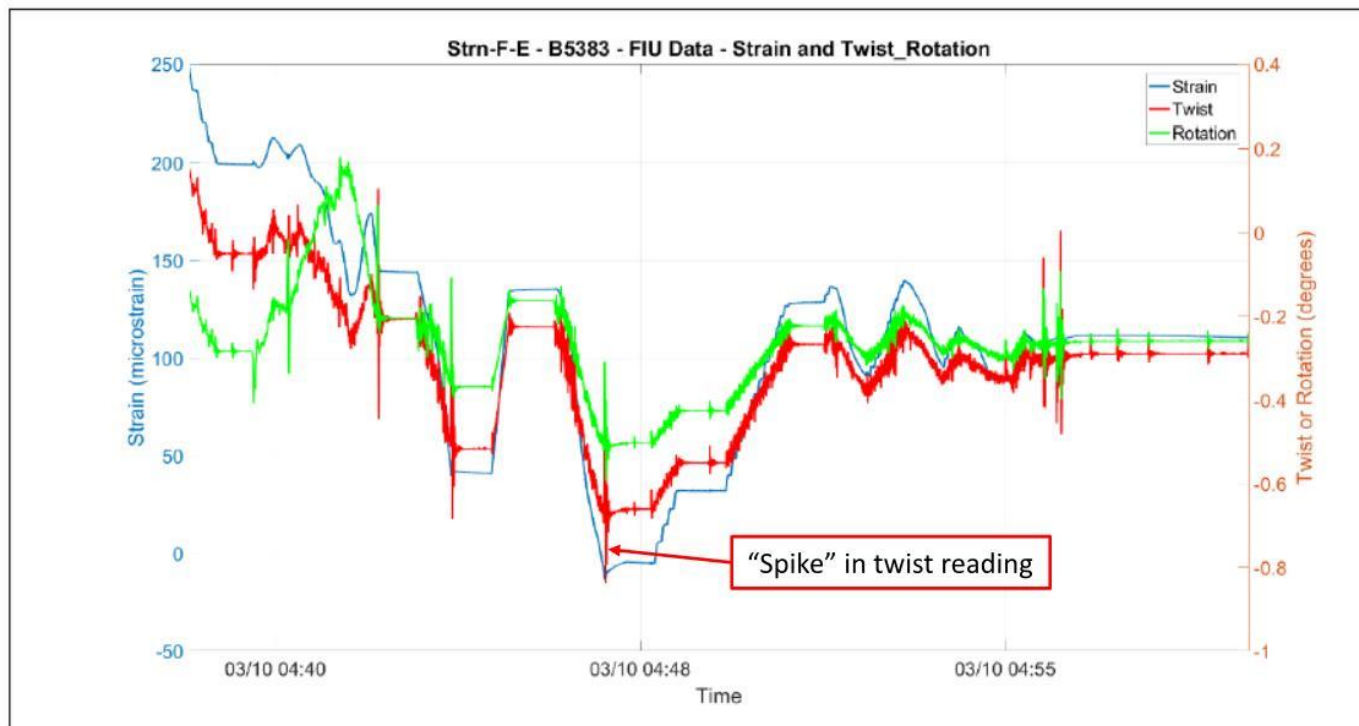
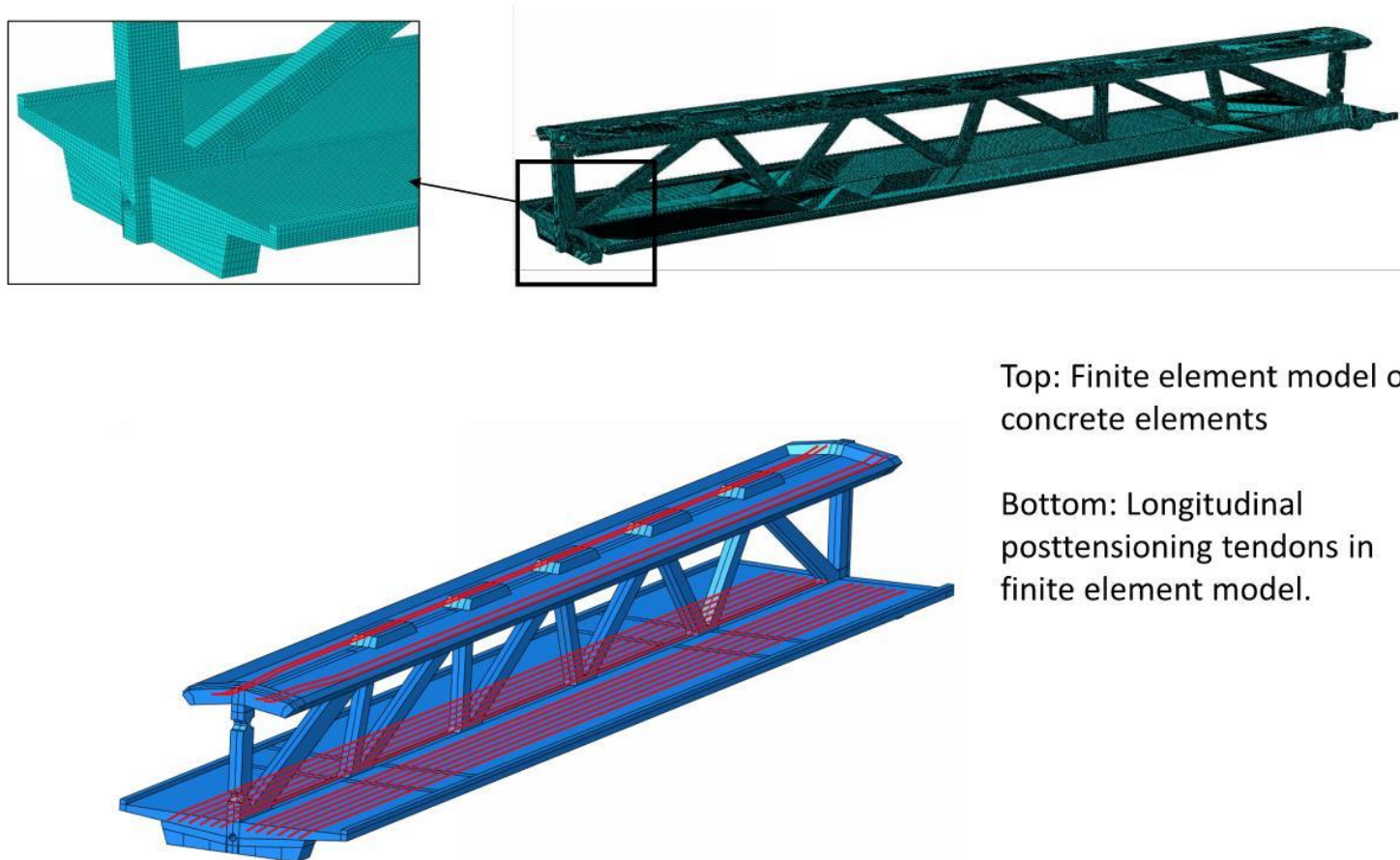


Figure 7 – Measured strain at Section F (east) with corresponding twist and rotation measurements

Exhibit 7.3.1. Finite element model



Top: Finite element model of concrete elements

Bottom: Longitudinal posttensioning tendons in finite element model.

Exhibit 7.3.2. Twist deformation looking southwest (deformations exaggerated 20x)

- Self-weight and PT effects are subtracted

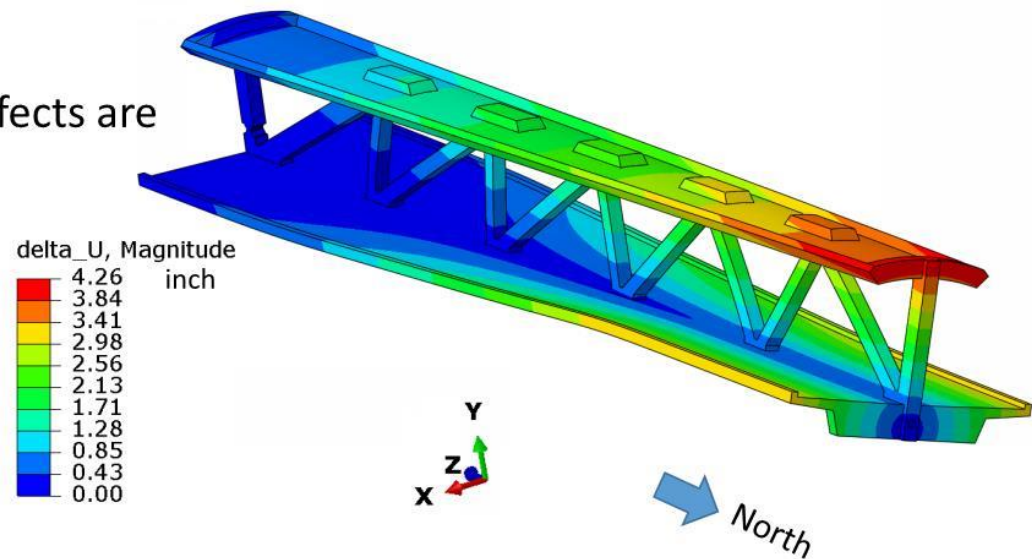
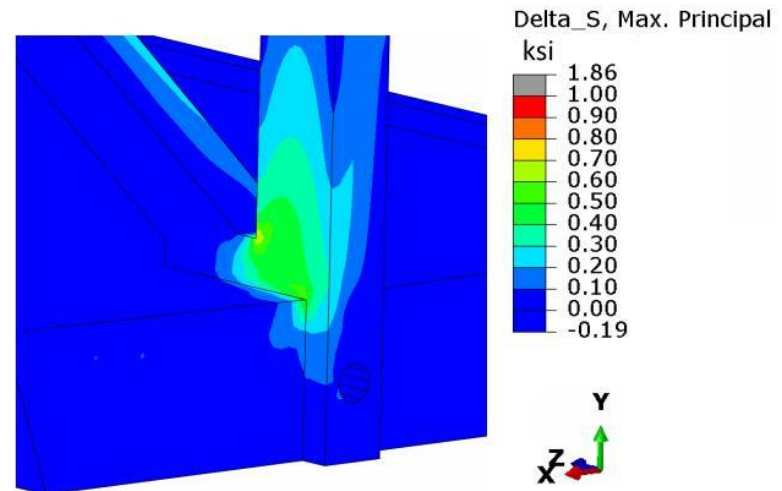


Exhibit 7.3.3. Maximum principle tensile stress due to twist only

Looking southwest at north end and east face. Green color indicates more than 500 psi tensile stress.

Dark blue areas have zero tensile stresses or they are compression dominant



8 RE-STRESSING OF MEMBER 11

WJE evaluated crack monitoring during re-stressing of Member 11 five days after the main span was set in its final position and Member 11 was de-stressed. The objective of the evaluation is twofold: 1) determine the extent to which cracks in the north diaphragm of the main span were monitored during re-stressing of the northernmost diagonal, and 2) assess the means by which changes in crack width could have been monitored and the likelihood of detecting increases in crack width.

8.1 Timeline and History of Cracking near the North End

The following is a brief timeline of events that substantially changed forces in the truss members, which led to distress near the north end and the eventual collapse.

Event	Date/Approximate Start Time
Shoring removal in casting yard	February 24, 2018
Initial lifting by transporter	March 9, 2018
Placement of the main span on the south pier and central pier	March 10, 2018, 12:27 p.m.
De-stressing of Member 11 by Structural/VSL	March 10, 2018, 4:17 p.m.
Re-stressing of Member 11 by Structural/VSL	March 15, 2018, 11:51 a.m.

The distress associated with the above events is described in the following paragraphs.

February 24-28, shoring removal. Cracks in the north-end truss members were first reported by BPA (on-site construction inspectors) in a February 28 email to FIGG. The cracks were observed shortly after removal of the shoring in the casting yard. Exhibit 8.1.1 shows narrow cracks on the top of the north-end diaphragm. Exhibit 8.1.2 shows a crack in the chamfer at the base of Member 11 visible on February 24. This crack is referred to as the “wedge” crack.

March 10, after the move. The cracks in the north end worsened significantly by mid-afternoon on March 10, 2018, after the main span was moved and supported in its final position between the south pier and central pier. Placement of the span in its final position would have resulted in a compressive force of more than 1700 kips in Member 11³⁴ due to the combined effects of dead load and post-tensioning. Exhibit 8.2.1 shows wide cracks on the top of the north-end diaphragm that were apparent several hours after the move, but prior to de-stressing. These photos were taken at about 3:10 p.m. on March 10. The cracks shown in Exhibit 8.2.1 are much wider than those visible before the move in Exhibit 8.1.1. Also, as can be seen by comparing Exhibit 8.1.2 and Exhibit 8.2.2, the wedge crack also widened significantly after the move.

March 10, after de-stressing. Even though de-stressing would have reduced the compressive force in Member 11, Structural/VSL reported that as they began to de-stress the post-tensioning (PT) bars of Member 11, cracks began to appear at multiple locations. The Structural/VSL supervisor took pictures of the cracks and forwarded them in an internal text stating “it cracked like hell.” SW 8th Street was re-open to traffic around 8 p.m. that evening.

On March 12, 2018, MCM’s project manager emailed several photographs of distress to FIGG, the first crack photos sent to FIGG since February 28. The photographs were taken near the north end of the main

³⁴ See Table 5.3

on March 12, two days after de-stressing of Member 11³⁵. Exhibits 8.3.1 and 8.3.2 show that cracking in the north-end diaphragm and near the base of Member 11 worsened somewhat after de-stressing, but the cracks were not substantially different than those visible in Exhibits 8.2.1 and 8.2.2, which were taken before de-stressing began.

March 14. Photographs taken on March 13 and 14, 2018, show that the cracks in the north-end diaphragm continue to widen, as can be seen in Exhibits 8.4.1 and 8.4.2.

8.2 Re-Stressing of Member 11

Based on the observations and events described above, as well as phone conversations between MCM and FIGG, the project team was under the impression that the worsening of the cracking was related to de-stressing of Member 11. FIGG also understood that the cracks had not grown since the de-stressing. On March 13, 2018, FIGG sent an email to MCM recommending re-stressing of Member 11. Each post-tensioning bar was to be re-stressed in 50 kip increments, alternating between the top and bottom bars, up to the originally specified prestressing force of 280 kips in each bar.

The March 13 email instructed MCM to closely monitor the north-end diaphragm “to ensure that the crack size does not increase.” FIGG anticipated the crack size would either remain the same or more probably decrease in size. Nevertheless, the FIGG email also indicated that “If the crack size increases, the post-tensioning bar stressing shall stop and FIGG be notified immediately.”

Also, the stressing safety guidelines in the Structural/VSL post-tensioning shop drawings state “Immediately cease prestressing and remove all personnel from the area if any existing crack widening, new concrete cracking, bearing plate movement, or unusual sounds are observed.” Thus, it would be expected that Structural/VSL would implement some type of monitoring of the existing cracks during re-stressing.

8.3 Actual Crack Monitoring

Wood blocks were mounted across cracks on the north face of the north-end diaphragm, as shown in Figure 8.1. Lines transcribed across the blocks indicate they were intended for monitoring changes in crack width. The extent to which these crack gauges were used is not known; however, as described below, time-lapse video does indicate they were not used to monitor changes in crack width during re-stressing.

³⁵ Occupational Safety and Health Administration, "Investigation of March 15, 2018 Pedestrian Bridge Collapse at Florida International University," June 2019, page 48.



Figure 8.1. Wood blocks mounted across cracks on the north face of the north and diaphragm

Two cameras near SW 8th Street recorded time-lapse images of construction activity: one west of the main span on the south side of SW 8th Street, and a second east of the main span on the north side of SW 8th Street. March 15 screenshots, mainly from the camera on the south side of SW 8th Street, are provided in Exhibits 8.5.1 to 8.5.10.

The following are examples of observations made from these screenshots:

Approximate Time (3/15/18)	Observation(s)
11:45 a.m.	Start of re-tensioning. Apparently, the five-person crew gained access from a green manlift (left side of screenshot). The hydraulic ram used for de-tensioning was positioned with a white crane (next to the manlift).
11:53 a.m.	Two persons (red arrows) can be seen on the east side of the deck near the railing at the north end.
1:42 p.m.	A person (red arrow) can be seen on the west side of the deck near the railing at the north end. Repositioning of the ram is evidenced by movement of the crane boom and ball on the crane line. The ram was repositioned numerous times during the course of the re-stressing. The number of times the ram was repositioned is consistent with the FIGG email to re-stress in 50 kip increments, alternating between the top and bottom bars, up to the originally specified pre-stressing force of 280 kips in each bar.
1:43 p.m.	The person seen in the previous image has moved a few feet southward.
1:44 p.m.	The person seen in the previous image has moved northward to his 1:42 p.m. position.
1:46 p.m.	One minute before collapse. No change from previous screenshot.
1:47 p.m.	First screenshot after collapse.

As described in the next section, closely monitoring cracks in the north-end diaphragm would have required electronic instrumentation or continual arm's-length or closer access to the cracks, either from a manlift on the north side of the diaphragm or on hands and knees on the deck at the north end. There is no record of electronic instrumentation and none of the time-lapse video images showed a person with arm's-length access to the cracks, either from the deck or from a manlift. Apparently, the cracks were not closely monitored as instructed by FIGG.

8.4 Possible Crack Monitoring

In light of FIGG's email to monitor cracks during re-stressing and the Structural/VSL stressing safety guideline regarding cracking during stressing, WJE evaluated possible means for monitoring cracks in the north-end diaphragm. Figure 8.2 shows a concrete slab in WJE's Northbrook laboratory used for evaluating anchors installed in cracked concrete. The specimen is mounted on a tensioning frame that induces cracks. A 0.1-inch-wide crack was induced in the concrete specimen to simulate an existing crack in the north-end diaphragm.

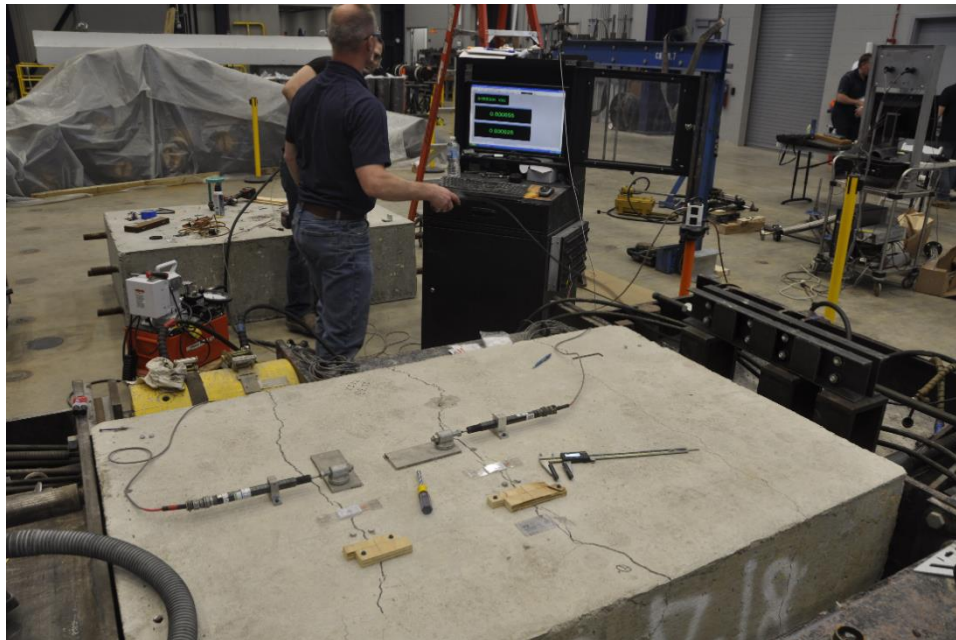


Figure 8.2. Crack induced in concrete specimen in WJE Northbrook laboratory

The crack frame was then used to increase the crack width to 0.2 inches in 0.02 inch increments, based on displacement transducer readings. Five methods for monitoring changes in crack width were evaluated:

1. Displacement transducer
2. Humboldt crack gauge
3. Dial caliper and measurement points
4. Wood block crack gauge (similar to that used at the site)
5. Crack width ruler (crack comparator)

The devices used in these five methods are shown in Figure 8.3. The numbers in the blue boxes correspond to the numbers in the above list.

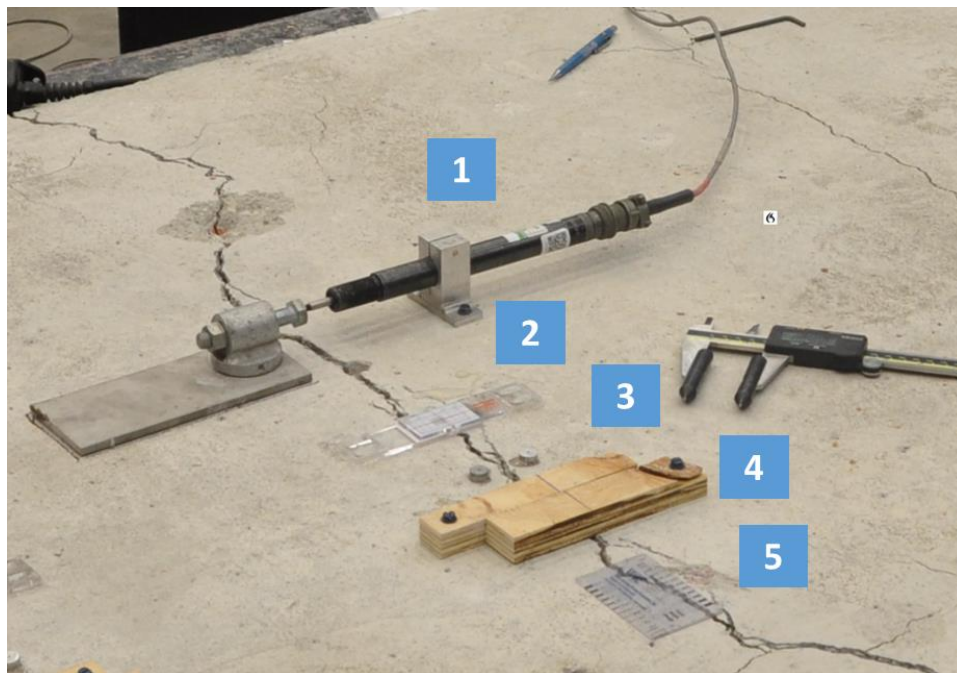


Figure 8.3. Crack monitoring methods evaluated

The effectiveness of these methods is summarized in Table 8.1. Effectiveness of crack monitoring methods. As indicated in Table 8.1. Effectiveness of crack monitoring methods, the first four methods, including the wood block crack gauge (similar to that used on the north end diaphragm), were effective in detecting changes in crack width as small as 0.02 inches. Much smaller changes could be detected with the displacement transducer or digital calipers. The crack comparator was only effective if used in combination with close-up photographs. Exhibit 8.6.1 provides photographs of the Humboldt crack gauge, wood block crack gauge, and crack comparator after a 0.02 inch increase in crack width.

Small changes in crack width could have been monitored remotely using a displacement transducer. (The readout from the displacement transducer used by WJE can be seen in Figure 8.2.) All other methods would have required arm's-length or closer access to the crack.

Table 8.1. Effectiveness of crack monitoring methods

Method	Effectiveness
Displacement transducer	Very accurate and effective; detects crack width changes of less than 0.001 inches.
Humboldt crack gauge	Requires close examination, but effective in detecting 0.02-inch increase in crack width.
Digital caliper	Very accurate and effective; detects crack width changes as small as approximately 0.002 inches.
Wood block crack gauge	Effective in detecting 0.02-inch increase in crack width.
Crack comparator	Requires close examination; effective if used in combination with close-up photographs.

8.5 Discussion and Findings

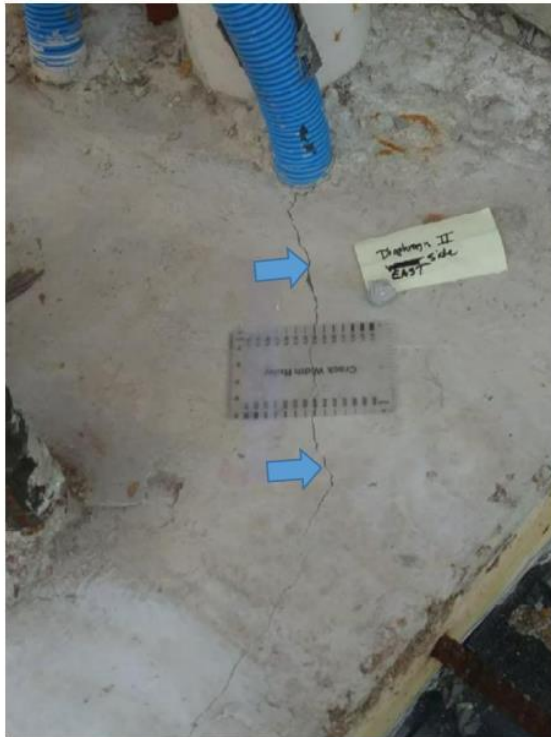
As described above, the cracks in the region of the connection of the northernmost diagonal to the deck increased dramatically during the course of the move from the casting yard to the final location. Even though the truss member forces were very similar before and after the move, several factors could have contributed to the additional damage. These factors are described in Section 7.

The damage observed after de-stressing is only slightly greater than the damage observed about three hours after the move. Therefore, the additional damage was related to the move and placement of the span in its final position, rather than de-stressing. Placement of the span in its final position would have resulted in a compressive force of almost 1700 kips in Member 11. The damage is consistent with horizontal sliding of Member 11 relative to the deck in combination with horizontal breakout failure of the north-end diaphragm, which are aggravated by additional compressive force in Member 11. On the other hand, de-stressing reduced the compressive force in Member 11, although a small increase in the post-tensioning force would have been required to loosen the nut on the post-tensioning rod in the first de-tensioning step. (No records of the de-stressing force used are available.)

Analysis of time-lapse video indicates that, contrary to FIGG instructions and Structural/VSL Safety Guidelines, no one closely monitored cracks in the north-end diaphragm during re-stressing of Member 11. Review of the time-lapse video also shows that Member 11 was re-stressed in increments. As such, Structural/VSL must have been aware of the instructions in FIGG's March 13 email to MCM. However, WJE does not know if MCM delegated responsibility for closely monitoring cracks during de-stressing to Structural/VSL.

Because the construction joint was not roughened and re-stressing Member 11 in incremental steps over two hours would have increased the compressive force by up to 560 kips, the existing cracks would have widened. If closely monitored by MCM, Structural/VSL, BPA or Corradino, increases in crack width could have been readily detected by several means, including use of wood block crack gauges, which were already used at the site. Increases in crack width would have required stopping the re-stressing in accordance with FIGG instructions and Structural/VSL safety guidelines and thereby prevented the collapse.

Exhibit 8.1.1. Crack in north end diaphragm approximately two weeks before move



East side of Member 12. Photo 13 from BPA crack inspection after formwork/scaffolding removal, February 28. Crack is indicated by blue arrows. Crack width ruler appears to indicate 0.020 inches.



West side of Member 12. Photo 12 from BPA crack inspection report after formwork/scaffolding removal, February 28. Crack is indicated by blue arrows. Crack width ruler appears to indicate 0.014 inches.

Exhibit 8.1.2. Diagonal “wedge” crack at Member 11 approximately two weeks before move



Diagonal “wedge” crack along the bottom of Diagonal 11 on the east face. Photo taken by BPA on February 24, 2018, prior to the move.

Exhibit 8.2.1. Cracks in north end diaphragm approximately three hours after move



East side of Member 12. March 10 photo by Corradino showing same crack after move at 3:14 p.m.



West side of Member 12. March 10 photo by Corradino at 3:14 p.m.

Exhibit 8.2.2. Diagonal “wedge” crack at Member 11 approximately three hours after move



Diagonal “wedge” crack at base of Member 11 after the move on the east face. Photo taken by Corradino on March 10, 2018 at 3:07pm.

Exhibit 8.3.1. Cracks in north end diaphragm

PHOTO 5: Diaphragm 2, Eastside top view crack



East side of Member 12. Photo taken March 12, 2018 by MCM.

PHOTO 1: Diaphragm 2, Westside top view, crack



West side of Member 12. Photo taken March 12, 2018 by MCM.

Exhibit 8.3.2. Diagonal “wedge” crack at Member 11



Diagonal “wedge” crack at base of Member 11 on the east face. Photo taken by MCM on March 12, 2018.

Exhibit 8.4.1. Cracks in north end diaphragm



East side of Member 12. Photo taken March 14, 2018 by BPA.



West side of Member 12. Photo taken March 13, 2018 by BPA.

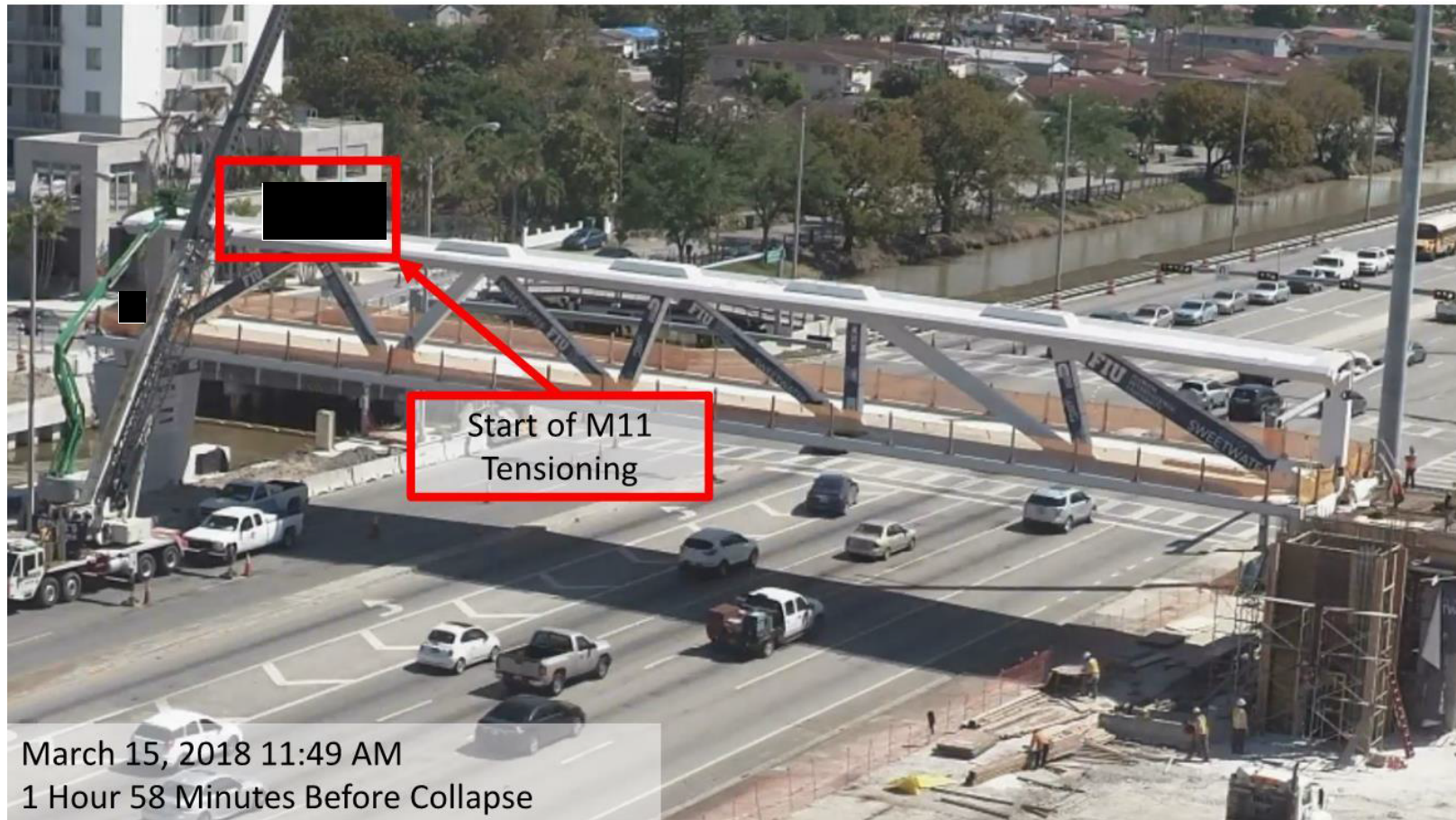
Exhibit 8.4.2. Diagonal “wedge” crack at Member 11



8

Diagonal “wedge” crack at base of Member 11. Photo taken by BPA on March 13, 2018. Note the spall seen in Exhibit 3.2 has been removed.

Exhibit 8.5.1. Time-lapse video



Note: Redaction in "Exhibit 8.5.1 Time-lapse video" as per NTSB Operations Bulletin CIO-GEN-016.

Exhibit 8.5.2. Time-lapse video



Note: Redaction in "Exhibit 8.5.2 Time-lapse video" as per NTSB Operations Bulletin CIO-GEN-016.